PL-TR--
92-1049

(2)

SEMICONDUCTOR LASER WITH A SELF-PUMPED PHASE-CONJUGATE EXTERNAL CAVITY

Bruce William Liby

October 1992

Final Report

APPROVED FOR PUBLIC RELEASE; DISTRIBUTION UNLIMITED.

PHILLIPS LABORATORY
Lasers and Imaging Directorate
AIR FORCE MATERIEL COMMAND
KIRTLAND AIR FORCE BASE, NM 87117-6008

PL-TR--92-1049

This final report was prepared by the Phillips Laboratory, Kirtland Air Force Base, New Mexico, under Job Order 2301Y401. The Laboratory Project Officer-in-Charge was Dr Bruce W. Liby (LIDC).

When Government drawings, specifications, or other data are used for any purpose other than in connection with a definitely Government-related procurement, the United States Government incurs no responsibility or any obligation whatsoever. The fact that the Government may have formulated or in any way supplied the said drawings, specifications, or other data, is not to be regarded by implication, or otherwise in any manner construed, as licensing the holder, or any other person or corporation; or as conveying any rights or permission to manufacture, use, or sell any patented invention that may in any way be related thereto.

This report has been authored by an employee of the United States Government. Accordingly, the United States Government retains a nonexclusive royalty-free license to publish or reproduce the material contained herein, or allow others to do so, for the United States Government purposes.

This report has been reviewed by the Public Affairs Office and is releasable to the National Technical Information Service (NTIS). At NTIS, it will be available to the general public, including foreign nationals.

If your address has changed, if you wish to be removed from the mailing list, or if your organization no longer employs the addressee, please notify PL/LIDC, Kirtland AFB, NM 87117-6008 to help maintain a current mailing list.

This report has been reviewed and is approved for publication.

BRUCE W. LIBY
Project Officer

FOR THE COMMANDER

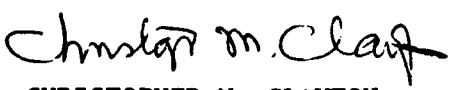

CHRISTOPHER M. CLAYTON
Acting Chief, Nonlinear Optics Branch

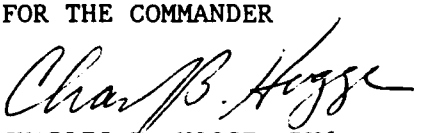

CHARLES B. HOGGE, DV6
Acting Director, Lasers and Imaging Directorate

DO NOT RETURN COPIES OF THIS REPORT UNLESS CONTRACTUAL OBLIGATIONS OR NOTICE ON A SPECIFIC DOCUMENT REQUIRES THAT IT BE RETURNED.

REPORT DOCUMENTATION PAGE

Form Approved
OMB No. 0704-0188

1. AGENCY USE ONLY (Leave blank)	2. REPORT DATE	3. REPORT TYPE AND DATES COVERED
	October 1992	Final 1 Oct 90 - 31 Jul 92

4. TITLE AND SUBTITLE

SEMICONDUCTOR LASER WITH A SELF-PUMPED PHASE-CONJUGATE EXTERNAL CAVITY

5. FUNDING NUMBERS

PE: 61102F
PR: 2301
TA: Y4
WU: 01

6. AUTHOR(S)

Bruce William Liby

7. PERFORMING ORGANIZATION NAME(S) AND ADDRESS(ES)

8. PERFORMING ORGANIZATION REPORT NUMBER

9. SPONSORING/MONITORING AGENCY NAME(S) AND ADDRESS(ES)

Phillips Laboratory
Kirtland AFB, NM 87117-6008

10. SPONSORING/MONITORING AGENCY REPORT NUMBER

PL-TR--92-1049

11. SUPPLEMENTARY NOTES

This dissertation was submitted in partial fulfillment of the requirements for the degree of Doctor of Philosophy in Physics.

12a. DISTRIBUTION/AVAILABILITY STATEMENT

Approved for public release; distribution unlimited.

12b. DISTRIBUTION CODE

13. ABSTRACT *(Maximum 200 words)*

This dissertation is intended to study the effects of self-pumped phase-conjugate feedback on a semiconductor laser. The concept of the unidirectional ring passive phase-conjugate mirror (PPCM) external cavity semiconductor laser (URECL) is introduced. This device consists of a laser diode coupled to a self-pumped ring phase-conjugate mirror. The URECL is compared and contrasted with a conventional external cavity semiconductor laser (CECL) that models a simple dielectric reflector for the feedback device, and with a phase-conjugate external cavity laser (PCECL) that models theoretically ideal phase conjugation as the feedback mechanism. The effective reflectivities for the different types of reflectors are derived and compared. The rate equations for all three cases are derived and plotted for comparison. The boundary conditions for the phase-conjugate cases are derived and experimental evidence is used to support the claim that a $2n\pi$ phase shift occurs for the PCECL and URECL. The multimode behavior of the free running laser, the CECL, and the URECL are compared. Experimental evidence of coherence collapse is presented and discussed. The dynamic rate equations are given and contrasted. The beam quality of the unidirectional ring PPCM is considered.

14. SUBJECT TERMS	15. NUMBER OF PAGES
External Cavity Lasers, Semiconductor Lasers, Coupled Cavity Lasers, Phase Conjugation, Photorefractive, Optical Feedback, Barium Titanate, Self-Pumped Phase Conjugation	170
	16. PRICE CODE

17. SECURITY CLASSIFICATION OF REPORT	18. SECURITY CLASSIFICATION OF THIS PAGE	19. SECURITY CLASSIFICATION OF ABSTRACT	20. LIMITATION OF ABSTRACT
Unclassified	Unclassified	Unclassified	SAR

ACKNOWLEDGMENTS

I would like to thank: David Statman for being my advisor, mentor, and, most importantly, friend. John McInerney for rescuing my Ph.D. You have my gratitude. Jack McIver for sticking around all these years. Jeanne Williams for her love and support. Her editing and typing made me look good. Karl Gass for his friendship and extensive help with the preparation of the text and graphics. Lee Schelonka for the extra effort when it counted. Chris Clayton for his indulgence in letting me puruse my reseacrh. Greg Dente for always having the time to answer my questions. Hua Li for her help in the lab. Mike Kelly. And have some more bread, Mike. Shelly Avery for all kinds of stuff. Teresa Manschesky for being *someone I could count on.* Steve Post for his friendship and some tech help in the crunch. Phil Peterson for being available to answer my questions. Tome Crowe, Sr. and the Litton crew; It was fun while it lasted. Fritz for making it all a little easier – so long, pal. To everyone I missed, I'm sorry. If you made a difference, you know it, and I thank you.

Most of all, I want to thank my father, William, who didn't get to see this; my mother, Geraldine; and my brother, Roger. Without their love and support this work would have not only been impossible, but meaningless. Thank you for your love.

TABLE OF CONTENTS

Chapter		Page
	LIST OF ILLUSTRATIONS	viii
	LIST OF TABLES	xiii
	LIST OF ACRONYMS	xiv
1	INTRODUCTION	1
	Photorefractives	1
	Semiconductor Lasers	2
	Optical Feedback	3
	Semiconductor Lasers with Phase-Conjugate Feedback	3
	Coupled Cavities	4
	Introduction to the Chapters	4
2	GENERAL ANALYSIS OF THE THREE GEOMETRIES	6
	Choice of the Phase Conjugate Reflector	6
	Effective Reflectivity for the Conventional Mirror	8
	Effective Reflectivity for the Ideal Phase-Conjugate Mirror	12
	Effective Reflectivity for the Unidirectional Ring	14
	Comparison	20
	Fundamental Assumptions for the Derivation of the Rate Equations	39
	Rate Equations with Conventional Feedback	41
	Rate Equations with Ideal Phase-Conjugate Feedback	45
	Rate Equations with Feedback from the Ring	48

CONTENTS – Continued

Chapter		Page
	Summary	52
3	STATIC AND SPECTRAL PHENOMENA	54
	Experimental Geometry	54
	Boundary Conditions for the URECL	59
	Measurement of Effective Reflectivities	66
	Coupling Factor	70
	Linewidth Narrowing and Broadening	71
	Multimode Spectra	80
	Summary	95
4	DYNAMIC PHENOMENA: COHERENCE COLLAPSE	96
	Experimental Set-Up	96
	Experimental Technique	98
	Results	98
	Discussion of the Coherence Collapse Data	107
	External Cavity Mode Suppression	110
	Rate Equations: Multiple Round Trips	113
	Rate Equations: One Round Trip	115
	Discussion of the Rate Equations	116
	Summary	117
5	BEAM QUALITY ASPECTS OF THE URECL	118
	Experimental Geometry #1	119
	Time Response	121
	Beam Quality	123
	Other Considerations	125

CONTENTS – Continued

Chapter		Page
	Experimental Geometry#2	127
	Beam Profile	127
	Summary	135
6	CONCLUSIONS AND FUTURE WORK	139
	Future Work	141
7	BIBLIOGRAPHY	144

LIST OF ILLUSTRATIONS

Figure		Page
2.1	Schematic of effective reflectivity.	9
2.2	Schematics of the three geometries: (a) CECL, (b) PCECL, and (c) URECL.	10
2.3	Unidirectional ring PCM diagrams: (a) PCM and (b) photorefractive grating.	15
2.4	Four wave mixing in kerr type media.	18
2.5	Effective versus external reflectivity. $R_2 = 0.9$. (a) All (a) All cases 1 RT, (b) all cases NRT. Solid line – CECL, dashed line – PCECL, and dotted line – URECL	21
2.5	Continued ... (c) CECL, (d) PCECL, and (e) URECL. Solid line – NRT, chain dot line – 1 RT.	22
2.6	Effective versus external reflectivity. $R_2 = 0.32$. (a) All cases 1 RT, (b) all cases NRT. Solid line – CECL, dashed line – PCECL, and dotted line – URECL.	23
2.6	Continued ... (c) CECL, (d) PCECL, and (e) URECL. Solid line – NRT, chain dot line – 1 RT.	24
2.7	Effective versus external reflectivity. $R_2 = 0.1$. (a) All cases 1 RT, (b) all cases NRT. Solid line – CECL, dashed line – PCECL, and dotted line – URECL.	25
2.7	Continued ... (c) CECL, (d) PCECL, and (e) URECL. Solid line – NRT, chain dot line – 1 RT.	26
2.8	Effective versus external reflectivity. $R_2 = 0.01$. (a) All cases 1 RT, (b) all cases NRT. Solid line – CECL, dashed line – PCECL, and dotted line – URECL.	27
2.8	Continued ... (c) CECL, (d) PCECL, and (e) URECL. Solid line – NRT, chain dot line – 1 RT.	28
2.9	Effective versus external reflectivity. $R_2 = 0.0001$. (a) All cases 1 RT, (b) all cases NRT. Solid line – CECL, dashed line – PCECL, and dotted line – URECL.	29
2.9.	Continued ... (c) CECL, (d) PCECL, and (e) URECL. Solid line – NRT, chain dot line – 1 RT.	30

LIST OF ILLUSTRATIONS – Continued

Figure		Page
2.10	Effective versus external reflectivity. $R_2 = 0.32$, phase $= \pi/2$. (a) All cases 1 RT, (b) all cases NRT. Solid line – CECL, dashed line – PCECL, and dotted line – URECL.	31
2.10	Continued ... (c) CECL, (d) PCECL, and (e) URECL. Solid line – NRT, chain dot line – 1 RT.	32
2.11	Effective versus external reflectivity. $R_2 = 0.32$, phase $= \pi$. (a) All cases 1 RT, (b) all cases NRT. Solid line – CECL, dashed line – PCECL, and dotted line – URECL.	33
2.11	Continued ... (c) CECL, (d) PCECL, and (e) URECL. Solid line – NRT, chain dot line – 1 RT.	34
2.12	Effective reflectivity versus $\omega\tau$. $R_2 = 0.01$. (a) 1 RT and (b) NRT.	35
2.13	Effective reflectivity versus $\omega\tau$. $R_2 = 0.1$. (a) 1 RT and (b) NRT.	36
2.14	Effective reflectivity versus external phase. $R_2 = 0.1$. (a) PCECL and (b) URECL.	37
2.15	Change in gain versus change in frequency. $R_3 = 0.01$. (a) CECL, (b) PCECL, and (c) URECL. Solid line – NRT, chain dot line – 1 RT.	50
2.16	Change in gain versus change in frequency. $R_3 = 0.0001$. (a) CECL, (b) PCECL, and (c) URECL. Solid line – NRT, chain dot line – 1 RT.	51
3.1	Unidirectional ring PPCM external cavity laser.	55
3.2	Schematic for boundary conditions.	60
3.3	Threshold gain versus effective reflectivty.	62
3.4	$L - I$ curves for external cavity lasers. (a) CECL, and (b) URECL. Solid line – free running, dashed line – decreased output, dotted line – increased output.	63

Figure		Page
3.5	Rear facet output power as measured by the spectrum analyzer (a) without feedback and (b) with feedback.	65
3.6	Effective reflectivity versus change in output power. Free running output power = 0.5.	67
3.7	Effective reflectivity versus change in threshold current. . . .	69
3.8	Coupling factor "f" versus effective reflectivity.	72
3.9	Linewidth reduction factor versus effective reflectivity. Solid line – CECL; dashed line – URECL, CECL as noted. .	76
3.10	Linewidth reduction factor versus effective reflectivity. Solid line – CECL; dashed line – URECL, CECL as noted. .	77
3.11	Linewidth reduction factor versus $\omega\tau$. Dotted line – CECL; solid line – URECL.	79
3.12	Linewidth narrowing for $r_3 = .045$. (a) with feedback and (b) without feedback.	81
3.13	Linewidth narrowing for $r_3 = .0136$. (a) with feedback and (b) without feedback.	82
3.14	Free running laser. (a) 105% current threshold, (b) 110% current threshold, and (c) 120% current threshold.	84
3.14	Continued ... (d) 130% current threshold, (e) 140% current threshold, and (f) 150% current threshold.	85
3.15	Laser with conventional feedback. (a) 105% threshold current, (b) 110% threshold current and (c) 120% threshold current. .	86
3.15	Continued ... (d) 130% threshold current, (e) 140% threshold current and (f) 150% threshold current.	87
3.16	Laser with phase-conjugate feedback. (a) 105% threshold current, (b) 110% threshold current and (c) 120% threshold current.	88
3.16	Continued ... (d) 130% threshold current, (e) 140% threshold current and (f) 150% threshold current.	89

LIST OF ILLUSTRATIONS (Continued)

Figure		Page
3.17	Model of multimode spectra. (a) CECL and (b) URECL. Dotted line – experimental, solid line – model.	92
3.18	Poor quality feedback from ring.	93
3.19	Good quality feedback from ring.	94
4.1	Coherence Collapse Geometry.	97
4.2	Fabry-Perot spectra of laser with feedback. (a) free running, and (b) $r_3 < 0.0141$.	99
4.2	Continued – (c) $r_3 < 0.0141$, and (d) $r_3 = 0.0265$.	100
4.2	Continued – (e) $r_3 = 0.0300$, and (f) $r_3 = 0.0316$.	101
4.2	Continued – (g) $r_3 = 0.0458$, and (h) $r_3 = 0.0520$.	102
4.3	Noise spectra of laser with feedback. (a) $r_3 < 0.0141$, (b) $r_3 = 0.0265$, and (c) $r_3 = 0.0300$.	103
4.3	Continued – (d) $r_3 = 0.0316$, (e) $r_3 = 0.0458$, and (f) $r_3 = 0.0520$.	104
4.4	Longitudinal spectra during coherence collapse. (a) Free running laser, (b) $R < 2 \times 10^{-4}$, and (c) $R = 7 \times 10^{-4}$ and above.	105
4.5	Noise spectra showing alternate cavity mode suppression. . .	111
4.6	Noise spectra showing external cavity mode suppression. . . .	112
5.1	Experimental Geometry #1.	120
5.2	Time Response of Barium Titanate. Squares – reflectivity, and circles – beam quality.	122
5.3	Beam quality versus reflectivity. Squares – conventional mirror, and circles – phase conjugate mirror.	124

LIST OF ILLUSTRATIONS (Continued)

Figure		Page
5.4	Beam quality versus reflectivity with aberration. Squares – conventional mirror, circles – phase conjugate mirror, and triangle – static hologram.	126
5.5	Experimental Geometry#2.	128
5.6	Output profile of laser. (a) Free running, and (b) with feedback.	129
5.7	Return beam profiles. (a) Conventional, (b) phase conjugate, (c) conventional showing interference effects, and (d) background.	131
5.8	Progress of phase conjugate buildup with off-axis beam. (a) Background, (b) 2.5 minutes, (c) 5 minutes, (d) 7.5 minutes.	132
5.8	Continued – (e) 10 minutes, and (f) 12.5 minutes.	133
5.9	Progression of phase conjugate buildup (a) Background, (b) 2.5 minutes, (c) 5 minutes, (d) 7.5 minutes.	136
5.9	Continued – (e) 10 minutes, (f) 12.5 minutes, and (g) 15 minutes.	137

LIST OF TABLES

Table		Page
2.1	Multiple round trips with boundary conditions imposed. . .	52
2.2	One round trip with boundary conditions imposed.	53
3.1	Change in facet output power normalized to free running. . .	64
3.2	Effective reflectives and coupling factors. $f_d = 135\text{GHz}$, $\tau_p = 2.1\text{ps}$	68

LIST OF ACRONYMS

PCM – Phase-conjugate Mirror. A device that returns the phase-conjugate of the electric field that is incident upon it. This is in contrast to a conventional mirror, which provides only specular reflection.

PPCM – Passive Phase-conjugate Mirror. This is a PCM in which four-wave mixing is self-induced. It is sometimes described as self-pumped.

UR – Unidirectional Ring PPCM. A ring PPCM that is constrained to oscillate in only one direction.

CECL – Conventional External Cavity Laser. This device is a coupled cavity formed by a semiconductor laser coupled to a conventional external reflector.

PCECL – Phase-conjugate External Cavity Laser. This conceptual device is a coupled cavity formed by an "Ideal" phase conjugate mirror coupled to a semiconductor laser. Ideal in this sense means perfect, not a laboratory model.

URECL – Unidirectional Ring External Cavity Laser. This device is the actual experimental phase-conjugate external cavity used in the experiments. It consists of a unidirectional ring passive phase-conjugate mirror coupled to a semiconductor laser. The unidirectional ring PPCM is described in the text, essentially it is a ring resonator that is constrained to oscillate in only one direction, clockwise or counterclockwise, around the ring cavity.

1 RT – One Round Trip. The approximation where the light in the external cavity makes one round trip before coupling back into the laser.

NRT – N Round Trips. The complete solution where the light in the external cavity makes an infinite number of round trips, coupling a portion of itself into the laser each time.

CHAPTER 1

INTRODUCTION

The field of nonlinear optics has always had the potential to impact other areas of physics. The science of imaging has reaped the greatest benefit of these techniques to date. The natural progression into other research domains consists of replacing conventional reflectors with their phase-conjugate counterparts. This simple idea lead to the work presented in this dissertation. Both semiconductor laser physics and nonlinear optics are relatively mature fields that have plenty of issues left to resolve. Their cross-fertilization enhances not only the rich physics to be found, but also the potential for device application.

Photorefractives

The two fields of semiconductor lasers and nonlinear optics are about the same age. Although the possibility of utilizing the higher order nonlinear effects of materials had been suggested for some time (for example, Gabor's holograms) it was not until the high intensities provided by the laser were available that significant research could be done. Then the field exploded with investigations into the second, third and higher order effects[1]. The laser also made practical holography possible [2]. That the former could be used for the latter was discovered almost by accident. Streaks in lithium niobate, thought to be optical damage caused by high laser light intensities, turned out to be the photorefractive effect [3]. This discoloration was due to an intensity dependent component of the index of refraction. Almost immediately this property began to be investigated as a potential mechanism for optical data storage.

Around the same time that the field of optical memory began to blossom investigators started to exploit the third order optical susceptibility ($X^{(3)}$) of

nonlinear materials [4,5]. It was found that through four-wave mixing in appropriate nonlinear materials the phase conjugate of an incident beam could be returned. This process became known as optical phase conjugation or real-time (dynamic) holography. The latter term is in contrast to static holograms recorded on film. The process is actually quite similar.

When it was realized that diffraction gratings could be written in $X^{(2)}$, or photorefractive, media, the process of photorefractive phase conjugation was developed [6,7]. The significant feature of this phenomena is that there is a $\pi/2$ phase shift between the index gratings and the scattered beam. Thus energy could be transferred between beams, and oscillation with gain could take place . Additionally, photorefractive phase conjugators can be self-pumped [8]. A single laser beam can write the grating, and, through either internal or external reflection, scatter off of it. The need for counter-propagating pump beams, as with $X^{(3)}$ materials, is eliminated. In those, the beams are coupled through a nonlinear polarization. In photorefractive media, the beams are coupled through scattering off refractive index gratings, creating an effective $X^{(3)}$. The experiments presented in this dissertation use Barium Titanate ($BaTiO_3$) as the nonlinear medium. Many other nonlinear materials, such as $LiNiO_3$, BSO, or SBN, would exhibit similar effects. The phase conjugation is treated as to be completely general; the results are applicable to any other material.

Semiconductor Lasers

Shortly after the development of the first lasers, lasing in semiconductor materials was achieved [9-12]. The first diode lasers were simple devices requiring significant cooling and large current densities. This field progressed rapidly and by the time optical phase conjugation was being researched laser diodes were commonplace. Their appeal is enormous; they are relatively inexpensive, easy

to manufacture, small, compact, and energy efficient (efficiencies of greater than 60% have been attained). And for the scientist they are rich in physics. As a result, laser diodes have not only become a common device in many everyday applications (e.g. CD players), their operation continues to be an area of active research [13, 14].

Optical Feedback

The great efficiency of semiconductor laser allows for lasing with relatively low cavity reflectivities. In fact, the Fresnel reflection off the laser facet is frequently sufficient. This is the case for the HLP1400 laser diode used in all of this dissertation's experiments. The semiconductor material used in laser diodes is optically nonlinear. The high gain, low reflectivity, and nonlinearity of these devices makes them extremely susceptible to optical feedback. This property can be detrimental to diode laser operation. It can also be used to control the behavior of these lasers with respect to frequency control, stability, linewidth and other considerations [15-19].

With the advent of nonlinear techniques, phase-conjugate mirrors were used to replace conventional reflectors in laser cavities. The success of these efforts spawned the field of phase conjugate resonators [20-25].

Semiconductor Lasers with Phase-Conjugate Feedback

The natural extension of the latter two fields was to investigate the effects of phase-conjugate feedback into lasers, particularly semiconductor lasers. The research has consisted largely of two areas: Optical feedback from a phase-conjugate mirror [26-31], and optical feedback from four-wave mixing in another semiconductor laser [32-34]. The latter topic is somewhat removed from the issues considered here. To date there have a number of experiments and calculations conducted, however, there has been no systematic study performed.

This dissertation is an attempt to put previous work in context, conduct new and significant research on the subject, and examine some of the commonly used assumptions.

Coupled Cavities

One of the primary motivations for this work was its extension to phase locking semiconductor lasers. The coupling of cavities, indeed oscillators, is a mature field that still receives a great deal of attention, especially with respect to laser diodes [37-45]. Several attempts have been made to couple lasers via nonlinear optical techniques [46-50]. Of particular interest are the efforts to phase lock diode lasers in this manner [51-54]. Experiments performed by the author prior to this work consisted of reproducing and extending that research [55]. During the course this research a number of questions arose that had not been addressed in previous work. They all related to one fundamental question: how does the impact of phase-conjugate feedback differ from feedback from a conventional mirror? The more important aspects have been studied for this dissertation.

Introduction to the Chapters

Throughout this work the effort has been made to distinguish between conventional feedback, Ideal phase-conjugate feedback and self-pumped phase conjugate feedback. Conventional feedback is the result of a reflection off a plane dielectric mirror. Ideal phase-conjugate feedback considers the theoretical *best case* of phase-conjugation. This can be thought of experimentally as phase conjugation due to $X^{(3)}$ four-wave mixing. The distinction is made because self-pumped phase conjugation is not *Ideal.* These concepts are modeled in Chapter 2, where the experimental geometries are introduced. They are: the Conventional External Cavity Laser (CECL), the Phase-conjugate External Cavity Laser (PCECL),

representing the Ideal case, and the Unidirectional Ring External Cavity Laser (URECL), which is the self-pumped geometry used for the experiments. In this chapter effective reflectivities and rate equations are derived for all three. Also included are the assumptions and approximations used throughout the dissertation.

In Chapter 3 the static behavior of the phase-conjugate external cavity is presented. It begins with a description of the experimental set-up. The boundary conditions for the phase conjugate cases are derived. This is of critical importance for understanding the process and its potential applications. Experimental evidence is used to support these findings. The quality of the coupling is presented. Linewidth narrowing is modeled and demonstrated. Finally, the multimode spectra of the free running and external cavity lasers are discussed.

Chapter 4 deals with the phenomena of coherence collapse. The experimental data is presented, clearly showing the onset of dramatic linewidth broadening due to optical feedback. External cavity mode suppression only seen with a phase-conjugate external cavity is demonstrated. The pertinent rate equations are given and compared. The chapter closes with suggestions as to future modeling.

Although whether one considers the system as a laser with feedback or a coupled cavity is purely conceptual, the distinction is made in this work when the nature of the feedback is considered independent of its effects on the laser. This occurs in Chapter 5, where the beam quality aspects of the self-pumped phase-conjugate external cavity laser are investigated. The time dependence of the reflectivity is noted and shown to be different than that of the beam quality. The beam quality of the ring PPCM, conventional mirror, and static hologram is measured. A series of images is presented that dramatically show this phenomenon, along with other interesting features of the device.

The conclusions are presented in Chapter 6. The dissertation ends with a discussion of potential follow on research.

CHAPTER 2

GENERAL ANALYSIS OF THE THREE GEOMETRIES

In this chapter the external cavity semiconductor laser geometries used in the experiments will be introduced. The first section will discuss the rationale for choosing the unidirectional ring passive phase-conjugate mirror external cavity semiconductor laser (URECL). The next three sections present the derivation of the effective reflectivities for the different geometries. Following this is a comparison of the three cases. Then the rate equations are introduced for the conventional external cavity semiconductor laser (CECL), formed by the laser and a plane dielectric mirror, the "Ideal" phase-conjugate external cavity semiconductor laser (PCECL), formed by the laser and an ideal, that is, theoretical phase-conjugate mirror, and then the URECL. This will place the device in context with previous work and provide a basis of understanding for the experiments that follow.

Choice of the Phase-Conjugate Reflector

This work features the unidirectional ring passive phase-conjugate mirror. The choice of this device was no accident; it was driven by several important considerations. The first was ensuring the generality of the work produced. The research leading up to this dissertation was directed towards the coupling of semiconductor lasers via the techniques of nonlinear optics. This technique is attractive for laser phasing because of the potential for aberration correction. Photorefractive methods are also self-aligning to some extent.

To date the most successful approach for coupling has been to employ a photorefractive crystal as the nonlinear medium, specifically Barium Titanate. This perovskite has become the workhorse of the phase-conjugation community. Its inclusion in this work was natural. At low powers in the near infrared there isn't anything that works nearly as well.

Phase conjugation in $BaTiO_3$ can be achieved in several fashions but self-pumped configurations are the most common [6]. This is because the photorefractive coupling coefficient of the crystal is large. Self-pumped phase-conjugate mirrors can originate from a single pump beam, such as the Cat mirror [7] and the Ring passive PCM [56], or they can originate from two beams, such as the Double Phase-Conjugate Mirror [57] or the Bird-wing mirror [58]. Ideally, for a nonlinear coupling medium, one would like a black box that returns the phase conjugate of whatever is incident upon it. Allowing for some gross alignment, this is virtually the case for the DPCM. It shows the greatest potential for laser phasing, of any geometry. In that device, two independent pump beams are crossed in the crystal, and couple into one another via the photorefractive effect. This provides a mechanism for injection locking. The URECL mimics a DPCM in that respect, except that only a single pump beam is used. Thus its study falls under the self-imposed guidelines of applicability for laser phasing.

A ring geometry was chosen for its ease of use. It is simple to align, allowing for a quick set-up. Additionally, ring PPCM's have become quite generally used in research on photorefractive phase conjugation. Despite this, untested assumptions about its behavior continue to prevail. So this and related work [59] has application outside the realm of coupling lasers because it sets several inferences on a sound footing.

The ring was constrained to be unidirectional so that phase and intensity instabilities (that plagues photorefractives) would not be an issue. Most of these

fluctuations arise from grating competition [60]. In a typical photorefractive device any two coherent beams can write a grating hologram [6]. So formed, these gratings can couple. The interaction is unstable in time thus their reflection or transmission strength will fluctuate. In the unidirectional ring PPCM, as in its cousin the DPCM, the beams are constrained so that only a single grating is written. Consequently, the reflection intensity is stable [61].

Other geometries were considered and a four-wave mixing mirror was set up and investigated. Unfortunately, the reflectivity of this device was quite low, less than 0.1%. This would have prohibited most of the experiments that were planned. This device is likely to suffer from grating competition as well, making it unsuitable for a wide range of experiments.

Effective Reflectivity for the Conventional Mirror

The differences in the external cavities are due to the nature of the reflected light. For the bare external cavity, i.e., one possessing no gain medium, we can consider the exit facet and external reflector an effective mirror. The effective reflectivity, r_{eff}, is then a function of r_2, r_3, (the amplitude reflectivities of the exit facet and external mirror, respectively), and the phase delay between them. This is shown conceptually in Fig. 2.1 [62].

To determine the effective reflectivity of the CECL consider Fig. 2.2. The electric field inside the laser is composed of E_i and E_r, incident and reflected fields, respectively. If E_r is expressed as a function of E_i, the following is attained:

$$E_r e^{i\omega\tau} = E_i \left[r_2 - t^2 r_3 e^{-i\omega\tau} - t^2 r_3^2 r_2 e^{-2i\omega\tau} - \ldots \right], \qquad (2.1)$$

where τ is the round trip time in the cavity and ω is the laser frequency with feedback. t_2, r_2, and r_3 are the Stokes parameters for dielectric mirrors. This is the source of the minus (-) sign in the equation; it represents the π phase

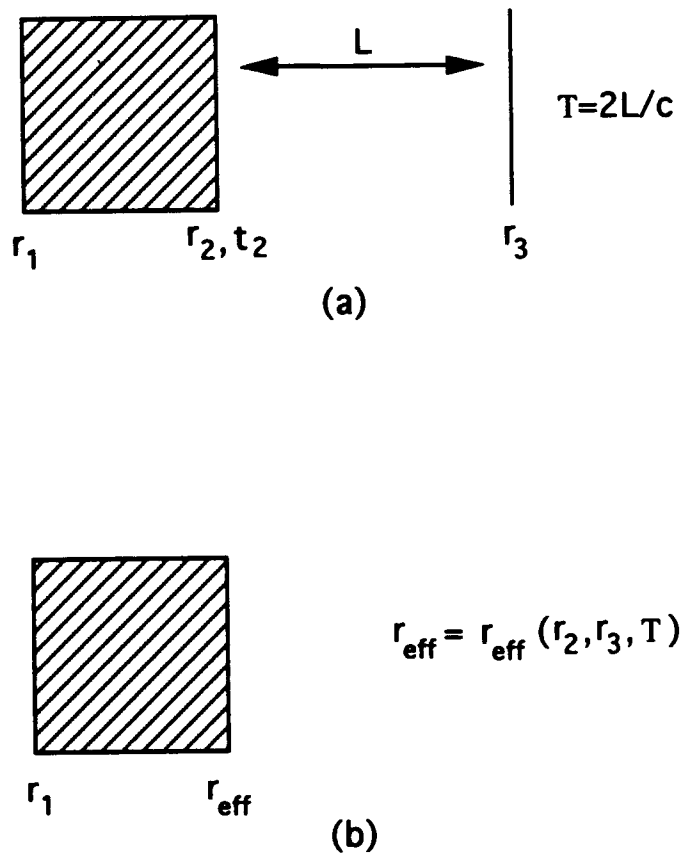

Fig. 2.1. Schematic of effective reflectivity.

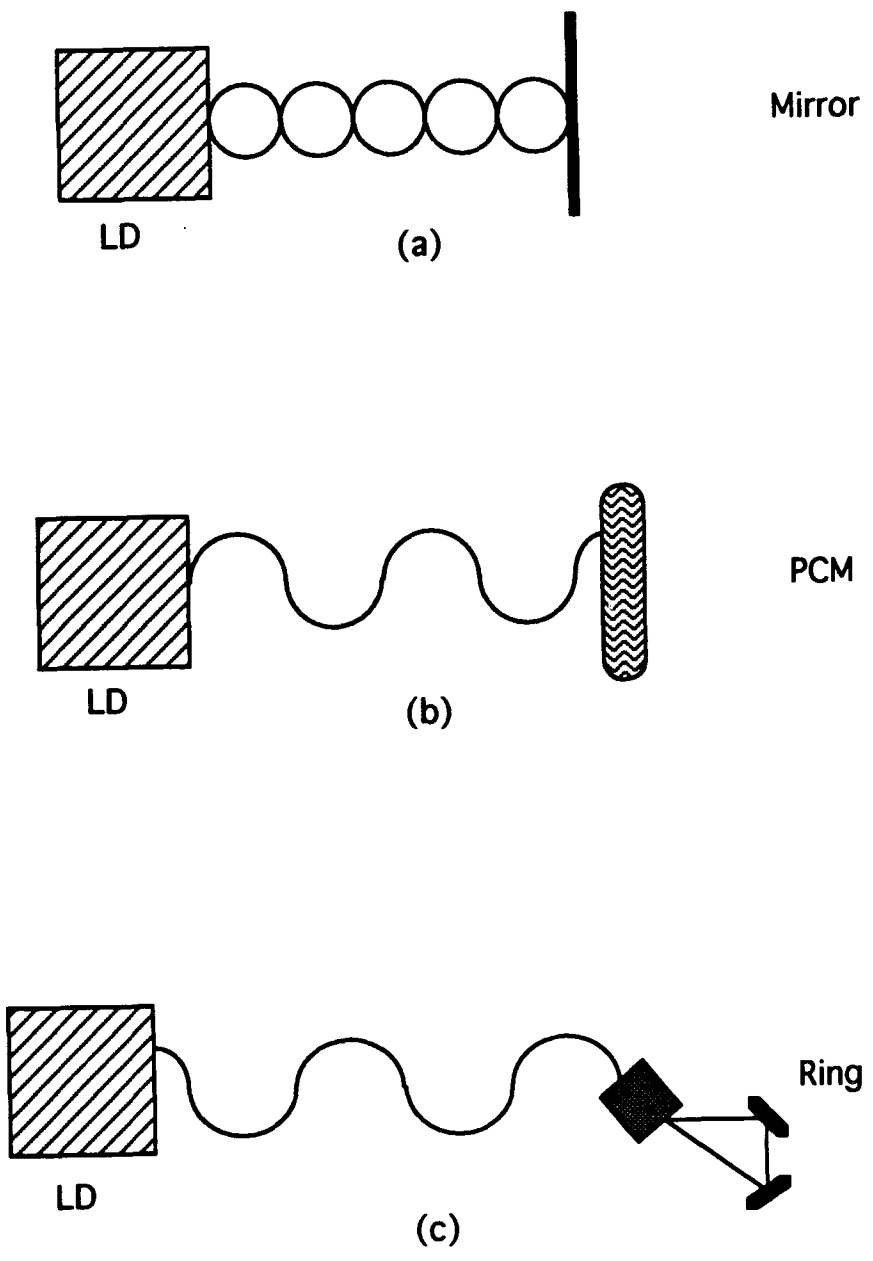

Fig. 2.2. Schematics of the three geometries: (a) CECL, (b) PCECL, and (c) URECL.

shift upon reflection off a dielectric surface of greater refractive index than the incident medium. Thus both r_2 and r_3 are negative. The increasing terms scale with additional reflections around the external cavity. In general the amount of light that actually couples into the gain region of the laser must be taken into account. This is called the coupling factor "f." Although this term is added empirically later, I have left it out here to simplify the equations for comparison and analysis. To solve for r_{eff}, take the ratio of E_i and E_r

$$r_{\text{eff}} = \frac{E_r}{E_i} = r_2 \left[1 - \frac{t^2 r_3}{r_2} e^{-i\omega\tau} - \frac{t^2 r_3^2 r_2}{r_2} e^{-2i\omega\tau} - \ldots \right]. \tag{2.2}$$

If this expression is summed

$$r_{\text{eff}} = r_2 \left[1 - \frac{t_2^2}{r_2^2} \sum_1^\infty (r_2 r_3 e^{-i\omega\tau})^m \right], \tag{2.3}$$

or

$$r_{\text{eff}} = r_2 \left[1 - \frac{(1 - r_2^2)}{r_2} \frac{e^{-i\omega\tau}}{1 - r_2 r_3 e^{-i\omega\tau}} \right]. \tag{2.4}$$

It follows immediately that

$$|r_{\text{eff}}|_{\text{conv:}N} = \left[\frac{r_2^2 + r_3^2 - 2r_2 r_3 \cos\omega\tau}{1 - 2r_2 r_3 \cos\omega\tau + r_2^2 r_3^2} \right]^{\frac{1}{2}}. \tag{2.5}$$

By squaring this quantity we get the power reflectivity. A complete discussion of the figures with varying parameters is included later in the chapter.

It is often the convention to include only one feedback term for low external reflectivity [15]. This is easily derived from Eq. (2.2) by simply truncating the expression after the first term

$$r_{\text{eff}} = r_2 \left[1 - \frac{t_2^2 r_3}{r_2} e^{-i\omega\tau} \right], \tag{2.6}$$

which reduces to

$$|r_{\text{eff}}|_{\text{conv:1}} = |r_2^2 + r_3^2 + 2(r_2^2 r_3 - r_2 r_3)\cos\omega\tau - 2r_2^2 r_3^2 + r_2^4 r_3^2|^{\frac{1}{2}}, \tag{2.7}$$

the amplitude reflectivity. Again the power reflectivity can be obtained just by squaring this term.

Effective Reflectivity for the Ideal Phase-Conjugate Mirror

The Ideal phase-conjugate mirror has a slightly different behavior. By definition the Ideal PCM reflects the phase conjugate of the light that is incident. To be complete, I allow the reflected light to accrue phase in the nonlinear medium [63]. In the conventional case, the path length in the external cavity impacted the phase of the returned light. This is not true for the Ideal PCM. Its phase is determined by the cavity boundary conditions (see Chapter 3) not its physical location. It does not reverse time as much as it undoes effects of the time delay. There is no time dependent phase because be the incident wave is reconstructed at every point by the reflected wave. Of course, this is only true if the delay time is less than the coherence time of the laser. The external cavity modes of the PCM will depend on the four-wave mixing phase-matching conditions and gain of the nonlinear media, not the resonator length. This has been established for phase-conjugate oscillators [20-25].

In the same manner as before consider the fields E_i and E_r in the coupled cavity (Fig. 2.2b). If E_r is expressed as a function of E_i then

$$E_r e^{i\omega t} = e^{i\omega t}\left[E_i r_2 + E_i t_2^2 r_3 e^{i\Phi_{pc}} - E_i t_2^2 r_2 r_3^2 + \ldots - \ldots\right], \qquad (2.8)$$

Φ_0 is the initial phase of the beam at the laser. Φ_{pc} is any accrued phase due to the nonlinear interaction. This term is included to keep the expressions entirely general. Note that there is no $\omega\tau$ term. For this analysis the cavity length must be shorter than the coherence length of the laser. r_3 is positive in this case because there is no phase shift upon reflection. The laser does not know where

the mirror is in space [64-66]. Take the phase out of the amplitude expression explicitly and solve for r_{eff}

$$A_r e^{i\phi_0} = r_2 \left[A_i e^{i\phi_0} + A_i^* e^{-i\phi_0} e^{i\Phi_{\text{pc}}} \frac{t_2^2 r_3}{r_2} - \ldots + \ldots \right], \tag{2.9}$$

$$r_{\text{eff}} = \frac{A_r}{A_i} = r_2 \left[1 + \frac{t_2^2 r_3}{r_2} \left(\sum_0^\infty (r_2 r_3)^{2m} e^{i(\Phi_{\text{pc}} - 2\phi_0)} - \sum_0^\infty (r_2 r_3)^{2m+1} \right) \right], \tag{2.10}$$

$$r_{\text{eff}} = r_2 \left[1 + \frac{t_2^2 r_3}{r_2} \left(\frac{e^{i(\Phi_{\text{pc}} - 2\phi_0)} - (r_2 r_3)}{1 - r_2^2 r_3^2} \right) \right], \tag{2.11}$$

$$|r_{\text{eff}}|_{\text{pc:}N} = \left| \frac{r_2^2(1 - r_3^2)^2 + r_3^2(1 - r_2^2)}{(1 - r_2^2 r_3^2)^2} + \frac{2 r_2 r_3 (1 - r_2^2)(1 - r_3^2) \cos(\Phi_{\text{pc}} - 2\phi_0)}{(1 - r_2^2 r_3^2)^2} \right|^{1/2}. \tag{2.12}$$

To get an expression for the single round trip simply truncate Eq. (2.9) after one reflection term to find

$$r_{\text{eff}} = \frac{A_r}{A_i} = r_2 \left[1 + \frac{t_2' r_3}{r_2} e^{i(\Phi_{\text{pc}} - 2\phi_0)} \right], \tag{2.13}$$

$$|r_{\text{eff}}|_{\text{pc:1}} = \left| r_2^2 + r_3^2 + r_2^4 r_3^2 - 2 r_2^2 r_3^2 + 2 r_2 r_3 (1 - r_2^2) \cos(\Phi_{\text{pc}} - 2\phi_0) \right|^{1/2}. \tag{2.14}$$

The phase terms were included in the phase conjugate case to keep it general in nature and to compare with the literature. In fact, those phase terms must disappear due to boundary conditions. The phase is required to be

$$\Phi_{\text{pc}} - 2\Phi_0 = 2n\pi. \tag{2.15}$$

This happens because the PCM chooses where it wants to phase conjugate. There is no node or anti-node as in a conventional mirror [64-66]. Thus the point of reference, for lack of a better term, can be anywhere within the interaction region

of the medium and the PCM will pick the point which satisfies the boundary conditions. For purposes of analysis choosing the external phase equal to zero will suffice.

In general, the epoch angle of the phase Φ_0 will be zero since there is a longitudinal node at each laser facet. But temporal instabilities could change that condition. For the semiconductor laser, which is a nonlinear and photorefractive medium, this is quite possible. The ideal phase conjugator does not just add a phase of $2n\pi$ to the wave, it adjusts so that the accrued cavity phase is zero. Naturally, the conventional cavity is under no such restraint.

Effective Reflectivity for the Unidirectional Ring

The Unidirectional Ring PPCM is a hybrid device, acting like a cross between a phase-conjugate mirror and a diffraction grating. (This mirror should not be confused with the unidirectional ring resonator [67].) Given its importance to this work, a short discussion on the physics of the device is warranted. A wave-mixing diagram of the mirror is shown in Fig. 2.3a. It consists of a single-crystal Barium Titanate, two conventional dielectric mirrors, a Faraday optical isolator, and a half-wave plate. The isolator keeps the device unidirectional and the half-wave plate keeps the polarization horizontal for maximum photorefractive coupling [6]. Note: the beam labels used here may differ from common usage, though there is no accepted standard. Light from the laser enters as Beam 1. It passes directly through the crystal, is turned by M1 and M2, and then is redirected to cross with itself in the crystal. This is now Beam 3. Beam 2 is formed by the asymmetric photorefractive scattering of Beam 1 in the $BaTiO_3$ [8]. It fans out towards the optic or *c*-axis. Beam 1 can write a continuum of photorefractive gratings with this fanned light. If Beam 3 is inside the angle formed by the *c*-axis and Beam 1, it can reflect off those gratings. The

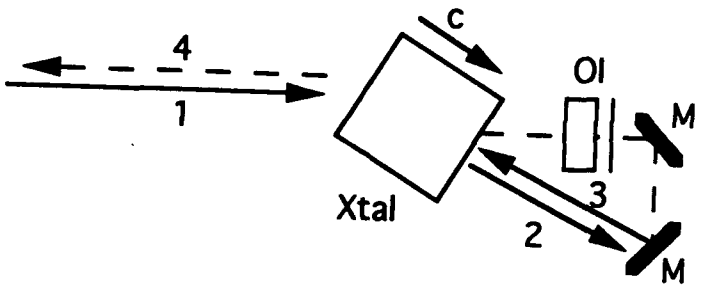

(a)

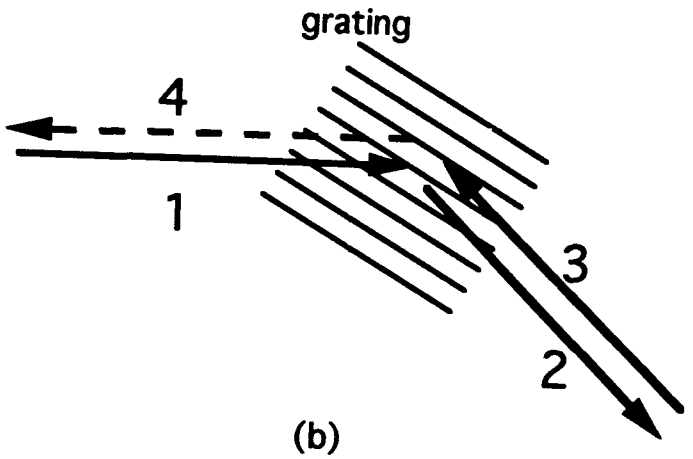

(b)

Fig. 2.3. Unidirectional ring PCM diagrams: (a) PCM and (b) photorefractive grating.

light that is reflected in the direction of the laser, counter propagating to Beam 1, will satisfy the phase matching conditions for four-wave mixing and will be enhanced via constructive interference. The other gratings will be washed out due to destructive interference. This all takes place during the "rise time" of the URECL. Once the fanning has ceased it is in the steady state [6]. The grating schematic is shown in Fig. 2.3b.

This is how a DPCM is formed as well, except that the beams to be mixed can come from two different sources (or a single source split before entering the crystal) that enter opposite faces of the crystal [57]. Without the isolator the process would proceed somewhat differently, the ring would be bidirectional, and there would be grating competition between multiple gratings [60,68]. The unidirectional ring, as well as the DPCM, has only a single grating in the steady state [61].

Let ϕ_0 be the initial phase of Beam 1 and Φ_R be the phase accrued in the crystal. The four-wave mixing phase matching condition can be written

$$\vec{k}_1 + \vec{k}_4 = \vec{k}_2 + \vec{k}_3, \tag{2.16}$$

where k_i is the k-vector of the ith beam. Phase conjugation demands that

$$e^{iP_1} e^{iP_4} = e^{iP_2} e^{iP_3}, \tag{2.17}$$

where P_i is the total phase of the ith wave. If d is the distance from the laser to the crystal, and D is the distance around the ring, then

$$P_1 = \phi_0 + |k \cdot d| + \vec{k}_1 \cdot \vec{r}, \tag{2.18a}$$

$$P_2 = \phi_0 + |k \cdot d| + \vec{k}_2 \cdot \vec{r}, \tag{2.18b}$$

$$P_3 = \phi_0 + |k \cdot d| + |kD| - \vec{k}_i \cdot \vec{r}, \tag{2.18c}$$

$$P_4 = P_2 + P_3 - P_1, \tag{2.19}$$

$$P_4 = \phi_0 + |kd| + |kD| - \vec{k}_1 \cdot \vec{r} + \phi_R, \tag{2.20}$$

where $\vec{r}$ is the position vector measured from some arbitrary point. It is clear that phase delay information has been retained and that phase conjugation, in the standard sense, has not taken place. The accrued phase is unspecified and must be determined by the boundary conditions. If the beam travels back to the laser it is easy to see that it will pick up another $|\vec{k} \cdot \vec{d}|$ in phase. The round trip time τ now corresponds to the total length from the laser to crystal through ring and back to the laser. It acts as an external ring cavity.

The ϕ_0 will drop out of the equations since it isn't conjugated. ϕ_R will keep adding to each team.

A comparison with Kerr media, or $X^{(3)}$, four-wave mixing might be helpful. As shown in Fig. 2.4 there are two counter-propagating pumps, Beams 1 and 2. If they are degenerate, as is typical, their phases cancel and the phase conjugate of Beam 3 is returned as Beam 4. No phase information of the pump beams is retained [69]. In contrast, the UR keeps the phase of its single pump.

With this understanding the effective reflectivity of the URECL can be derived in the same fashion as for the other mirrors. Figure 2.2c shows a conceptualization of this external cavity. Writing E_r as a function of E_i

$$E_r e^{i\omega t} = E_i e^{i\omega t} \left[r_2 + t_2^2 r_3 e^{i(\omega\tau - \phi_R)} - t_2^2 r_2 r_3^2 e^{2i(\omega\tau - \phi_R)} + \ldots \right]. \tag{2.21}$$

Note that r_3 is a positive quantity. Reflection off the Bragg angle of a grating yields zero phase shift. By again taking the ratio of E_r and E_i the following is obtained

$$\frac{E_r}{E_i} = r_{\text{eff}} = r_2 \left[1 + \frac{t_2^2 r_3}{r_2} e^{-i(\omega\tau - \phi_R)} - \frac{t_2^2 r_2 r_3^2}{r_2} e^{-2i(\omega\tau - \phi_R)} + \ldots - \ldots \right]. \tag{2.22}$$

This reduces to

$$r_{\text{eff}} = \frac{r_2 + r_3 e^{-i(\omega\tau - \phi_R)}}{1 + r_2 r_3 e^{-i(\omega\tau - \phi_R)}}, \tag{2.23}$$

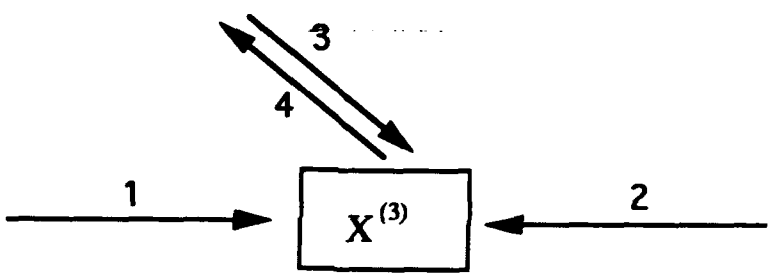

Fig. 2.4. Four wave mixing in Kerr type media.

and finally,

$$|r_{eff}|_{ring:N} = \left| \frac{r_2^2 + r_3^2 + 2r_2 r_3 \cos(\omega\tau - \phi_R)}{1 + 2r_2 r_3 \cos(\omega\tau - \phi_R) + r_2^2 r_3^2} \right|^{1/2}. \tag{2.24}$$

The single round trip can be easily calculated. Simply truncate Eq. (2.20) to yield

$$r_{eff} = \frac{E_r}{E_i} = r_2 \left[1 + \frac{t_2^2 r_3}{r_2} e^{-i(\omega\tau - \phi_R)} \right], \tag{2.25}$$

and then

$$|r_{eff}|_{ring:1} = \Big| r_2^2 + r_3^2 - 2r_2^2 r_3^2 \mp r_2^4 r_3^2 + 2r_2 r_3 (1 - r_2^2) \cos(\omega\tau - \phi_R) \Big|^{1/2}. \tag{2.26}$$

The boundary conditions for four wave mixing demand that the reflected wave reconstruct itself after one round trip, just as in the Ideal PCM. As mentioned, the reflection off a diffraction grating at the Bragg angle yields zero phase shift. But the crystal will set the phase delay to be such that

$$\omega\tau - \Phi_R = 2n\pi, \tag{2.27}$$

to satisfy the boundary conditions. The grating will write, inside the crystal, at the physical location where this will happen. Any other gratings will suffer from destructive interference. The beam still retains its original phase information so the laser will be able to pump external cavity modes, i.e., the laser knows the spatial location of the mirror. The modes are ring cavity modes; they lase at

$$\Delta\nu = c/L. \tag{2.28}$$

Since the response time of Barium Titanate is slow at 830 nm, the gratings can exist in the crystal after a change in lasing or even after it is no longer being pumped; they form a hologram [2]. (They'll easily last overnight.) For

the experimental conditions, the medium took about two minutes to begin to respond to a new frequency or power level. During the intermediate time the gratings behaved like a static hologram (as opposed to the dynamic holography of phase conjugation). So although the device will set the feedback phase as a phase conjugator, it can act as a conventional ring cavity as well. If a grating is written with a moderately high power pump beam (several millwatts), and the power is reduced to less than one percent of that, the gratings can last for many minutes, essentially providing feedback that is conventional or phase conjugate depending on whether the phase matching conditions are still met. This will be addressed in later chapters.

This quality makes the self-pumped photorefractive mirrors unique; the DPCM is similar. This may lend itself usefully in the coupling of lasers, particular with respect to the problem of "overcoupling" [45].

Comparison

Figures 2.5 through 2.14 plot the effective power reflectivities of all three geometries. The first set of figures, 2.5 through 2.9 plot the values of R_{eff} versus R_{ext} where R_{eff} is the effective reflectivity and R_{ext} is the power reflectivity of the external reflector. The feedback phase is set to zero for this set. For each set of five plots, the first three compare the single round trip (1RT) case with the multiple round trip (NRT) case. The next two compare the the different geometries versus one another, NRT and 1RT respectively.

One interesting feature for all of the curves is that the single round trip has a different functional form than for the multiple round trip. This is not generally considered in the study of feedback into semiconductor lasers. So while for low values of the curve the numbers match correspond, the functions are not behaving the same way. This could impact dynamical studies of the system, as well as other complex analysis.

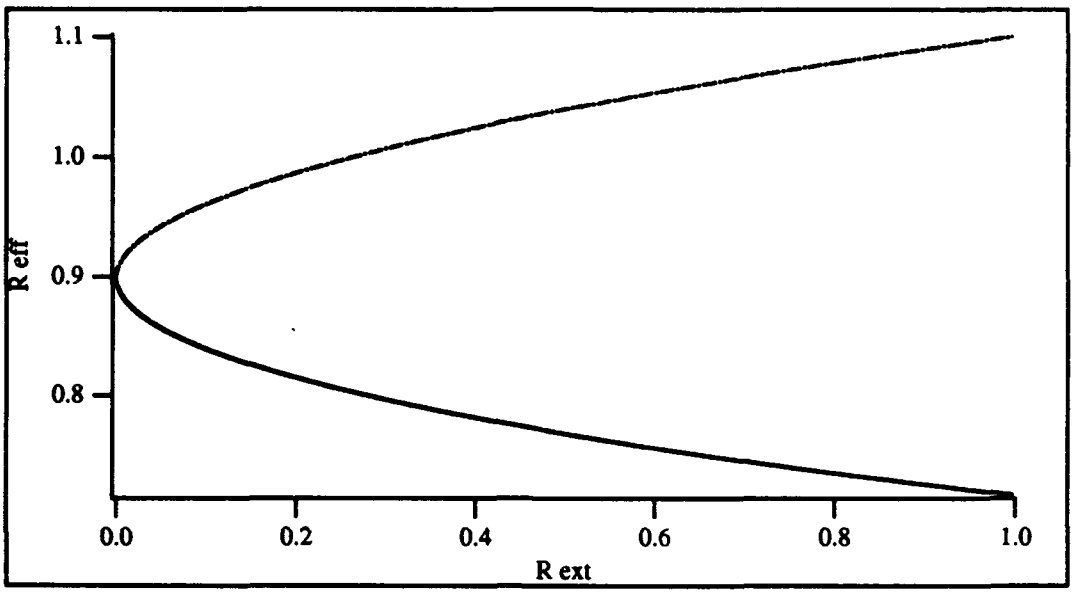

(a)

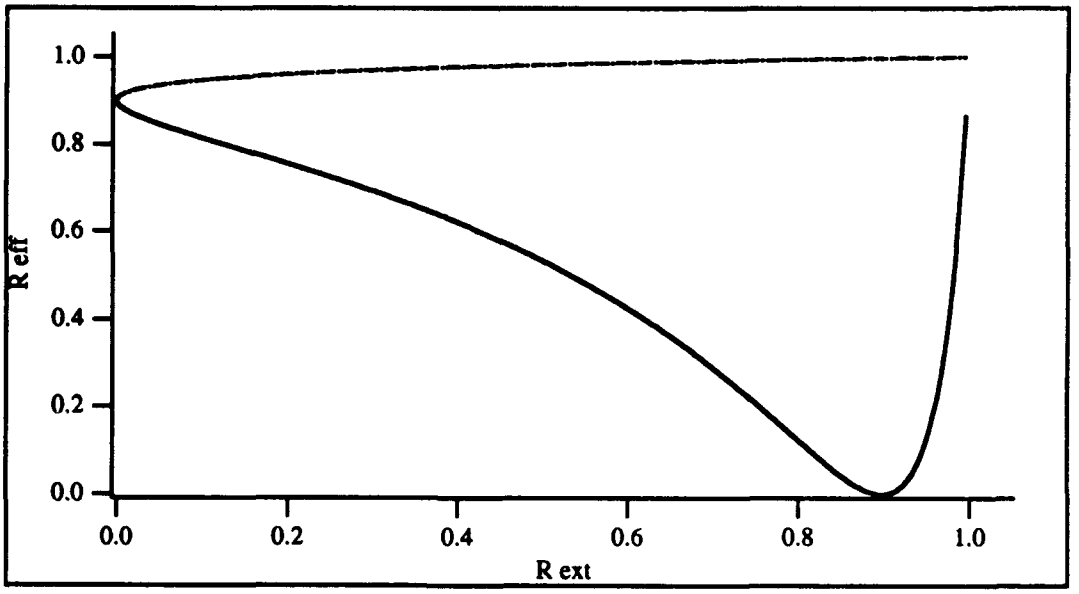

(b)

Fig. 2.5. Effective versus external reflectivity. $R_2 = 0.9$. (a) All cases 1 RT, (b) all cases NRT. Solid line – CECL, dashed line – PCECL, and dotted line – URECL.

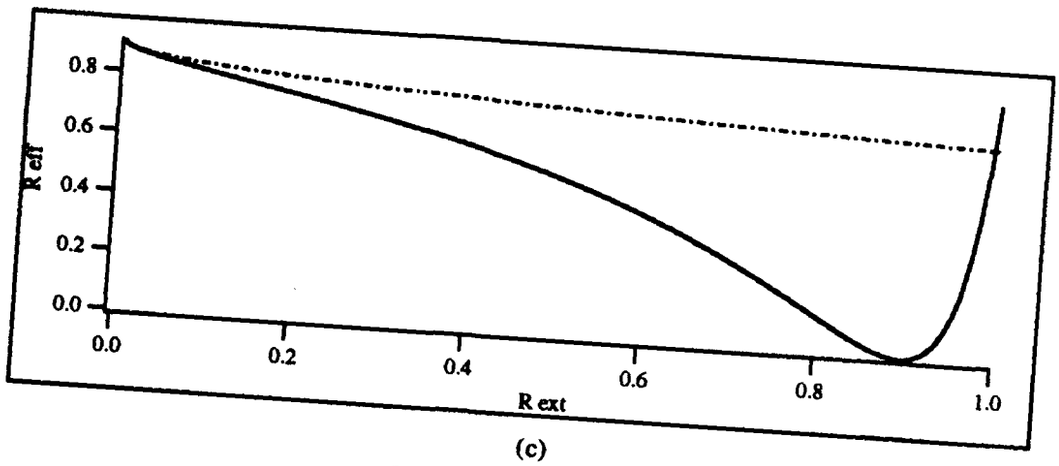

(c)

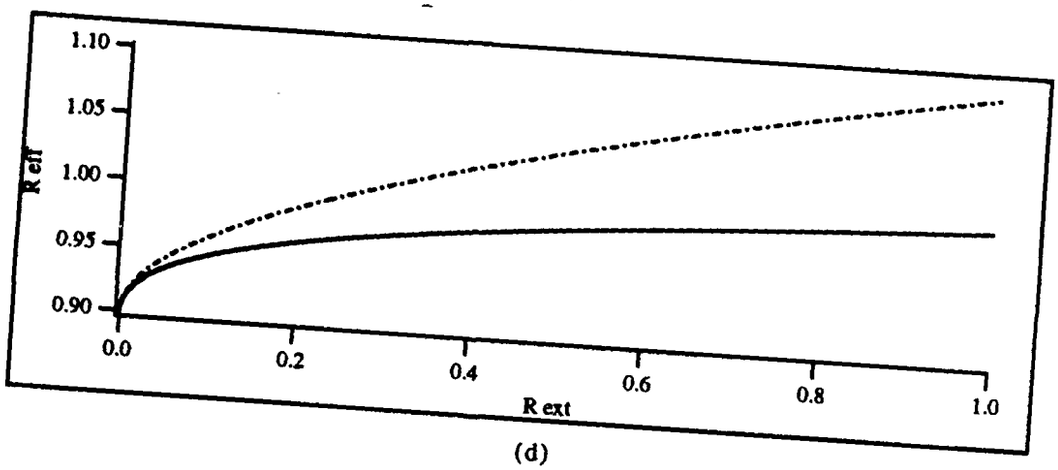

(d)

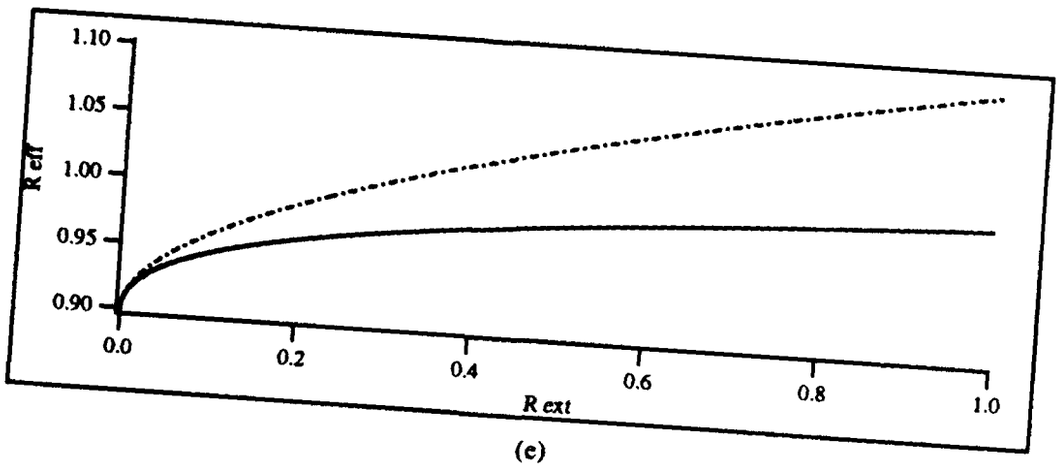

(e)

Fig. 2.5. Continued ... (c) CECL, (d) PCECL, and (e) URECL. Solid line – NRT, chain dot line – 1 RT.

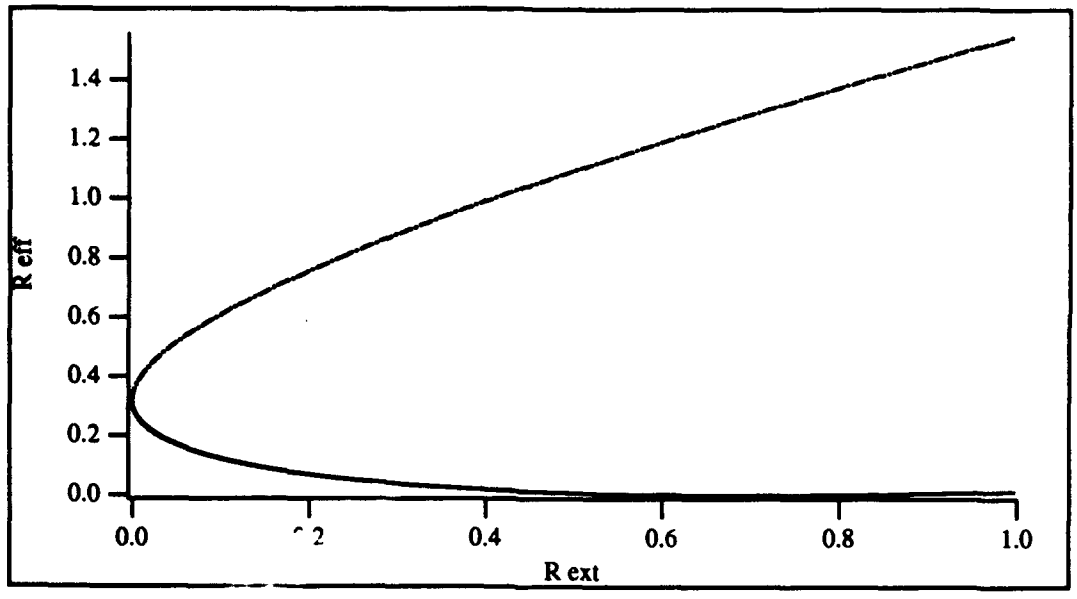

(a)

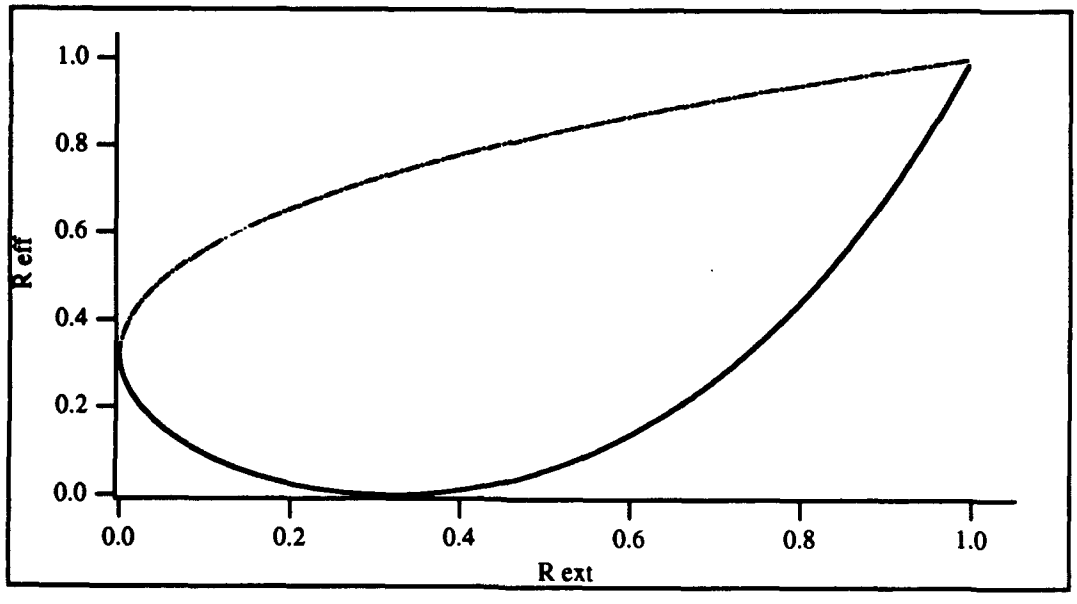

(b)

Fig. 2.6. Effective versus external reflectivity. $R_2 = 0.32$. (a) All cases 1 RT, (b) all cases NRT. Solid line – CECL, dashed line – PCECL, and dotted line – URECL.

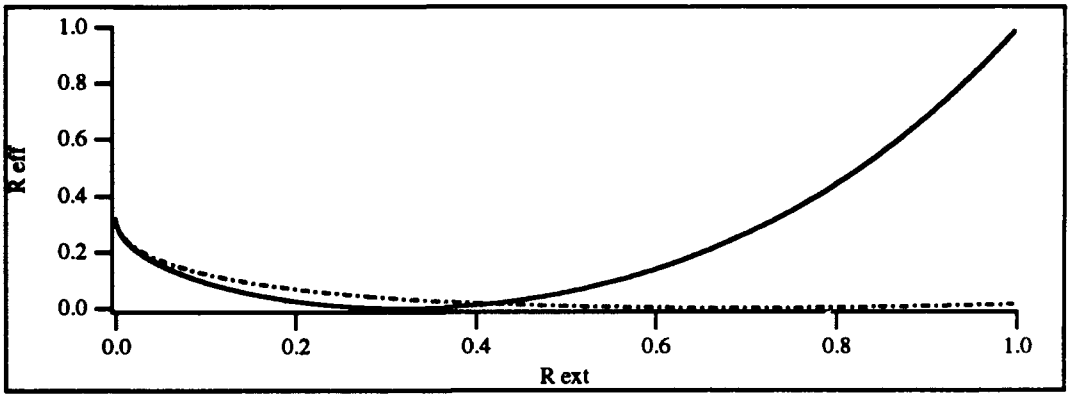

(c)

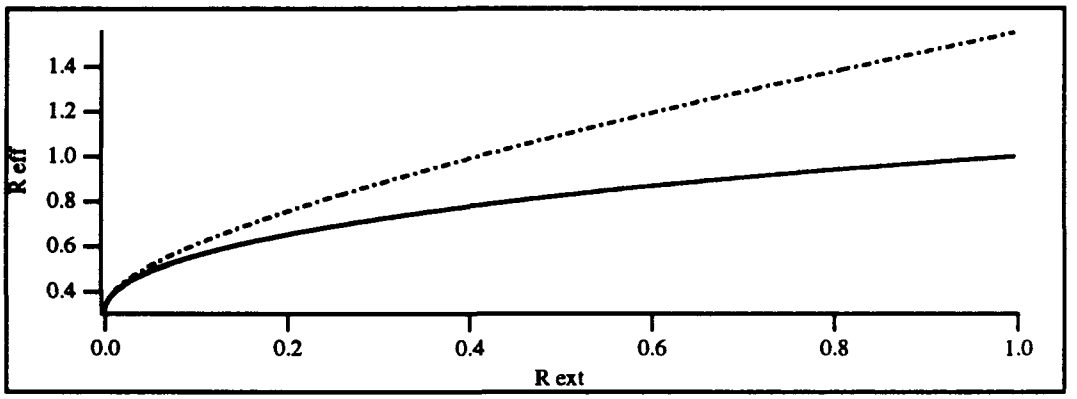

(d)

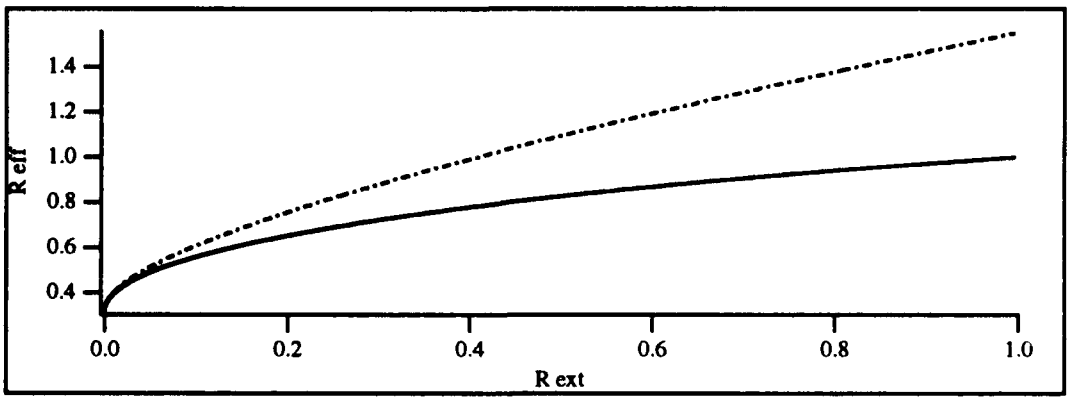

(e)

Fig. 2.6. Continued ... (c) CECL, (d) PCECL, and (e) URECL. Solid line – NRT, chain dot line – 1 RT.

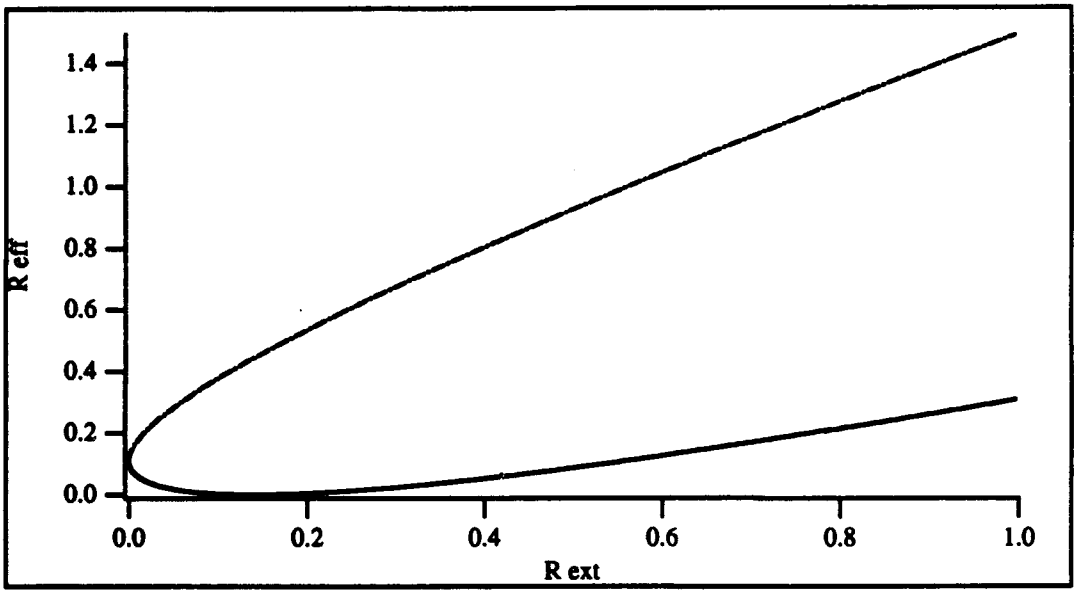

(a)

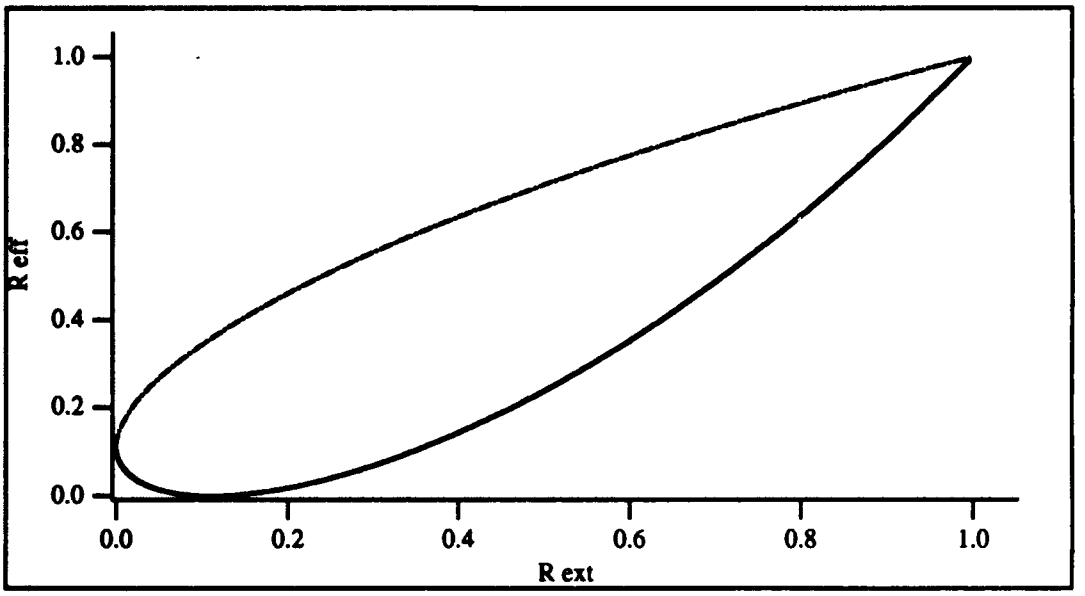

(b)

Fig. 2.7. Effective versus external reflectivity. $R_2 = 0.1$. (a) All cases 1 RT, (b) all cases NRT. Solid line – CECL, dashed line – PCECL, and dotted line – URECL.

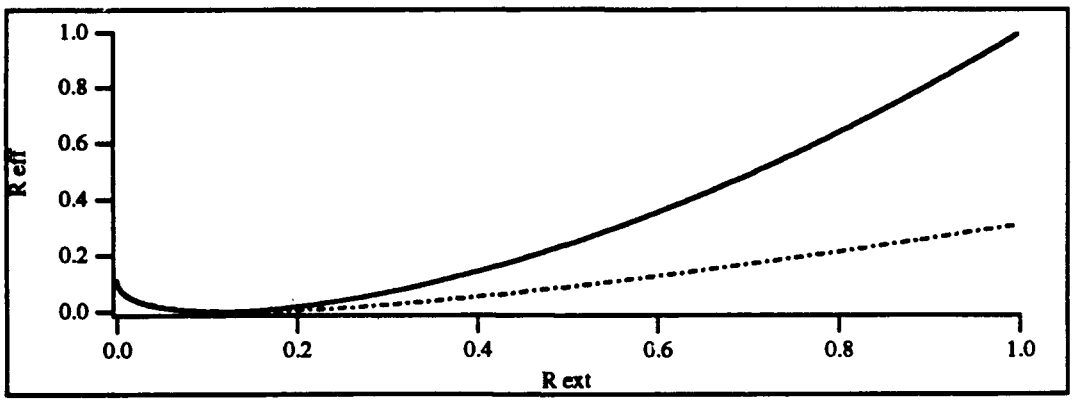

(c)

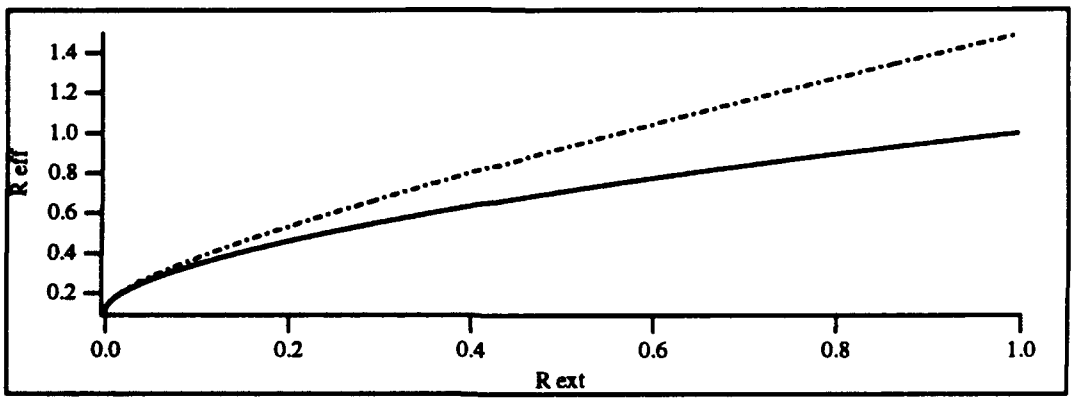

(d)

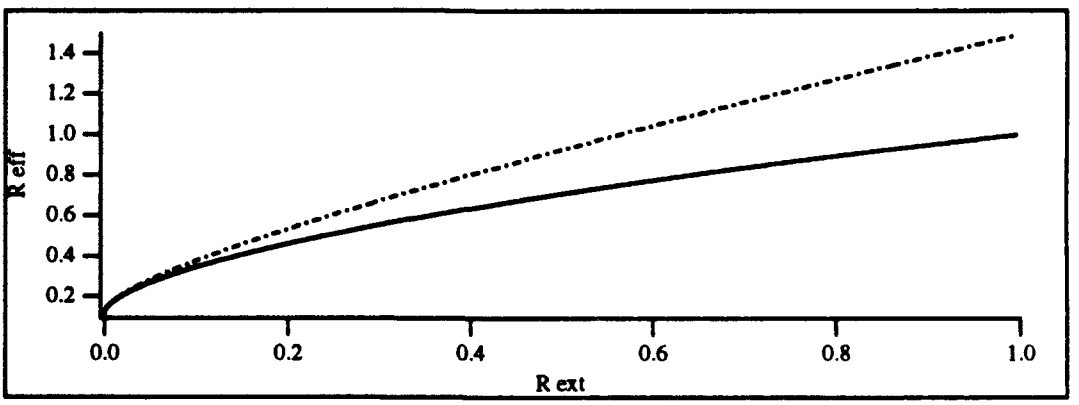

(e)

Fig. 2.7. Continued ... (c) CECL, (d) PCECL, and (e) URECL. Solid line – NRT, chain dot line – 1 RT.

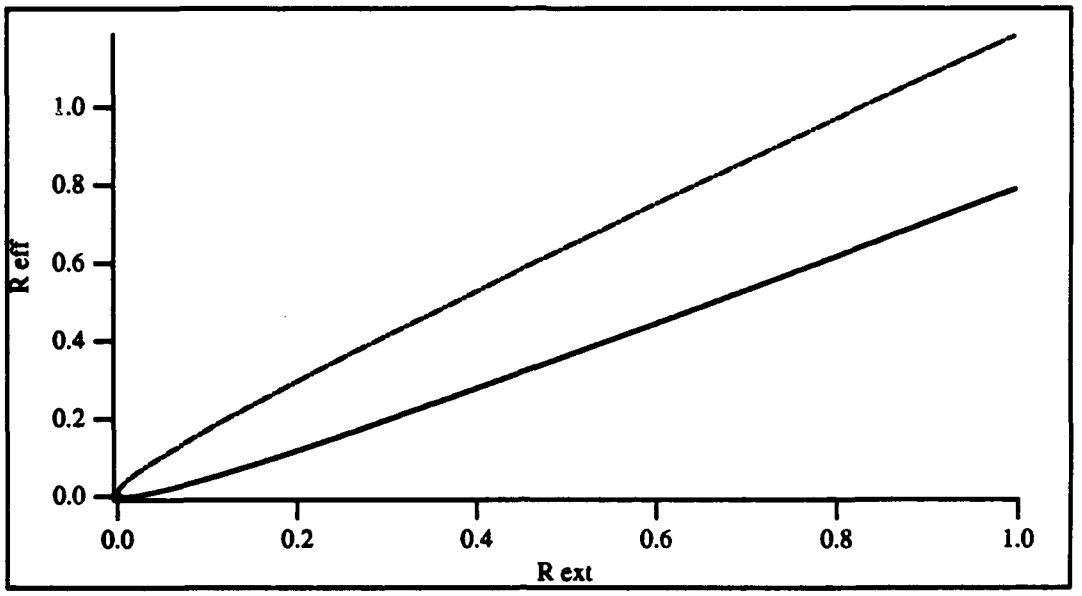

(a)

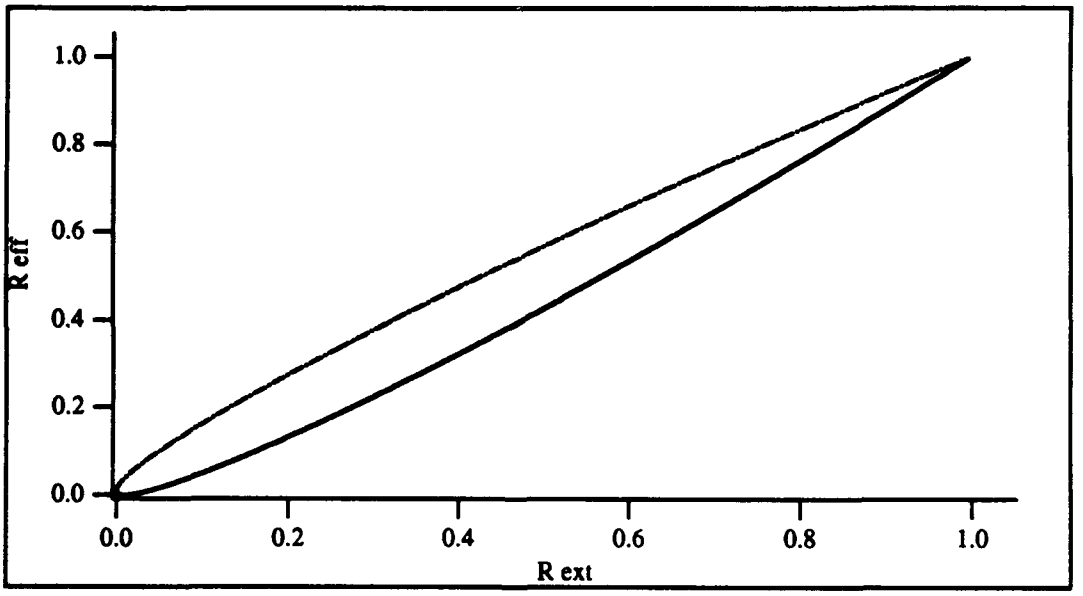

(b)

Fig. 2.8. Effective versus external reflectivity. $R_2 = 0.01$. (a) All cases 1 RT, (b) all cases NRT. Solid line – CECL, dashed line – PCECL, and dotted line – URECL.

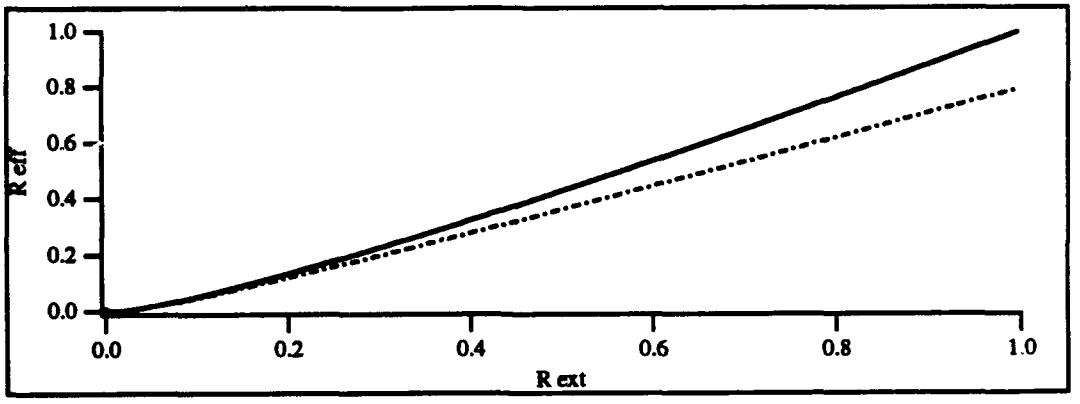

(c)

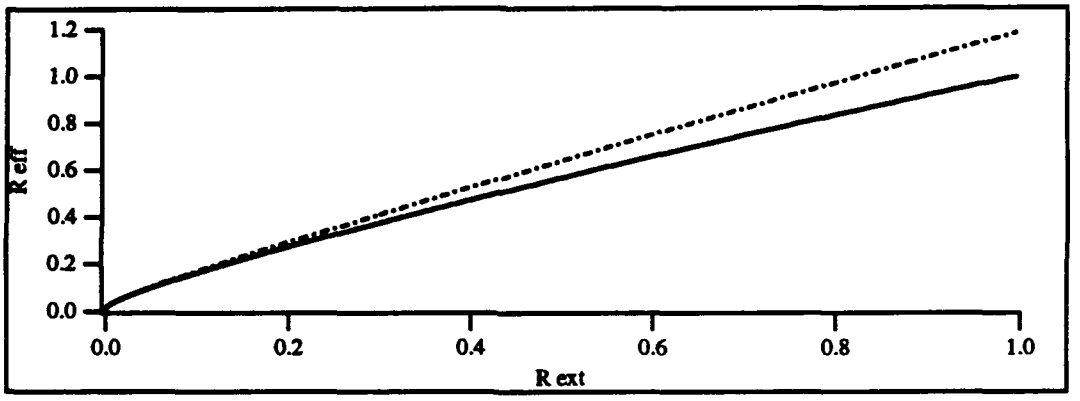

(d)

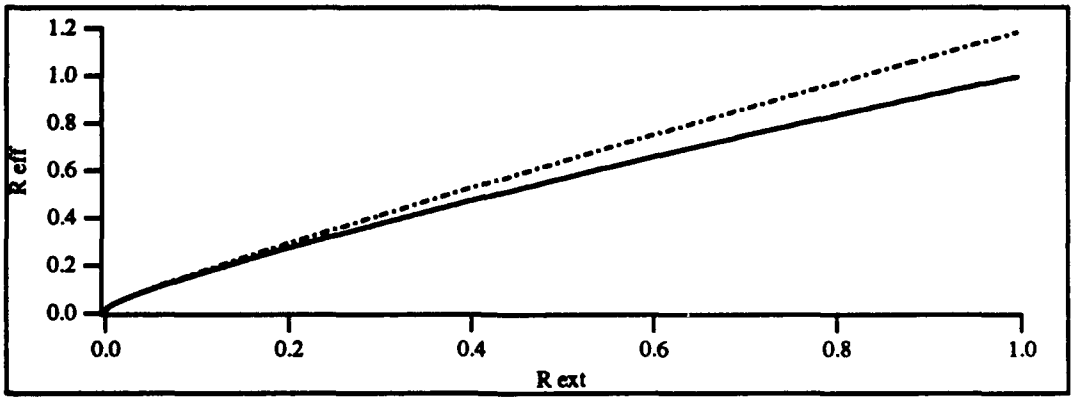

(e)

Fig. 2.8. Continued ... (c) CECL, (d) PCECL, and (e) URECL. Solid line – NRT, chain dot line – 1 RT.

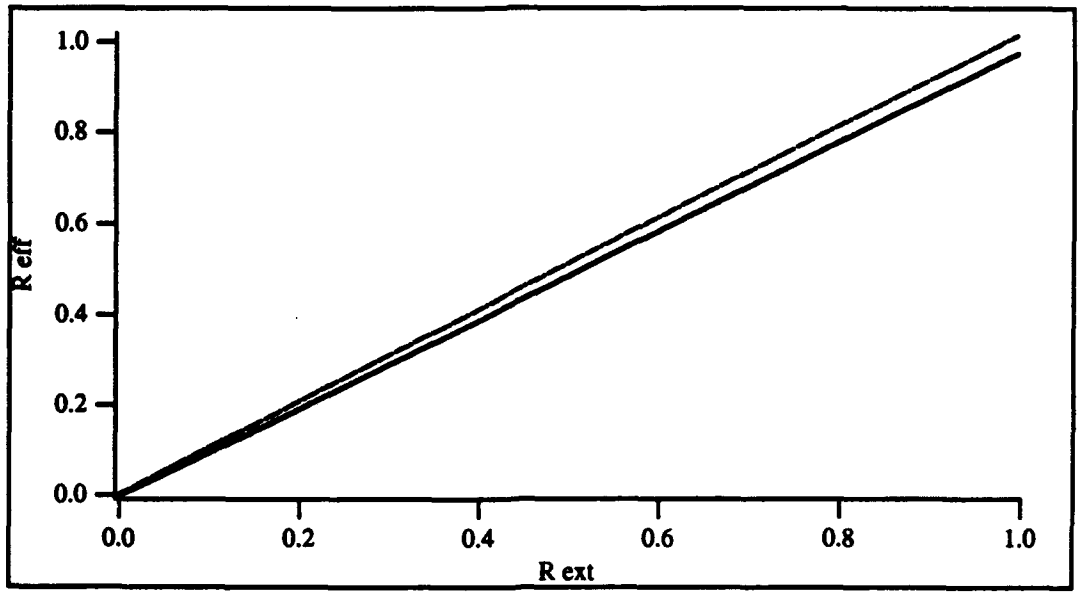

(a)

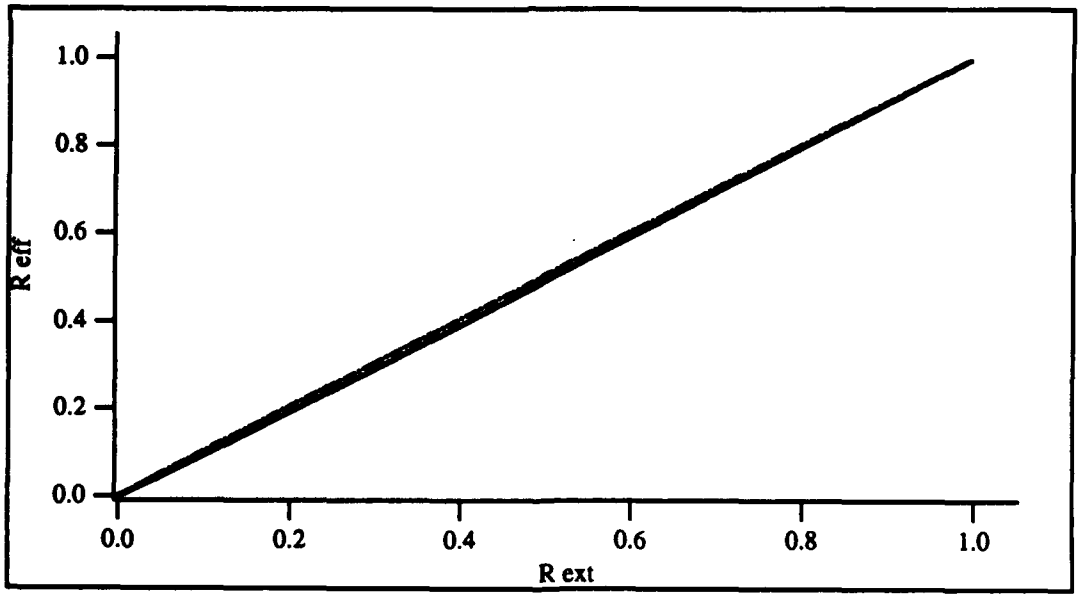

(b)

Fig. 2.9. Effective versus external reflectivity. $R_2 = 0.0001$. (a) All cases 1 RT, (b) all cases NRT. Solid line – CECL, dashed line – PCECL, and dotted line – URECL.

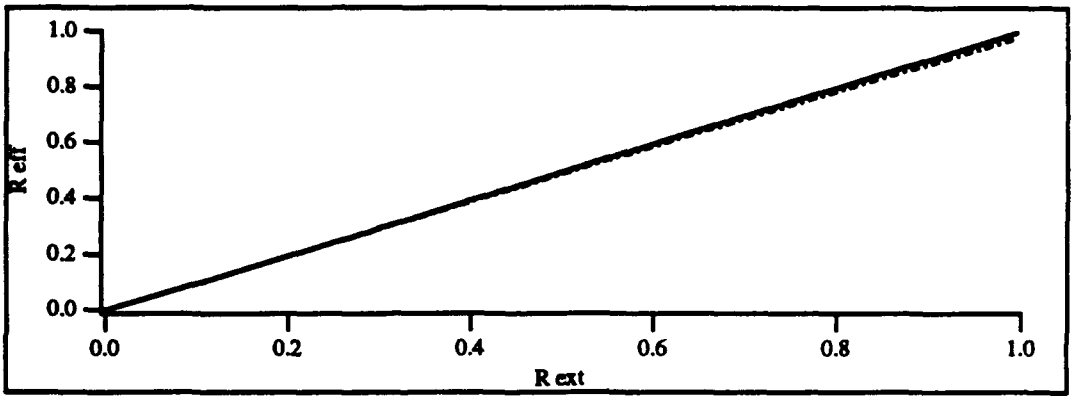

(c)

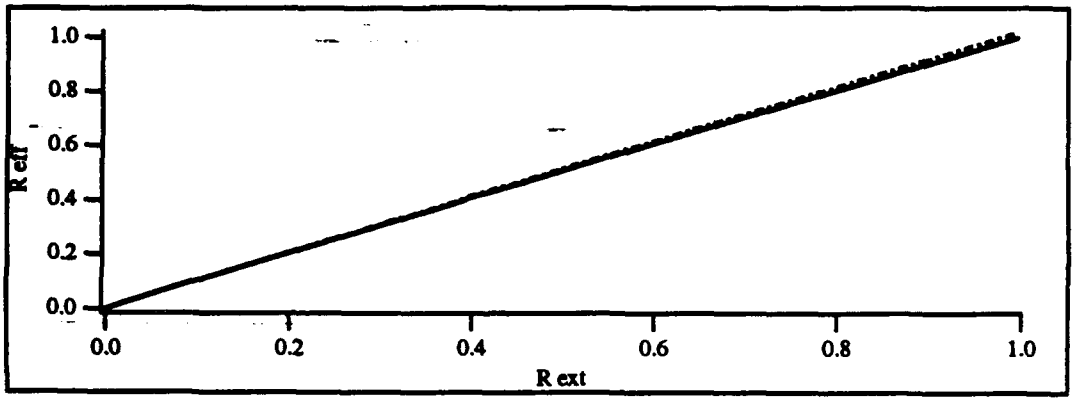

(d)

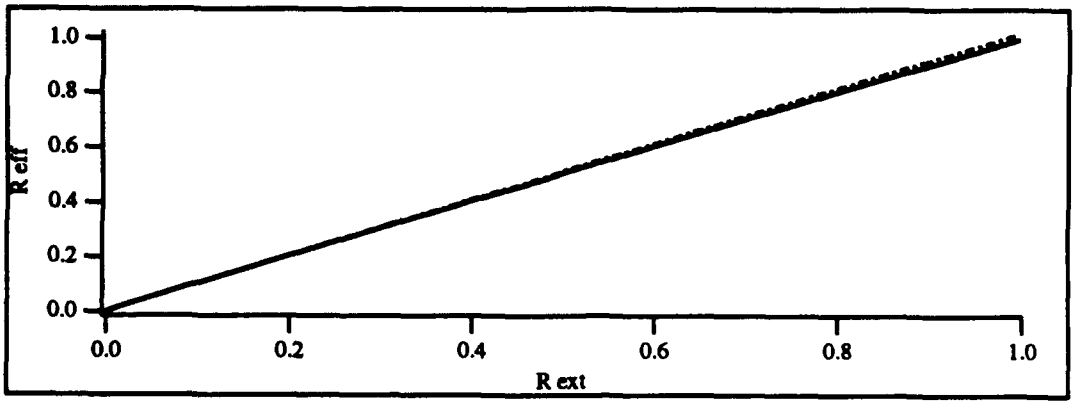

(e)

Fig. 2.9. Continued ... (c) CECL, (d) PCECL, and (e) URECL. Solid line – NRT, chain dot line – 1 RT.

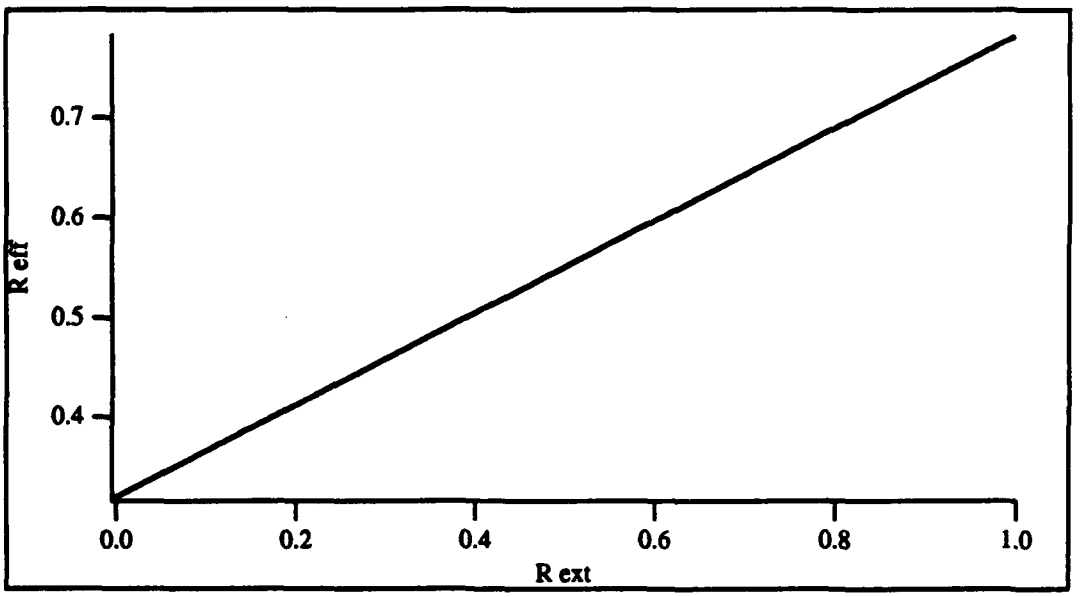

(a)

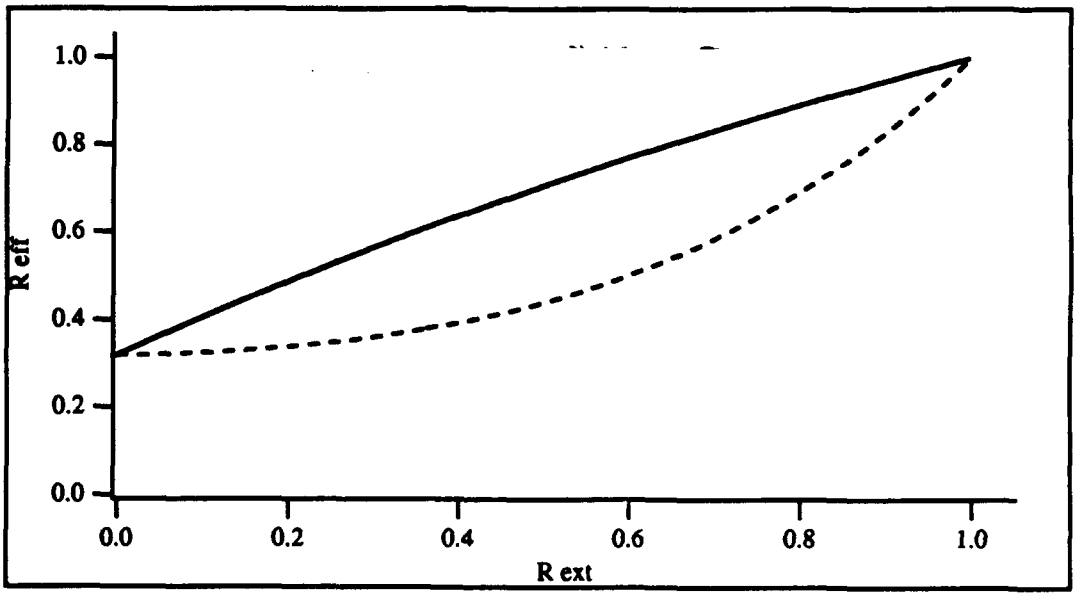

(b)

Fig. 2.10. Effective versus external reflectivity. $R_2 = 0.32$, phase $= \pi/2$. (a) All cases 1RT, (b) all cases NRT. Solid line – CECL, dashed line – PCECL, dotted line – URECL.

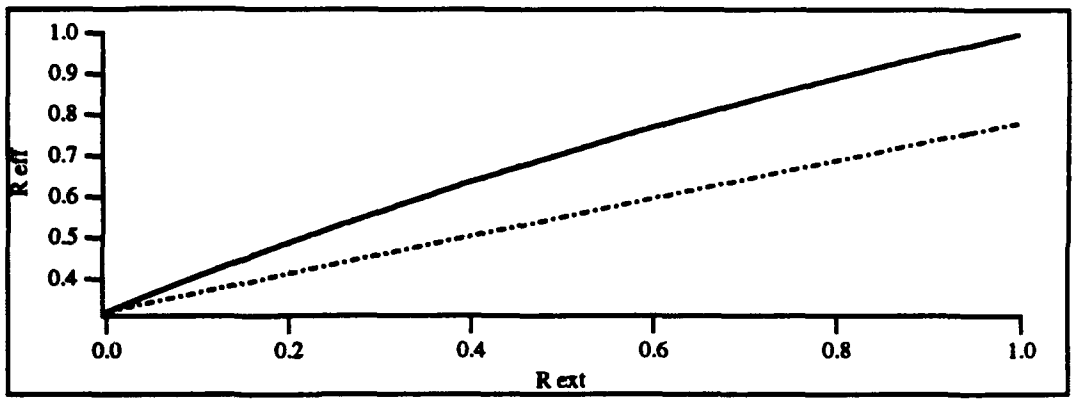

(c)

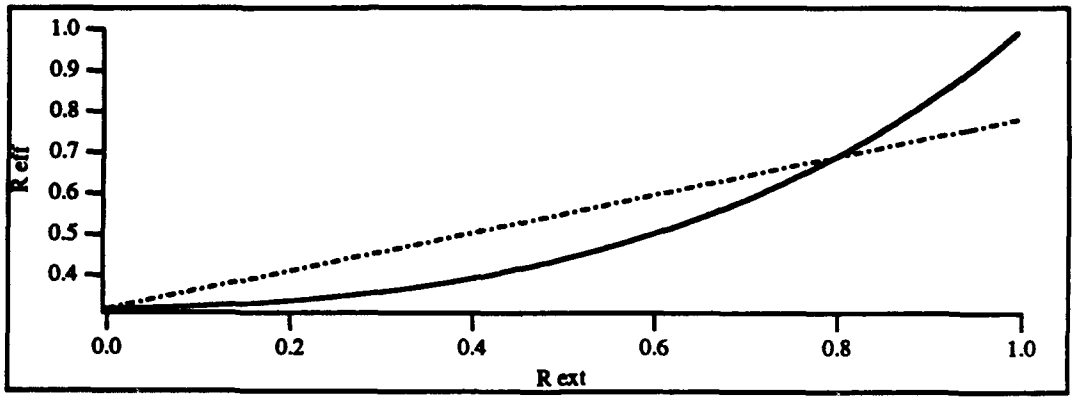

(d)

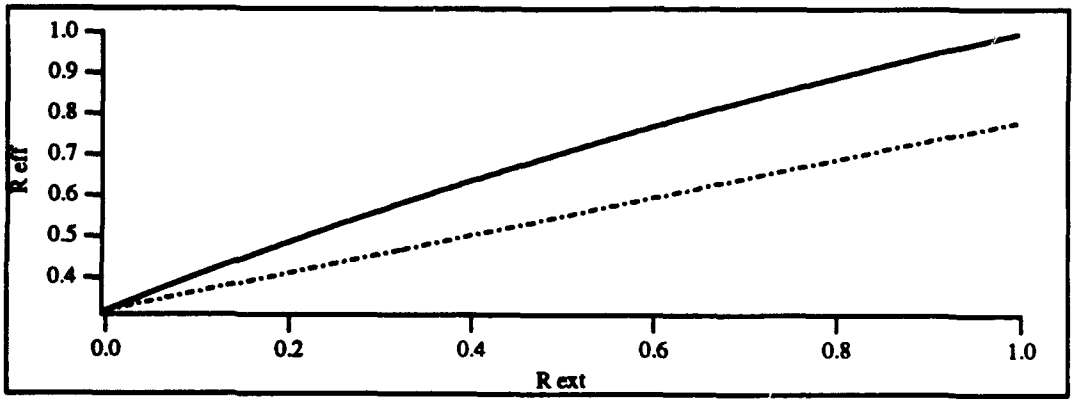

(e)

Fig. 2.10. Continued ... (c) CECL, (d) PCECL, and (e) URECL. Solid line – NRT, chain dot line – 1 RT.

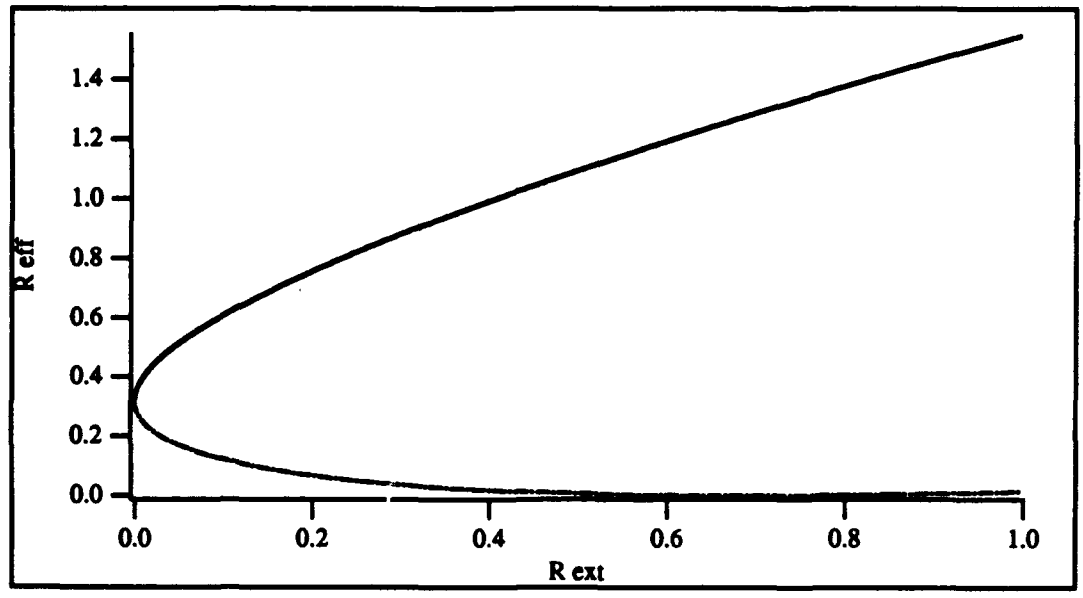

(a)

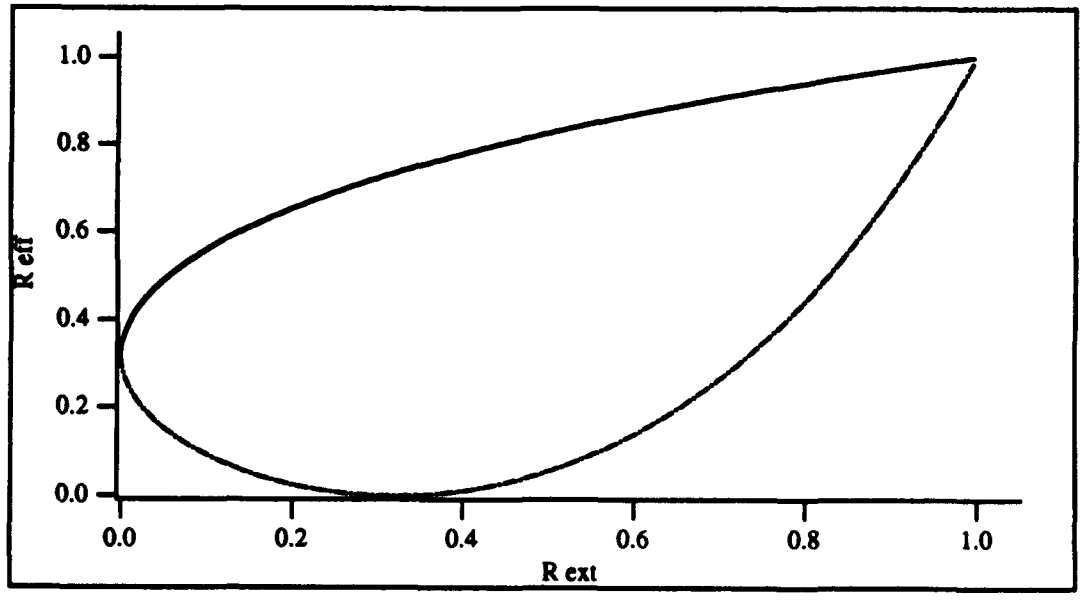

(b)

Fig. 2.11. Effective versus external reflectivity. $R_2 = 0.32$, phase $= \pi$. (a) All cases 1 RT, (b) all cases NRT. Solid line – CECL, dashed line – PCECL, and dotted line – URECL.

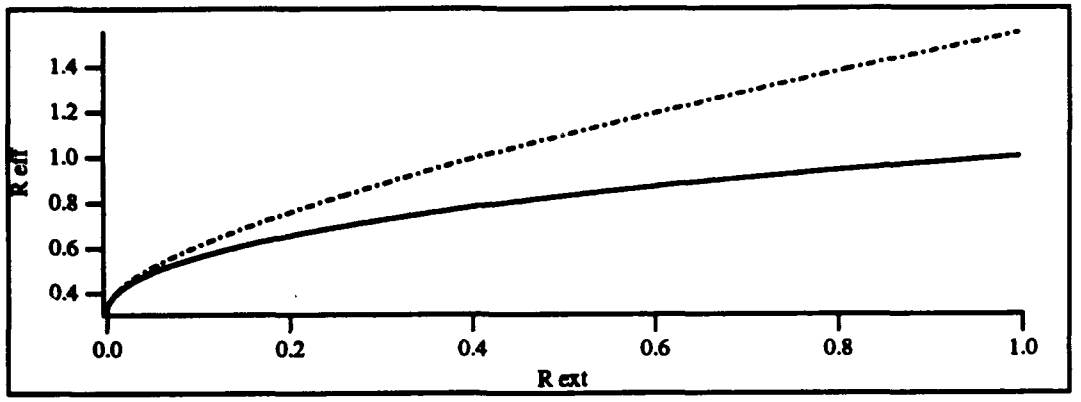

(c)

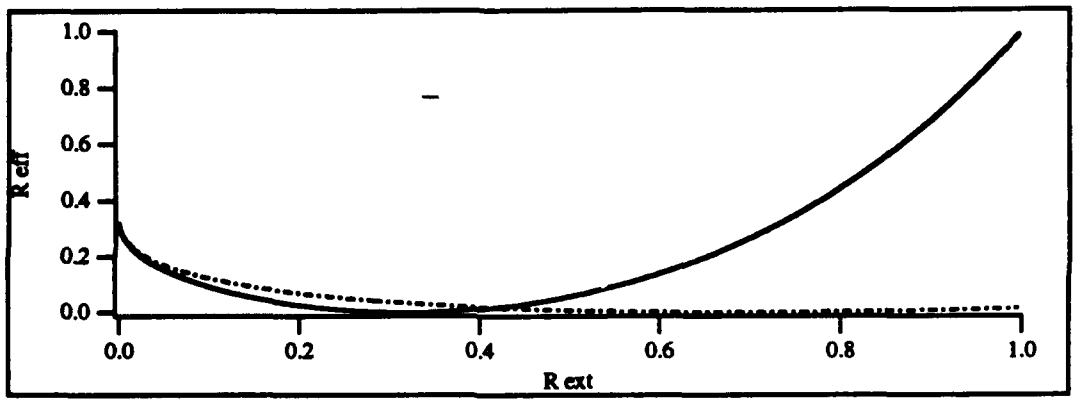

(d)

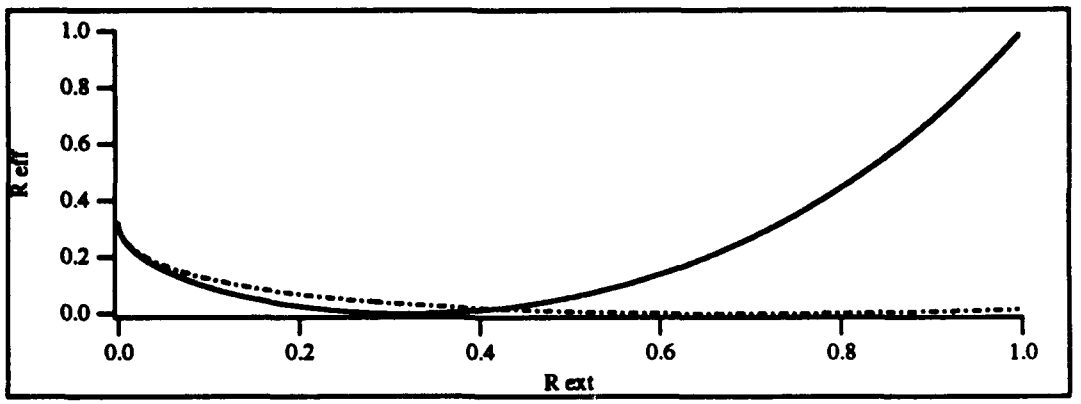

(e)

Fig. 2.11. Continued ... (c) CECL, (d) PCECL, and (e) URECL. Solid line – NRT, chain dot line – 1 RT.

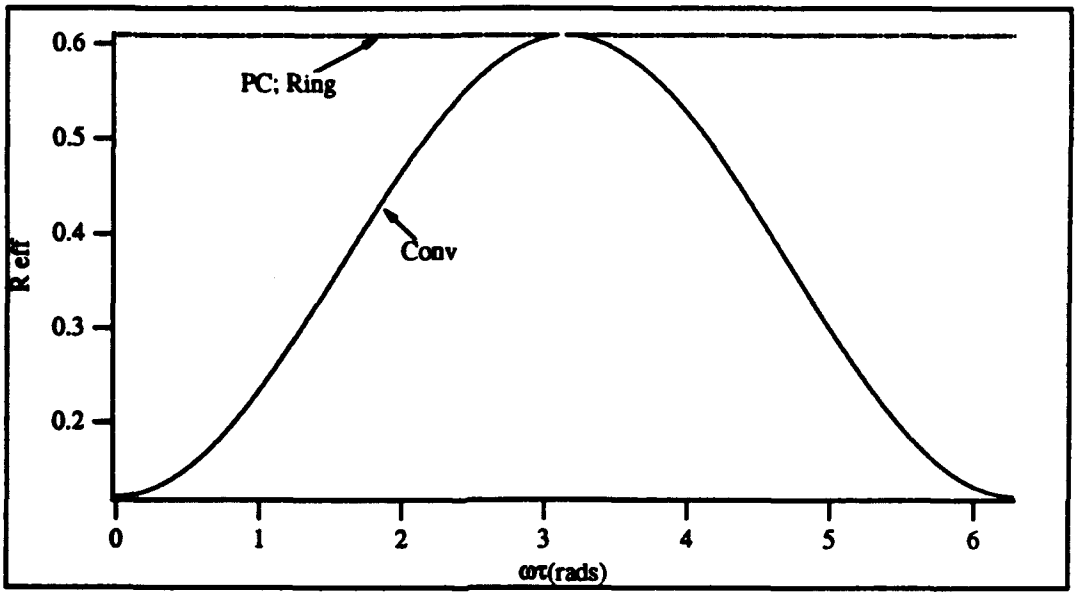

(a)

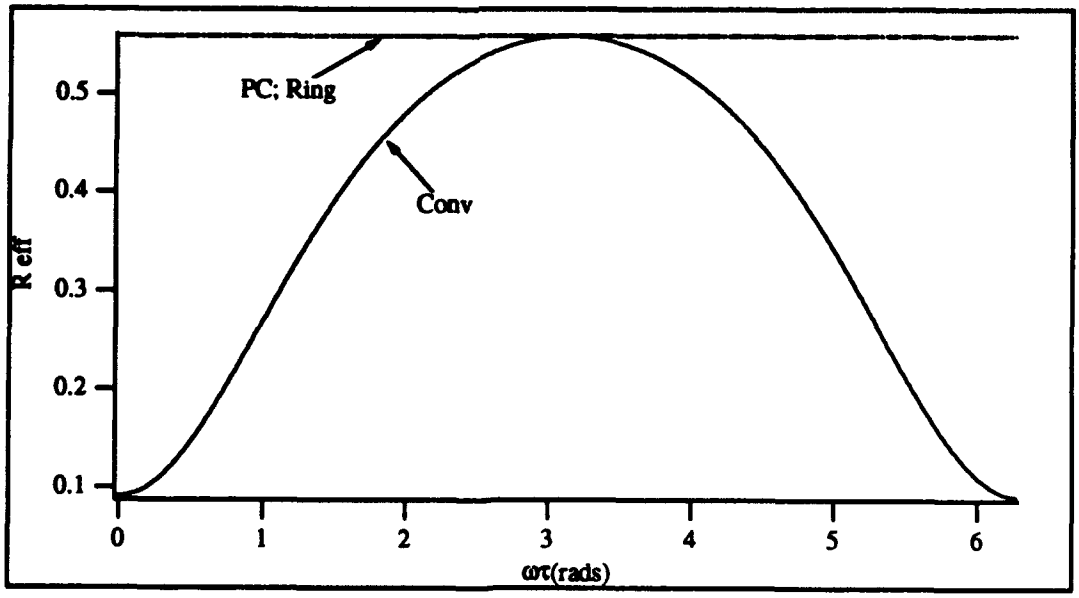

(b)

Fig. 2.12. Effective reflectivity versus $\omega\tau$. $R_2 = 0.01$. (a) 1 RT and (b) NRT.

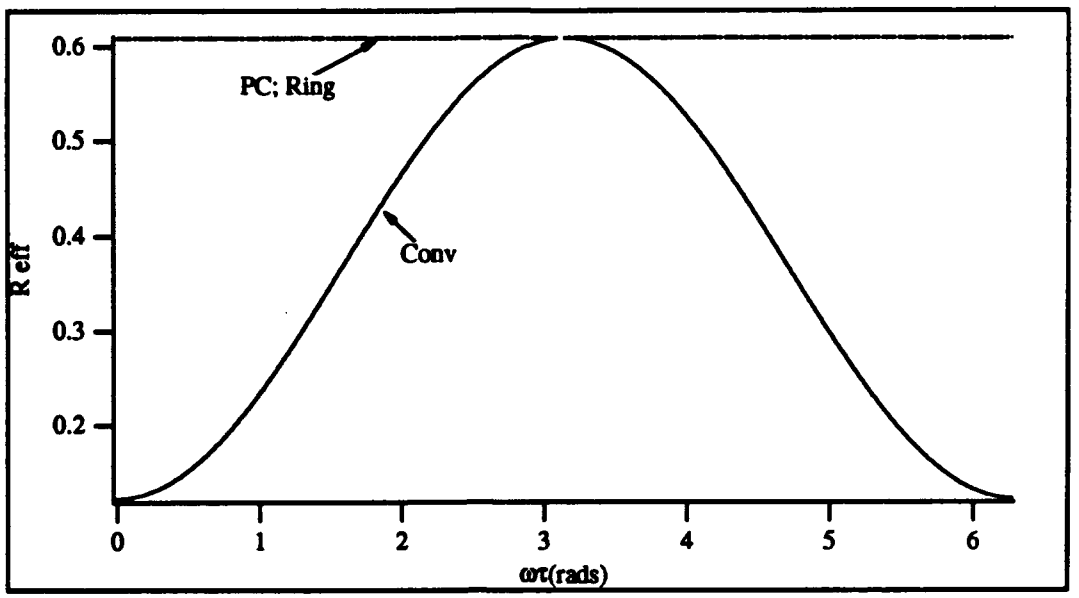

(a)

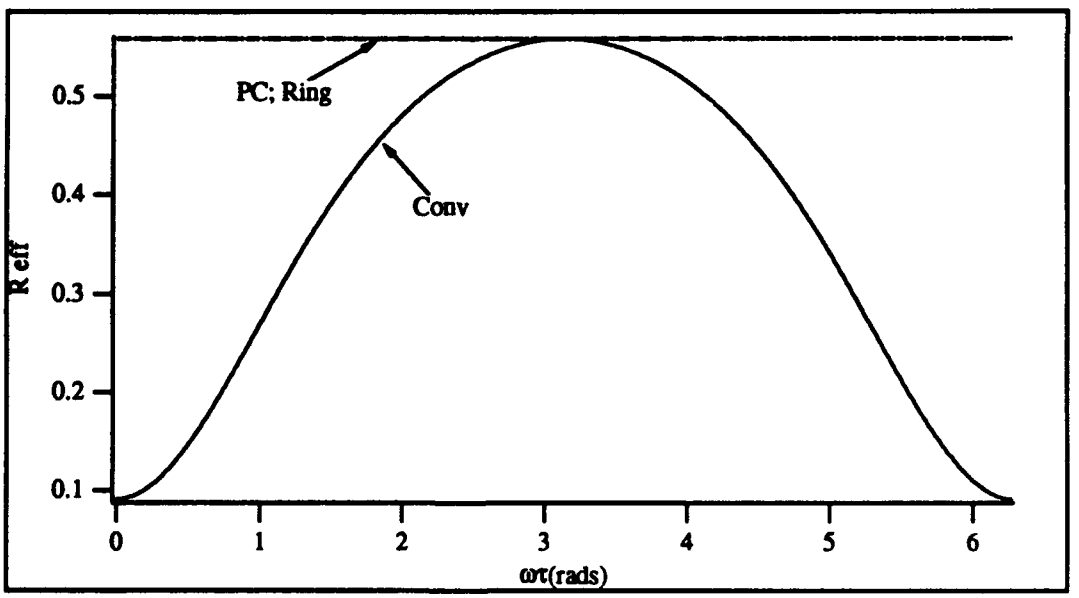

(b)

Fig. 2.13. Effective reflectivity versus $\omega\tau$. $R_2 = 0.1$. (a) 1 RT and (b) NRT.

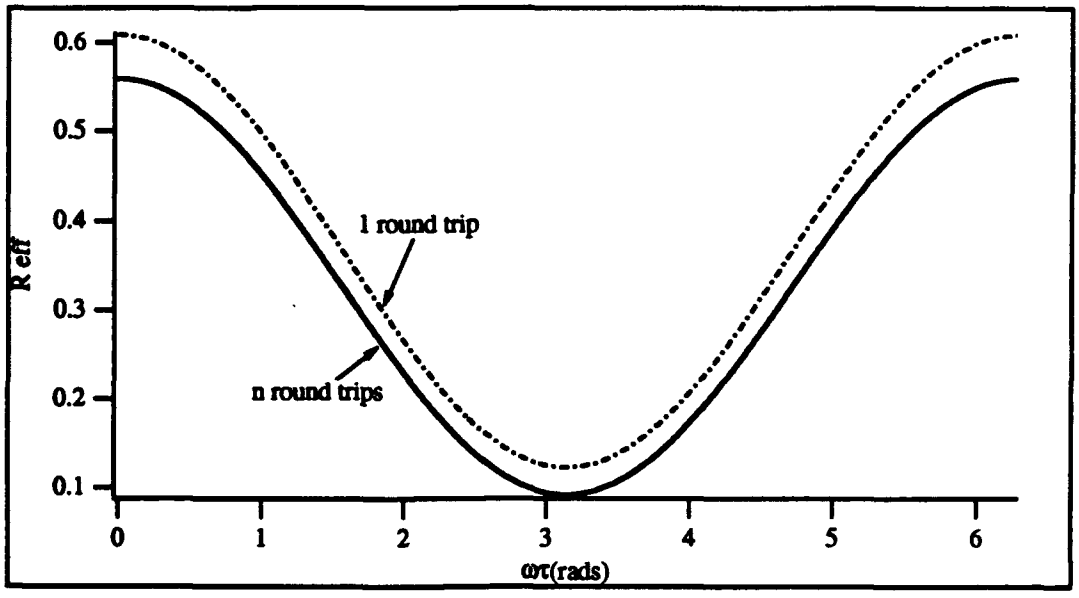

(a)

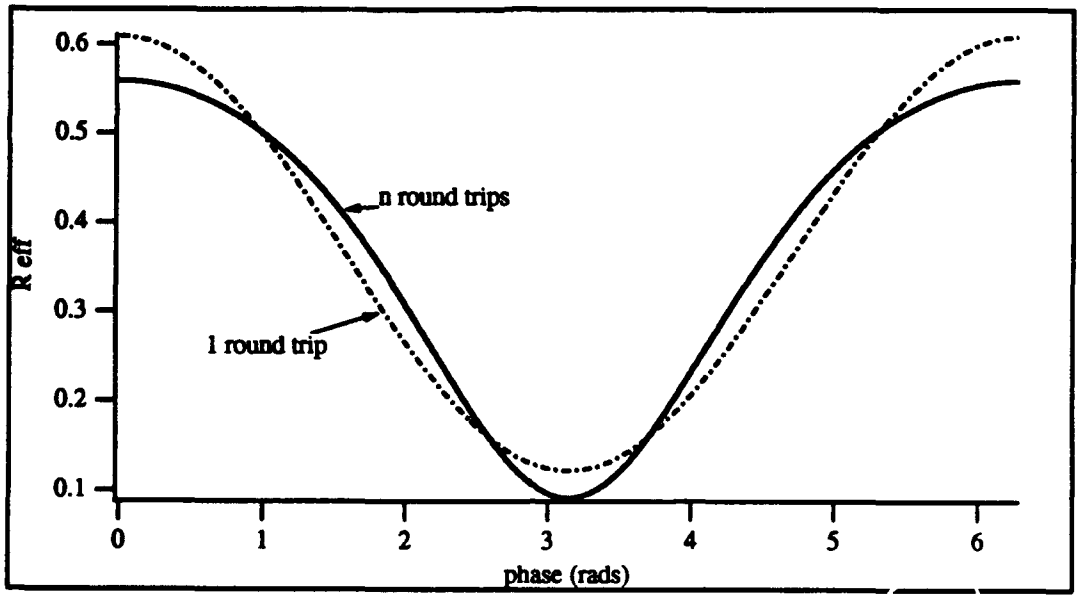

(b)

Fig. 2.14. Effective reflectivity versus external phase. $R_2 = 0.1$. (a) PCECL and (b) URECL.

Its also clear that the approximation becomes better for low values of R_2. Considering the equations, this makes sense. But, again, this is not typically taken into account in the literature, even though laser diodes are frequently coated for high or low reflectivity.

The CECL has a minimum reflectivity which edges back towards zero with decreasing R_2. This is due to destructive interference. As will be seen, the URECL and Ideal PCM would suffer from this as well if they could meet the appropriate phase conditions.

Keep in mind that all cases are covered in the models. In practice, the Ideal PCM and Unidirectional Ring (UR) PPCM will always have a set phase. This concept, too, is not usually considered in the study of feedback. In general, for the conventional case the phase is set to maximize the coupling. With the phase conjugate cases there is no choice.

For the case of $\Phi = 0$ or π, the Ideal phase conjugate mimics the behavior of the UR. This is as expected as the equations reduce to one another.

Figure 2.10 sets the delay phase at $\pi/2$ with $R_2 = 0.32$. Note that the URECL and the CECL are identical. All three are identical for the single bounce case. This points to another problem with the approximation. Figure. 2.11 sets the phase at π for the same reflectivity. Its clear that the CECL and the URECL are quite similar, only out of phase by π.

Figures 2.12 and 2.13 plot R_{eff} versus phase length delay. Obviously, the Ideal PCM is unaffected. The UR and conventional case are the same curves shifted by π. Please note that the behavior of the UR in this case is as a static hologram. When it acts as a phase conjugator it will be unaffected by delay length change in the steady state, as shown in Fig. 2.14. Figure 2.14 also plots the Ideal PCM versus change in phase, just to complete the model. But in reality, only the $2n\pi$ phase point can be reached.

In the longitudinal mode the differences between the three geometries are subtle. No information as to the aberration correction qualities of the mirrors is provided in the model, since this is a function of the transverse modes. This issue is treated qualitatively in Chapter 5. A rigorous study of the transverse mode structure is beyond the scope of this work; indeed it would be a thesis in itself.

A general note about all the graphs. This use of the single round trip approximation may often be experimentally justified, but its indiscriminate use is unwise. As the plots show, the magnitude of r_2, as well as r_3, dictates the validity of using that approach. The literature is not always clear in this respect.

Fundamental Assumptions for the Derivation of the Rate Equations

The clearest way to place the URECL in context is to compare the rate equations and effective reflectivities of the three external cavities. By taking the same approach to the modeling of all three, their differences and similarities will become evident. For the rest of this section the following assumptions are made [70], experimental considerations]:

The laser light is considered planar. In actuality, the HLP 1400 laser diode used in this experiment has a gaussian profile. This approximation is frequently made as it simplifies the theory. In the interactions regions of both the diode laser and the nonlinear medium, the beam waist is much greater than the interaction length, a reasonable justification for the approximation. Previous work approached in this fashion agrees well with the data.

The laser operates in a single transverse mode. For the Hitachi HLP 1400 laser diode this is true until the laser is run at above twice the threshold current. For these experiments this limit is never reached.

The laser runs single longitudinal mode. This is exactly the case for the free running laser for more than a few percent above threshold. Although not

all of the experiments with feedback were performed in this regime, this at least provides enough insight to get a grasp on the laser dynamics. Additionally, for the experimental observation of dynamical behavior (Chapter 4), single mode operation is achieved through the use of an etalon in the external cavity. The full multimode solution is, in principle, soluble, but beyond the scope of this work.

The electric field is sinusoidal inside the laser proper. This is not strictly true, as the gain medium is nonlinear. But it is a close approximation. The nonlinearity of the medium is contained in the "anti-guiding" factor α, which is the ratio of the real and imaginary parts of the susceptibility. Its importance is evident in the rate equations.

The feedback terms are added phenomenologically. Although they can be derived from first principles it becomes rather messy for more than one term. Additionally, the current convention is to use this successful technique.

The coupling constant is defined empirically and is considered constant in time. This is not strictly (for any real media) true. For Barium Titanate at 830 nm the rise time to steady state of the photorefractive grating is on the order of twenty minutes, for these experiments. Most of the experiments are done on a time scale that is slow compared to the rise time so this assumption is a good one. Further, the rate equations themselves are evaluated only in the steady state. A complete study of the dynamics, including transients, would have to include the time dependence. This is presented in Chapter 4. The coupling coefficient, C_m, can be rigorously derived [40,70]. But it is a difficult calculation for even the single round trip case, so in practice it is never done. The only suspicious terms in the coefficient are the variables f and τ_d. f is the fractional amount of light that is coupled back into the gain region of the laser. It can be empirically derived; this is shown in Chapter 3. τ_d is the round trip time in the laser cavity

and it corresponds to a photon lifetime, thus its inclusion is necessary even in the phase conjugate case.

The anti-guiding factor, α, is defined as:

$$\alpha = \frac{\mathrm{Re}\{\Delta n\}}{\mathrm{Im}\{\Delta n\}}, \tag{2.29}$$

the ratio of the real and imaginary parts of the change in refractive index. For my plots, I used $\alpha = -4$ [71]. Other works suggest a range of values values [14, 72-74]. This question has not been entirely resolved.

Rate Equations with Conventional Feedback

The above approximations are generally made in the literature, although their justification is usually assumed. They have been included for simplicity and universality. The approach taken follows that of Dente, et al. [74].

The rate equations for the conventional external cavity semiconductor laser (CECL) can be written

$$\dot{E}(t) = \left[i\omega(N) + \frac{1}{2}G(N) - \frac{1}{\tau_p}\right] E(t) + C_1 E(t-\tau) + C_2 E(t-2\tau) + \ldots, \tag{2.30}$$

$$\dot{N}(t) = R - \frac{N}{\tau_s} - G(N)|E(t)|^2. \tag{2.31}$$

where $E(t)$ the the total electric field inside the laser, $\omega(N)$ is the frequency of the laser with feedback, τ is the round trip time in the external cavity, τ_p is the photon lifetime in the laser diode, $N(t)$ is the carrier number, R is the pump rate, τ_s is the carrier lifetime, $G(N)$ is the carrier dependent gain. C_m is the mth coupling coefficient, which is measurement of how well the light that has made m round trips couples back into the gain medium of the laser. These equations can be derived from first principles [70].

The first term on the right-hand side of 2.26 is just the electric field rate equation for the free running laser [70]. The feedback terms are added phenomenologically as in Mork [75] and Park [62]. The carrier number equation is

also standard. The effect of the external cavity on the carrier number is expressed through its dependence on the gain and electric field.

The coupling coefficients are gleaned from Eq. (2.2) and correspond to the reflectivity terms [15]. Thus

$$C_m = -\frac{f}{\tau_d}\frac{(1-r_2^2)r_3}{r_2}(r_2 r_3)^{m-1}, \tag{2.32}$$

where f is the coupling factor mentioned earlier. It can vary between 0 and 1. Its value is limited by the beam quality of the laser and any aberrations to the beam. f is derived and measured in Chapter 3. The time dependent phase and the phase delay is left in the electric field. For generality any phase terms that are affected by phase conjugation are explicitly kept in the coupling coefficient. (There are not any for the conventional case.) A further notational shorthand is

$$C_m = -\kappa(r_2 r_3)^{m-1}, \qquad \kappa = \frac{f}{\tau_d}\frac{(1-r_2^2)r_3}{r_2}. \tag{2.33}$$

Substitute this expression into 2.26 along with the following

$$E(t) = A(t)e^{i\phi(t)}e^{i\Omega t} = A(t)e^{i\omega\tau}, \tag{2.34a}$$

$$\begin{aligned} E(t-m\tau) &= A(t-m\tau)e^{i\phi(t-m\tau)}e^{i\Omega(t-m\tau)} \\ &= A(t-m\tau)e^{i\omega(t-m\tau)}, \end{aligned} \tag{2.34b}$$

$$N(t) = N_0 + n(t), \tag{2.34c}$$

$$G(N) = G_0 + gn = G\left(N - N_{\text{th}}\right), \tag{2.34d}$$

$$\omega(N) = \Omega + \beta n = \Omega + \frac{|\alpha| gn}{2}, \tag{2.34e}$$

where $A(t)$ is the time dependent electric field amplitude, $\Phi(t)$ is the time dependent phase of the laser, Ω is the free running angular frequency, N_0 and G_0 are

the steady state values, n and g are the time dependent fluctuations off steady state, and Nth is the threshold value. Note that

$$\begin{aligned}\phi(t) &= (\omega - \Omega)t, \\ \phi(t - m\tau) &= (\omega - \Omega)t - (\omega - \Omega)m\tau, \\ \dot{\phi}(t) &= \omega - \Omega = \Delta\omega. \end{aligned} \tag{2.35}$$

where $\Delta\omega$ is the frequency change of the laser due to feedback. Substitute these values in, and let

$$\frac{1}{2}G_0 = \frac{1}{\tau_p}, \tag{2.36}$$

to get the result

$$\begin{aligned}\dot{A}e^{i\phi(t)}e^{i\Omega t} &+ i(\dot{\phi} + \Omega)A(t)e^{i\phi(t)}e^{i\Omega t} \\ &= i\left(\Omega + \beta n + \frac{1}{2}gn\right)A(t)e^{i\phi(t)}e^{i\Omega t} \\ &- \sum_{1}^{\infty} C_m A(t - m\tau)e^{i\phi(t)}e^{i\Omega t}e^{i\phi(m\tau)}e^{-im\Omega\tau}. \end{aligned} \tag{2.37}$$

In steady state

$$\begin{aligned}\dot{A}(t) &= 0, \\ A(t) &= A(t - m\tau) = A \equiv \text{constant}, \\ gn &\rightarrow gn_0 = \Delta G, \\ \beta n &\rightarrow \beta n_0. \end{aligned} \tag{2.38}$$

where ΔG is the change in gain due to feedback. Again substitute these values and separate the equation into its real and imaginary components:

$$\frac{1}{2}gn_0 = \kappa \mathrm{Re}\left\{\frac{e^{-i\omega\tau}}{1 - r_2 r_3 e^{-i\omega\tau}}\right\}, \tag{2.39}$$

$$\Delta\omega = \beta n_0 - \kappa \mathrm{Im}\left\{\frac{e^{-i\omega\tau}}{1 - r_2 r_3 e^{-i\omega\tau}}\right\}. \tag{2.40}$$

These reduce to

$$\Delta G = 2\kappa \frac{\cos\omega\tau - r_2 r_3}{1 - 2r_2 r_3 \cos\omega\tau + r_2^2 r_3^2}, \tag{2.41}$$

$$\Delta\omega = \frac{\kappa[\alpha\cos - \alpha r_2 r_3 + \sin\omega\tau]}{1 - 2r_2 r_3 \cos\omega\tau + r_2^2 r_3^2}. \tag{2.42}$$

By keeping only one feedback term the work by Dente, et al. [74] can be reproduced. Rewriting Eq. (2.30) and keeping only round trip in the external cavity yields

$$\dot{E}(t) = \left[i\omega(N) + \frac{1}{2}G(N) - \frac{1}{\tau_p}\right] E(t) + C_1 E(t-\tau). \tag{2.43}$$

A glance at Eq. (2.6) identifies

$$C_1 = -\frac{f}{\tau_d}\frac{(1-r_2^2)r_3}{r_2} = -\kappa. \tag{2.44}$$

Substituting this into Eq. (2.43), along with Eqs. (2.34) - (2.36), produces the dynamical equation

$$\begin{aligned}\dot{A}(t) + i(\Omega + \dot{\phi})A(t) &= i(\Omega + \beta n)A(t) \\ &+ \frac{1}{2}gnA(t) + \kappa A(t-\tau)\exp(-i\phi(t-\tau) - i\Omega\tau),\end{aligned} \tag{2.45}$$

which reduces, in the steady state, to

$$\Delta G = 2\kappa\cos\omega\tau, \tag{2.46}$$

$$\Delta\omega = \alpha\kappa\cos\omega\tau + \kappa\sin\omega\tau. \tag{2.47}$$

This is essentially the result of Dente, et al. This type of equation is typically used in the literature for modeling feedback.

The solution for the carrier number equation, Eq. (2.31) is simply achieved by making the previous and following substitutions:

$$\begin{aligned} N &= n_0 + n(t), \\ R &= R_0 + \frac{N_0}{\tau_s}, \\ G(N) &= G_0 + gn, \end{aligned} \tag{2.48}$$

and solving

$$\dot{n}(t) = R_0 + (G_0 + gn)|A(t)|^2 - \frac{n(t)}{\tau_s}. \tag{2.49}$$

This equation contains no specific dependence on the feedback. In fact, it would be the same for the free running case. The effects of the coupled cavity are contained in the terms for the gain and the electric field. It will not be necessary to reproduce this equation in the upcoming sections.

Rate Equations with Ideal Phase-Conjugate Feedback

The solutions for the PCECL are attained in the same fashion as the conventional case. The rate equation with feedback is written the same as Eq. (2.30). I rewrite it here as

$$\dot{E}(t)\left(i\omega(N) + \frac{1}{2}G(N) - \frac{1}{\tau_p}\right)E(t) + C_1E(t-\tau) + C_2E(\tau - 2\tau) + \ldots. \tag{2.50}$$

In this instance the coupling coefficients will have a different form, to reflect the phase conjugator. The coupling coefficients are taken from Eq. (2.10)

$$\begin{aligned} C_m &= \frac{f}{\tau_d}\frac{(1-r_2^2)r_3}{r_2}(-r_2r_3)^{m-1}e^{+i(\Phi_{pc}-2\phi_0)} \quad \text{ODD } m, \\ C_m &= \frac{f}{\tau_d}\frac{(1-r_2^2)r_3}{r_2}(-r_2r_3)^{m-1} \qquad\qquad\quad \text{EVEN } m, \end{aligned} \tag{2.51}$$

or

$$\begin{aligned} C_m &= \kappa(-r_2r_3)^{m-1}e^{+i(\Phi_{pc}-2\phi_0)} \quad \text{ODD } m, \\ C_m &= \kappa(-r_2r_3)^{m-1} \qquad\qquad\quad \text{EVEN } m. \end{aligned} \tag{2.52}$$

Note the phase differences compared to the conventional case. The inclusion of f/τ_d warrants further comment. At first thought, one might consider $f = 1$, since the Ideal PCM will perfectly recreate the output of the laser. However, it can do no more than return the original beam quality. If this is poor it will not couple back into the laser gain medium as well as single-mode aberration-free light and thus f can be less than one.

Although the phase delay is "conjugated out," the photon still has a lifetime. The inclusion of τ_d^{-1} has become the convention [15]. It occurs in the general theory of using Maxwell's equations for the coupled cavities and is determined by the boundary conditions [40].

The response time of the nonlinear media is considered instantaneous. This allows us to use a constant C_m and keeps the equations completely valid for both the transient and the steady state cases, unlike the URECL as will be discussed later.

As with the conventional case substitute Eq. (2.34a), (2.34c) - (2.34e) into Eq. (2.50) along with Eq. (2.52). In order to allow for the phase-conjugate process use the following in place of Eq. (2.34b)

$$E(t - m\tau) = A(t - m\tau)e^{i\phi(t)}e^{i\Omega t} = A(t - m\tau)e^{-i\omega t}. \tag{2.53}$$

Note now that there is no phase delay in the external cavity. This is by definition of the phenomenon. The result is the following rate equation

$$\begin{aligned}\dot{A}(t)e^{i\phi(t)}e^{i\Omega t} + i(\Omega + \dot{\phi})A(t)e^{i\phi(t)}e^{i\Omega t} = &\left[i\Omega + i\beta n + \frac{1}{2}gn\right]A(t)E^{i\theta(t)}e^{i\Omega t} \\ &+ \kappa A^*(t - \tau)e^{i\phi(t)}e^{i\Omega t}e^{+i(\Phi_{pc} - 2\phi_0)} - \kappa A(t - 2\tau)e^{i\phi(t)}e^{i\Omega t}r_2r_3 \\ &+ \ldots - \ldots.\end{aligned} \tag{2.54}$$

Note that in the steady state

$$A^*(t - m\tau) = A(t - (m + 1)\tau) = A(t) = A \equiv \text{constant}. \tag{2.55}$$

After canceling terms, separating real and imaginary components, and solving in the steady state Eq. (2.54) reduces to

$$\Delta G = g n_0 = -\frac{2\kappa(\cos(\Phi_{pc} - 2\phi_0) - r_2 r_3)}{1 - r_2^2 r_3^2}, \tag{2.56}$$

$$\Delta\omega = -\frac{\kappa}{1 - r_2^2 r_3^2}\left[\alpha\cos(\Phi_{pc} - 2\phi_0) - \alpha r_2 r_3 - \sin(\Phi_{pc} - 2\phi_0)\right]. \tag{2.57}$$

As expected this has the same form as the conventional case. There is no time dependent phase delay. Keep in mind that due to boundary conditions the phase shift for the Ideal PCM must equal zero. This will be shown in detail in Chapter 3. The general case is given here for the sake of comparison to previous work [58].

To find the expression for the single round trip merely keep only the first feedback term in Eq. (2.50)

$$\begin{aligned} A(t)e^{i\phi(t)}e^{i\Omega t} + i(\dot{\phi}|\Omega)A(t)e^{i\phi(t)}e^{i\Omega t} \\ = \left[i\Omega + i\beta n + \frac{1}{2}gn\right]A(t) \\ + \kappa A^*(t-\tau)e^{i\phi(t)}e^{i\Omega t}e^{i(\Phi_{pc} - 2\phi_0)}. \end{aligned} \tag{2.58}$$

Using the above assumptions this reduces to

$$\Delta G = -2\kappa\cos(\Phi_{pc} - 2\phi_0), \tag{2.59}$$

$$\Delta\omega = -\alpha\kappa\cos(\Phi_{pc} - 2\phi_0) + \kappa\sin(\Phi_{pc} - 2\phi_0), \tag{2.60}$$

which agrees with the derivation of Agrawal and Klaus [58].

Rate Equations with Feedback from the Ring

The rate equations for the URECL are solved in the same fashion as for the other two cases. Begin with the standard Eq. (2.30)

$$\dot{E}(t) = \left(i\omega(t) = \frac{1}{2}G(N) - \frac{1}{\tau_p}\right) E(t) + C_1 E(t-\tau) + C_2 E(t-\tau) + \ldots. \quad (2.61)$$

Now the coupling coefficients, from Eq. (2.21), take the form of

$$C_m = \frac{f}{\tau_d}\frac{(1-r_2^2)}{r_2} r_3 (r_2 r_3)^{m-1} e^{+im\phi_R}. \quad (2.62)$$

Again the substitutions given in Eq. (2.34a) - (2.34e) are used. The phase delay information is retained, just as in the conventional case.

$$\begin{aligned} E(t-m\tau) &= A(t-m\tau)e^{i\phi(t-m\tau)}e^{i\Omega(t-m\tau)} \\ &= A(t-m\tau)e^{i\omega(t-m\tau)}. \end{aligned} \quad (2.63)$$

After all the substitutions are made Eq. (2.61) becomes

$$\begin{aligned} \dot{A}(t)e^{i\phi(t)}e^{i\Omega t} + i(\dot{\phi}+\Omega)A(t)e^{i\phi(t)}e^{i\Omega t} \\ = \left[i\Omega + i\beta_n \cdot + \frac{1}{2}gn\right] A(t) \\ + \sum_1^{\omega} C_m A(t-m\tau)e^{-i\omega(\omega\tau-\phi_R)}. \end{aligned} \quad (2.64)$$

This reduces in steady state to

$$\Delta G = -2\kappa \mathrm{Re}\left\{\sum_1^{\infty}(-r_2 r_3)^{m-1} e^{im\phi_R} e^{-i\omega m\tau}\right\}, \quad (2.65)$$

$$\Delta\omega = \beta n_0 + \kappa \mathrm{Im}\left\{\sum_1^{\infty}(-r_2 r_3)^{m-1} e^{im\phi_R} e^{-i\omega m\tau}\right\}. \quad (2.66)$$

After further algebra the end result is achieved

$$\Delta G = -2\kappa\left(\frac{\cos(\omega\tau-\phi_R)+r_2 r_3}{1+2r_2 r_3\cos(\omega\tau-\phi_R)+r_2^2 r_2^2}\right), \quad (2.67)$$

$$\Delta\omega = -\frac{\kappa}{1 + 2r_2 r_3 \cos(\omega\tau - \phi_0) + r_2^2 r_3^2} \times \left(\alpha\cos(\omega\tau - \phi_R) + \alpha r_2 r_3 + \sin(\omega\tau - \phi_R)\right). \quad (2.68)$$

A comparison with Eqs. (2.41) and (2.42) shows the similarity between the two cases. However, note the sign differences due to the phase of the amplitude reflectivities.

The single round trip case can be easily derived from Eq. (2.64). The rate equation becomes

$$\dot{A}(t)e^{i\phi(t)}e^{i\Omega t} + i(\dot{\phi} + \Omega)A(t)e^{i\phi(t)}e^{i\Omega t} = \left(i\Omega + i\beta n + \frac{1}{2}gn\right)A(t)e^{i\phi(t)}e^{i\Omega t} + \kappa e^{i\phi_R}A(t-\tau)e^{i\phi(t-\tau)}e^{i\Omega(t-\tau)}, \quad (2.69)$$

which, in the steady state reduces to

$$\Delta G = -2\kappa\cos(\omega\tau - \phi_R), \quad (2.70)$$

$$\Delta\omega = -\alpha\kappa\cos(\omega\tau - \phi_R) - \kappa\sin(\omega\tau - \phi_R). \quad (2.71)$$

Figures 2.15 and 2.16 plot both the complete and single round trip solutions for all cases. The differences are slight for the reflectivities shown. As r_{ext} or r_2 is increased, they are more pronounced. However, it is interesting to note, that the curves are quite similar for changes in external phase. This is because although the phase conditions vary between the cases, the terms are consistent for ΔG and Δw in the individual cases, thus the behavior observed. The minima of the curves indicate the frequency that the laser with feedback will shift to. **The important point is that for the PCECL and URECL the steady state solutions are actually single valued due to boundary conditions.**

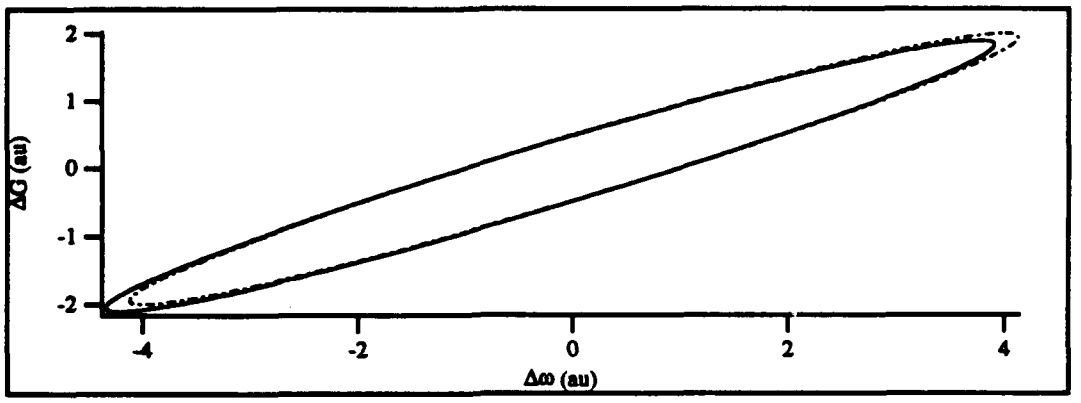

(a)

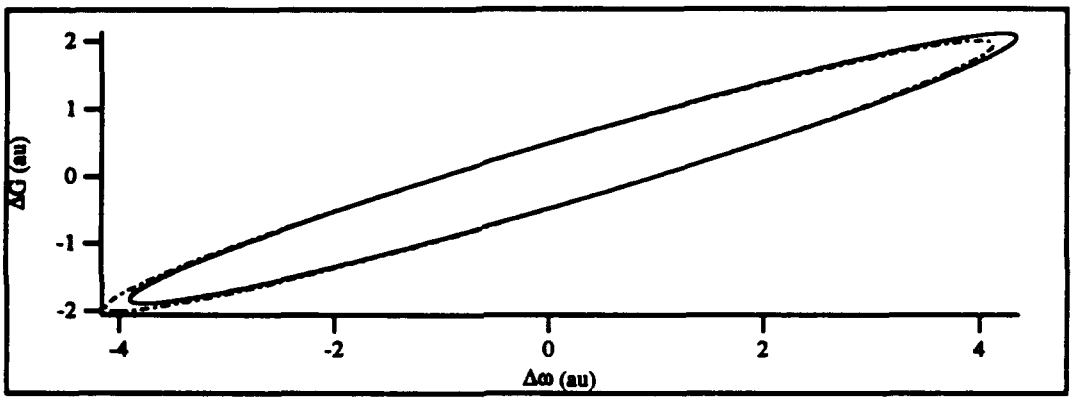

(b)

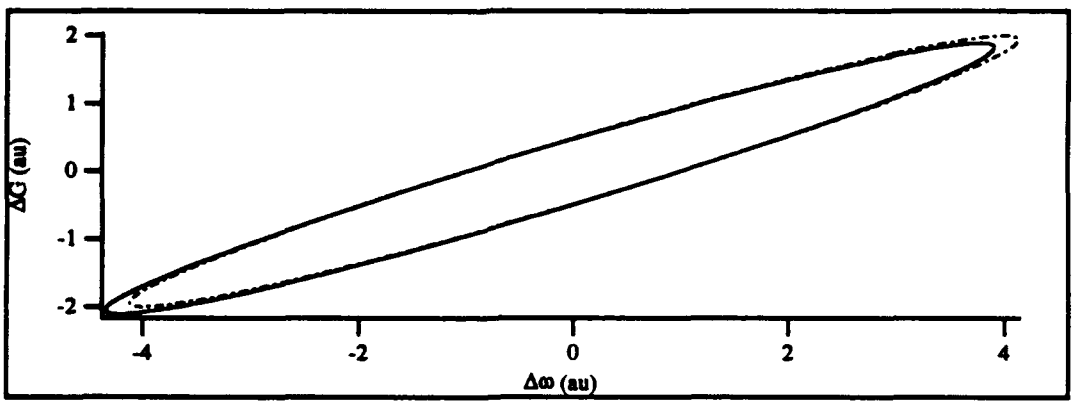

(c)

Fig. 2.15. Change in gain versus change in frequency. $R_3 = 0.01$. (a) CECL, (b) PCECL, and (c) URECL. Solid line – NRT, chain dot line – 1 RT.

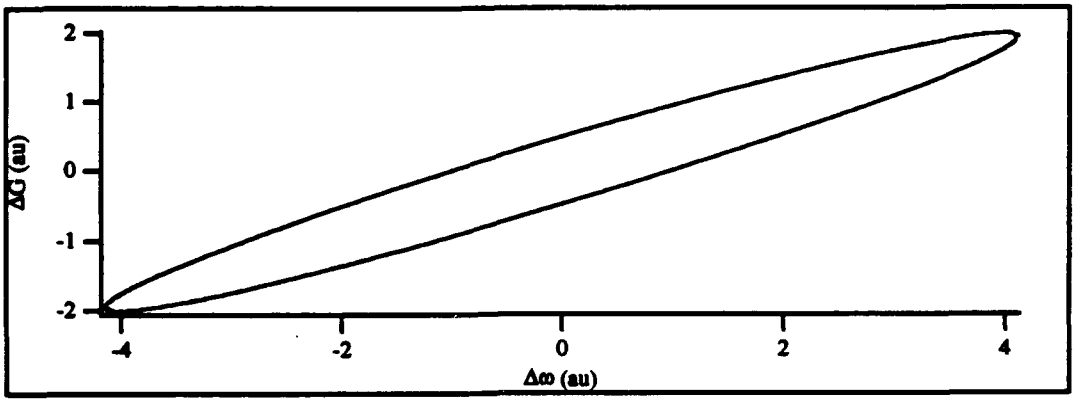

(a)

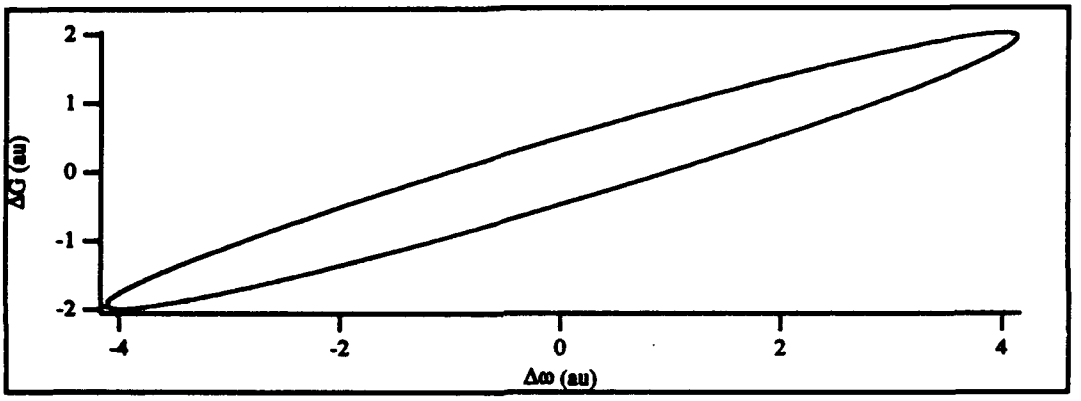

(b)

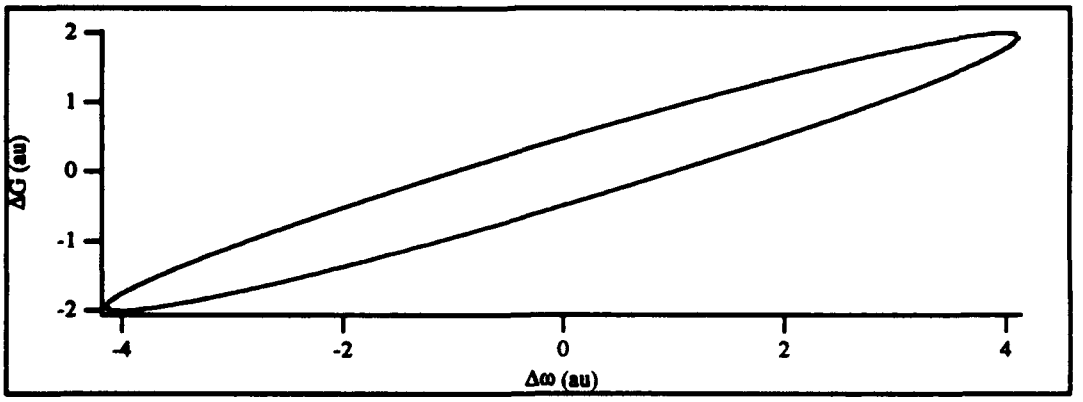

(c)

Fig. 2.16. Change in gain versus change in frequency. $R_3 = 0.0001$. (a) CECL, (b) PCECL, and (c) URECL. Solid line – NRT, chain dot line – 1 RT.

Summary

Three different geometries have been introduced. They are the Conventional External Cavity Laser (CECL), the Ideal Phase Conjugate External Cavity Laser (PECL), and the Unidirectional Ring Passive Phase Conjugate External Cavity Laser (URECL). The physical differences between them have been discussed. All of the standard assumptions made are presented and the quality of the approximations are justified. The effective reflectivities of the external cavities are derived as well as rate equations for each case.

Tables 2.1 and 2.2 compare the rate equations and effective reflectivities for all steady state cases. The phase differences are clear upon inspection. Both of the phase conjugate cases have boundary conditions that must be met; the effect of these is given in the table as well.

Table 2.1. *Multiple round trips with boundary conditions imposed.*

	CECL	PCECL	URECL
r_{eff}	$\left\lvert \frac{r_2^2 + r_3^2 - 2r_2 r_3 \cos\omega\tau}{1 - 2r_2 r_3 \cos\omega\tau + r_2^2 r_3^2} \right\rvert^{\frac{1}{2}}$	$\frac{r_2 + r_3}{1 + r_2 r_3}$	$\frac{r_2 + r_3}{1 + r_2 r_3}$
ΔG	$2\kappa \frac{\cos\omega\tau - r_2 r_3}{1 - 2r_2 r_3 \cos\omega\tau + r_2^2 r_3^2}$	$\frac{-2\kappa}{1 + r_2 r_3}$	$\frac{-2\kappa}{1 + r_2 r_3}$
$\Delta\omega$	$\kappa \frac{\alpha\cos\omega\tau - \alpha r_2 r_3 + \sin\omega\tau}{1 - 2r_2 r_3 \cos\omega\tau + r_2^2 r_3^2}$	$\frac{-\kappa\alpha}{1 + r_2 r_3}$	$\frac{-\kappa\alpha}{1 + r_2 r_3}$

Table 2.2. *One round trip with boundary conditions imposed.*

	CECL
r_{eff}	$\lvert r_2^2 + r_3^2 - 2r_2r_3(1-r_2^2)\cos\omega\tau - 2r_2^2r_3^2 + r_2^4r_3^2\rvert^{\frac{1}{2}}$
ΔG	$2\kappa\cos\omega\tau$
$\Delta\omega$	$\alpha\kappa\cos\omega\tau + \kappa\sin\omega\tau$
	PCEL
r_{eff}	$\lvert r_2^2 + r_3^2 + 2r_2r_3(1-r_2^2) - 2r_2^2r_3^2 + r_2^4r_3^2\rvert^{\frac{1}{2}}$
ΔG	-2κ
$\Delta\omega$	$-\alpha\kappa$
	URECL
r_{eff}	$\lvert r_2^2 + r_3^2 + 2r_2r_3(1-r_2^2) - 2r_2^2r_3^2 + r_2^4r_3^2\rvert^{\frac{1}{2}}$
ΔG	-2κ
$\Delta\omega$	$-\alpha\kappa$

There are three main differences between the CECL and the PECL and URECL. The first is that the phase of the reflectivity, and thus the feedback are different. This is due to the nature of the physical processes that produce the returned light. This is shown quite clearly in the equations through the sign of the terms and the phases in the exponent. Second, and most important is that the boundary conditions insist that for the PCECL and URECL the delay phase equal an integer multiple of 2π.

The third difference, only briefly touched upon, is the beam reconstruction qualities of the latter two systems. Any phase front defects or aberrations will not only be uncorrected in the conventional case, they will be compounded. The phase conjugators will correct for aberrations. This means that a cleaner signal will couple back into the laser. This shows up in the transverse properties of the beam, and so is not apparent in the equations presented in this chapter.

CHAPTER 3

STATIC AND SPECTRAL PHENOMENA

Although the dynamic behavior of a laser diode with feedback attracts the most interest, and will be treated in Chapter 4, the static characteristics of the external cavity semiconductor laser are interesting in their own right. This is particularly true for Ideal phase-conjugate feedback and feedback from the Ring PPCM. Ideal is again capitalized to emphasize its theoretical nature. This contrasts with the Ring PPCM, which is the actual experimental device. The distinction is made because there is some confusion in previous work as to the nature of the feedback from nonconventional reflectors. As shown in Chapter 2, the attributes of a self-pumped PCM are different from that of a four-wave mixing PCM.

In this chapter some of those aspects will be addressed. The chapter begins with a description of the experimental geometry that was used throughout this work. A derivation of the boundary conditions for the phase-conjugate and ring external cavities follows and is supported by the experimental data. This information allows for a calculation of the coupling factor f. Linewidth narrowing is then demonstrated and modeled. Finally, the multimode behavior of the laser diode is discussed and presented, for the free-running, conventional feedback and ring PPCM feedback cases.

Experimental Geometry

The experimental configuration used in this work is shown in Fig. 3.1. At its heart is a Hitachi HLP1400 semiconductor laser [76]. This device is a double heterojunction, channeled substrate, planar stripe, gain-guided GaAlAs laser, with a

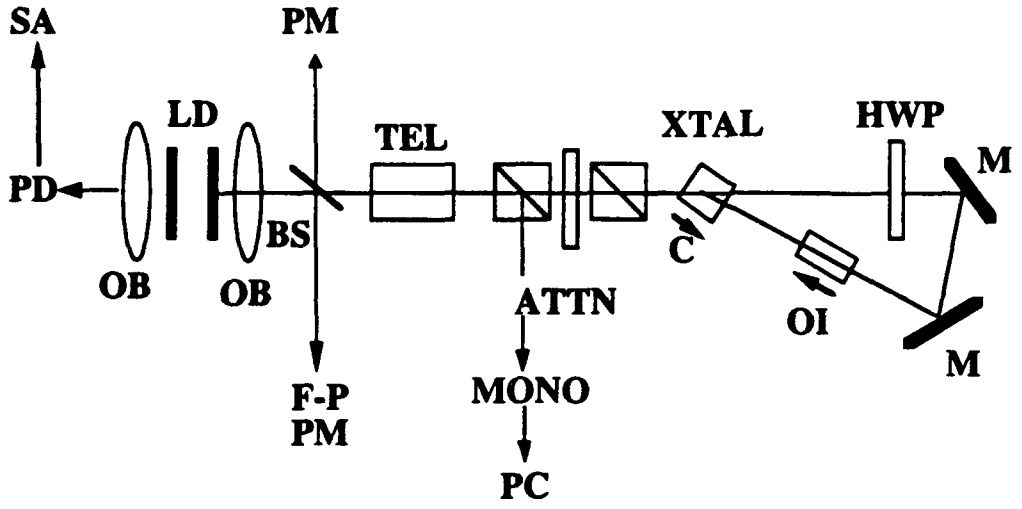

Fig. 3.1. Unidirectional ring PPCM external cavity laser.

nominal wavelength of 825 ± 25 nm. The actual lasing wavelength is determined by the pump current and temperature of the laser diode. It has a maximum cw output of 15 mW; the typical operating power was 5 mW. The laser is single longitudinal and transverse mode when free running. The lasing threshold, as later shown, is typically 50 mA. The maximum applied pump current was 90 mA, although it can be driven at higher currents. In general the laser was operated between 70 and 80 mA. The laser chip is mounted on a copper stem which also serves as ground and as a heat sink. No attempt was made to tune the laser frequency. The lasing frequency of the laser is very dependent upon temperature. No external cooling was employed. Temperature stability was provided by mounting the device onto a copper heat sink. Over the course of the experiment the lasers were fairly stable, i.e., they did not suffer from significant frequency drift or mode hopping, and they remained single mode. When the laser did not behave in this fashion the data was not used.

This laser was chosen because they are single mode, rugged and reliable. The open air construction makes them well suited for laboratory work. Additionally, they are commonly used by researchers in the field. Several laser diodes were used during the course of the experiments and their individual characteristics noted. Since the absolute wavelength was not a concern, interchanging lasers was not a problem if done between different experimental runs. If a laser developed problems during a run, it was replaced and that set of measurements was retaken.

As shown in Fig. 3.1 light from the rear facet suffers from a degradation in beam quality caused by self-interference with reflected light off the stem (it acts as a Fresnel biprism). One fringe was screened, collected with a lens, and directed onto an Antel AR-S2 photodiode (response time 30 ps). This, in turn, was connected to a Tektronix MDL2755 21 GHz spectrum analyzer. This device has a maximum resolution of 1 MHz (for this experiment).

The front facet light was sent to the phase conjugator. It was collimated with an NRC FL-20 objective lens (NA = 0.5, FL = 8.6 mm). Then it passed through a beam splitter (approximately 16% R). This beam splitter sent the output from the laser to either a CCD camera, a power meter, or a set of Fabry-Perot Interferometers, FP1, FP2, and FP3. FP1 was a plane-plane type with a Free Spectral Range of 4000 GHz [77] and a finesse of 300. FP2 was also plane-plane with a FSR of 16.5 GHz and a finesse of 300. FP3 was a spherical confocal type with a FSR of 750MHz and a finesse of 100. The outputs of the Fabry-Perot's were sent to a digital storage oscilloscope, where they could be viewed or sent to a plotter.

Two types of power meters were used. The first was a NRC MDL 815-SL digital power meter with a range of from 0.2 to 2000 mW. The second was fashioned form a large area photodiode, bias circuit electronics, and voltmeter. This was calibrated to the previous device.

The CCD video camera was used in the beam quality measurements and will be described in Chapter 5.

The return beam was sent by a beam splitter to either a power meter or the beam quality measurement device, described in Chapter 5. The reflectivity of the ring PPCM could be measured by taking the ratio of the two power meters coupled via the beam splitter.

After the beam splitter the light was sent through a fixed position 6X telescope backwards to shrink the beam. This was to get the beam diameter small enough to send through the $BaTiO_3$ and keep the overlap within the crystal good. The beam diameter out of the collimation objective was 8.8 mm $\times$ 4.0 mm, the long direction vertical. The beam was horizontally polarized in the plane of the laser junction.

The output of the telescope was sent through an attenuator which consisted of two polarizing cube beam splitters on either side of a half-wave plate that

could be rotated. The attenuation ranged from 0% to approximately 100%, the former figure was too low to be accurately measured. However, the reflectivity could be kept below the amount that has an effect on laser performance.

The polarizers deflect light with vertical polarization. The output of the first polarizer was collected with an objective and sent to the monochromator via an fiber optic input. Greater than 30% of this light passed through the fiber. The monochromator was a Spex 1m Czerny-Turner type spectrometer with adjustable entrance and exit slits. The diffraction grating was blazed at 500 nm and had 600 lines/mm. The exit light could be directed to either a CCD camera connected to a video monitor for a real-time, low-resolution image, or to a photomultiplier tube that fed a PC. The output could be displayed and stored.

The light then entered the Barium Titanate as shown. This photorefractive element is a single crystal of $BaTiO_3$ approximately 6mm on a side. It was grown by Sanders [78]. The *c*-axis of the Barium Titanate is normal to one set of faces. It is uncoated; the index of refraction is 2.365 so there are some reflection losses. Experiments were carried out at room temperature. As a consequence the photorefractive effect was relatively weak due to the low nonlinear coefficient at the operating wavelength.

The crystal was aligned so that the *c*-axis was pointing away from the input beam and so the light would be horizontally polarized in the nonlinear medium. After exiting the it passed through a half-wave plate, was turned by two mirrors and then sent through a Faraday Optical Isolator from Optics for Research, model NIR-IO5. The half-wave plate rotated the polarization to match the input polarizer of the isolator. The isolator was set to pass 830 nm light. The stated isolation was $> 99.9\%$ extinction. The measured amount was $> 98.0\%$. This feedback contribution was found to be negligible after passing back through all the associated optics; it did not have an effect on the experiments.

After the isolator, the beam was sent back into the crystal. The beam was returned such that within the angle formed by the c-axis of the crystal and the pump beam. This is a necessary condition for phase conjugation as described in Chapter 2. All beams were kept co-planar. The phase-conjugate return beam then passed back through the described optics and experiments were performed.

Boundary Conditions for the URECL

In a conventional external cavity laser, the boundary conditions are set arbitrarily. This is not the case for a phase-conjugate external cavity, either photorefractive or Ideal. As described in the previous chapter, the four-wave mixing phase matching conditions will determine the phase of the return beam [64-66]. These are, in turn, set by by the steady state coupled cavity parameters. The PCM can meet two requirements: the phase-conjugate return beam is in phase with either the light transmitted through or reflected off the rear facet of the diode laser. In Fig. 3.2, E_i is the light incident on facet 2 which has amplitude reflectivity and transmittance r_2 and t_2, respectively. Er and Et are the corresponding reflected and transmitted beams. E_1 has made one round trip in the cavity and just reflected off facet 2. Likewise for E_2 except that it has just transmitted back into the laser diode. Now to satisfy the first requirement means that

$$E_r = AE_2, \tag{3.1}$$

where A is the appropriate amplitude coefficient. Thus

$$E_i r_2 = t_2^2 r_3 E_i e^{i\phi}, \tag{3.2}$$

or

$$e^{i\phi} = 1, \quad \phi = 2n\pi, \quad n = 0, 1, 2 \ldots . \tag{3.3}$$

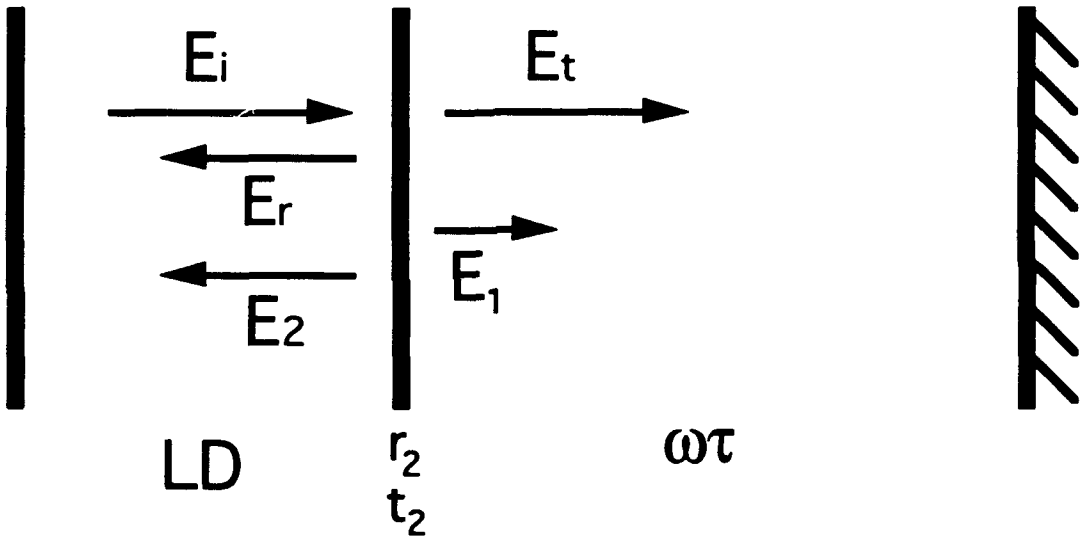

Fig. 3.2. Schematic for boundary conditions.

To meet the second requirement

$$E_t = AE_2, \tag{3.4}$$

$$t_2 E_i = -t_2 r_2 r_3 E_i e^{i\phi}, \tag{3.5}$$

so that

$$e^{i\phi} = -1; \quad \phi = (2n+1)\pi, \quad n = 0, 1, 2, \ldots . \tag{3.6}$$

This is exactly how the effective reflectivities were solved for. For either the Ring PPCM or the Ideal phase-conjugate mirror the following expressions are obtained.

$$\frac{r_2 + r_3}{1 + r_2 r_3}; \quad \phi = 2n\pi, \tag{3.7}$$

$$\frac{r_2 - r_3}{1 - r_2 r_3}; \quad \phi = (2n+1)\pi. \tag{3.8}$$

Note that for $\phi = 2n\pi$ the effective reflectivity is greater than the facet reflectivity and for $\phi = (2n+1)\pi$ it is less. In Fig. 3.3 the threshold gain is plotted against r_{eff} for a small range. As r_{eff} increases, g_{th} decreases. So the PCM will always set its phase such that the threshold gain decreases; its phase will be effectively zero for all cases. This is true for the ideal case as well. This can also be seen by taking the derivative of the power reflectivity, $|r_{\text{eff}}|^2$, to find that it has a maximum at $2n\pi$.

The evidence for this case can be seen in Fig. 3.3, which shows the light-current (L-I) curves for both the conventional and ring feedback configurations. The conventional mirror can be adjusted to either increase or decrease the effective reflectivity. For increased r_{eff}, the output power goes down, conversely for decreased r_{eff}. This is accomplished by simply translating the mirror. Feedback from the ring PPCM always decreases the facet output power, regardless of alignment. These phenomena are demonstrated with the L-I curves shown in Fig. 3.4. Figure 3.4a shows the change in output power for the conventional case; it can

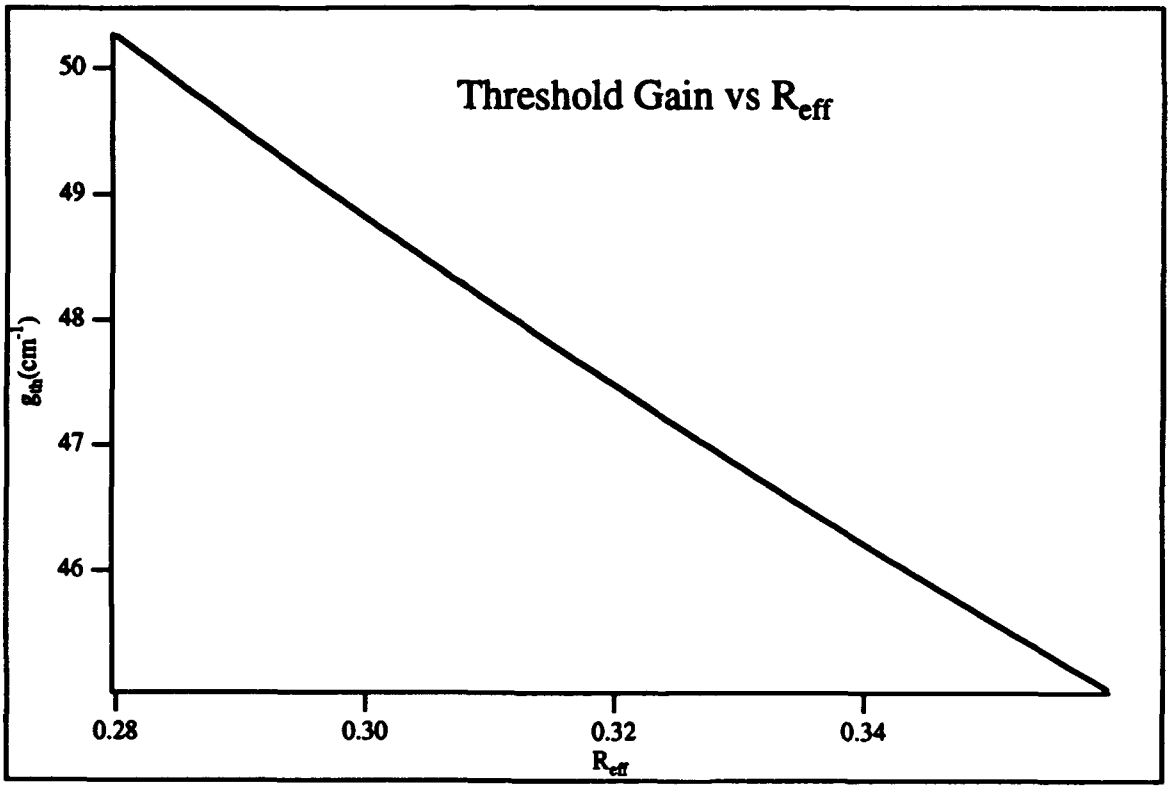

Fig. 3.3. Threshold gain versus effective reflectivty.

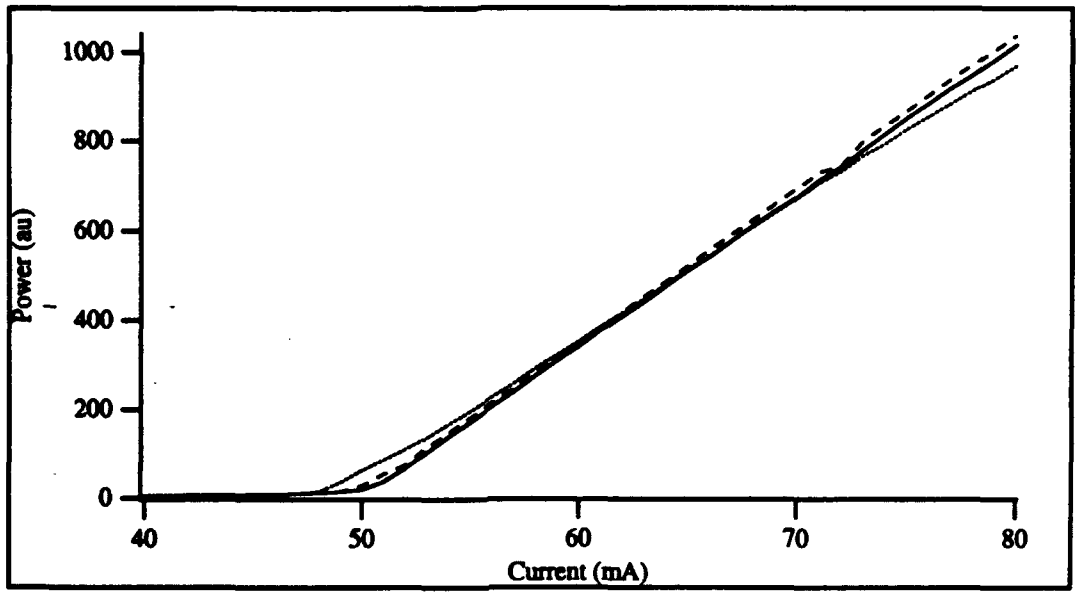

(a)

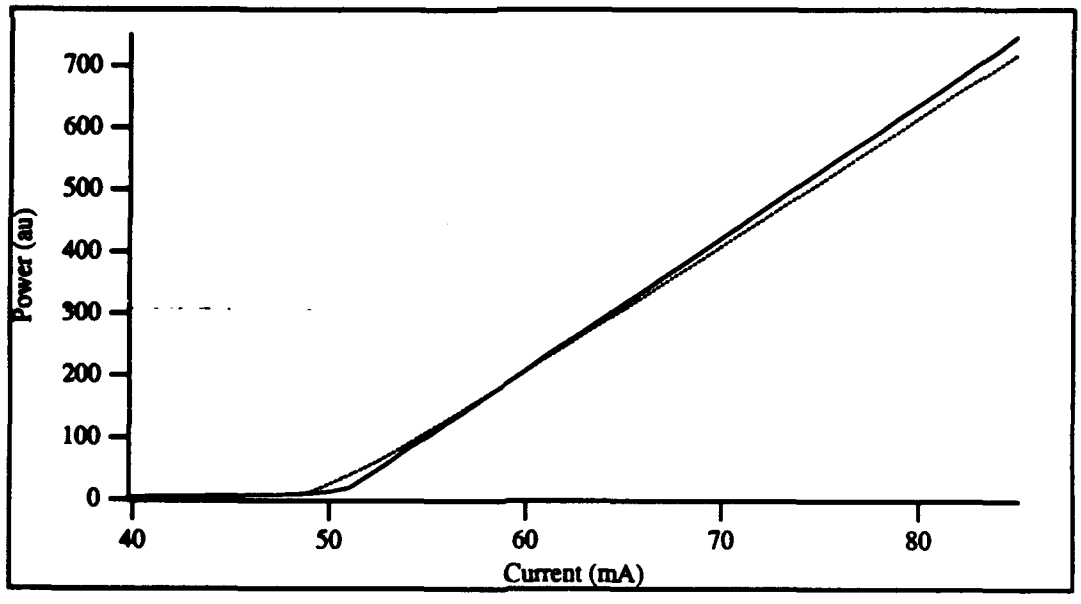

(b)

Fig. 3.4. $L - I$ curves for external cavity lasers. (a) CECL, and (b) URECL. Solid line – free running, dashed line – decreased output, dotted line – increased output.

either increase or decrease. Figure 3.4b is a typical L-I curve for the URCEL. Increased power output from the external cavity facet was never observed. In both cases the laser has multimode longitudinal modes. In the conventional case the mirror was adjusted at 80 mA applied current. The ring PPCM gratings were written at this same pump current. The measured error for these plots is less than 0.5%

The total output power from both facets must be measured for a detailed analysis of the L-I curves. But a relationship can be found to relate the individual facet powers. It is given by [79]

$$\frac{P_1}{P_2} = \frac{R_1^{-1/2} - R_1^{1/2}}{R_2^{-1/2} - R_2^{1/2}}, \tag{3.9}$$

where $P_{1,2}$ is the facet output power and $R_{1,2}$ is the power reflectivity for that facet. If the P_2 decreases while P_1 increases then R_2 must be increasing. Single measurements done with the URCEL confirm this (see Table 3.1). In this case the measured intensity from the back facet and from the front facet simultaneously. P_1 is the rear facet. Due to the experimental arrangement I could not collect all of the power exiting off the rear. The reflectivity was approximately 50% (measured without the optical isolator for convenience). The trend, however, is clearly indicated. This proves that the reflectivity is increasing, the result of a $2n\pi$ phase shift. Additionally, the noise spectra data, Fig. 3.5, show an increase in back facet output power for the URECL , as compared to free running, in every case. (Further discussion of the noise spectra will be given in Chapter 4.)

Table 3.1. *Change in facet output power normalized to free running.*

	P_1	P_2	R
Free Running	1	1	-
With Feedback	1.02	0.94	51%

As the current is increased from below threshold to maximum, the wavelength will change, thus the product $\omega\tau$ for any mode will not be constant.

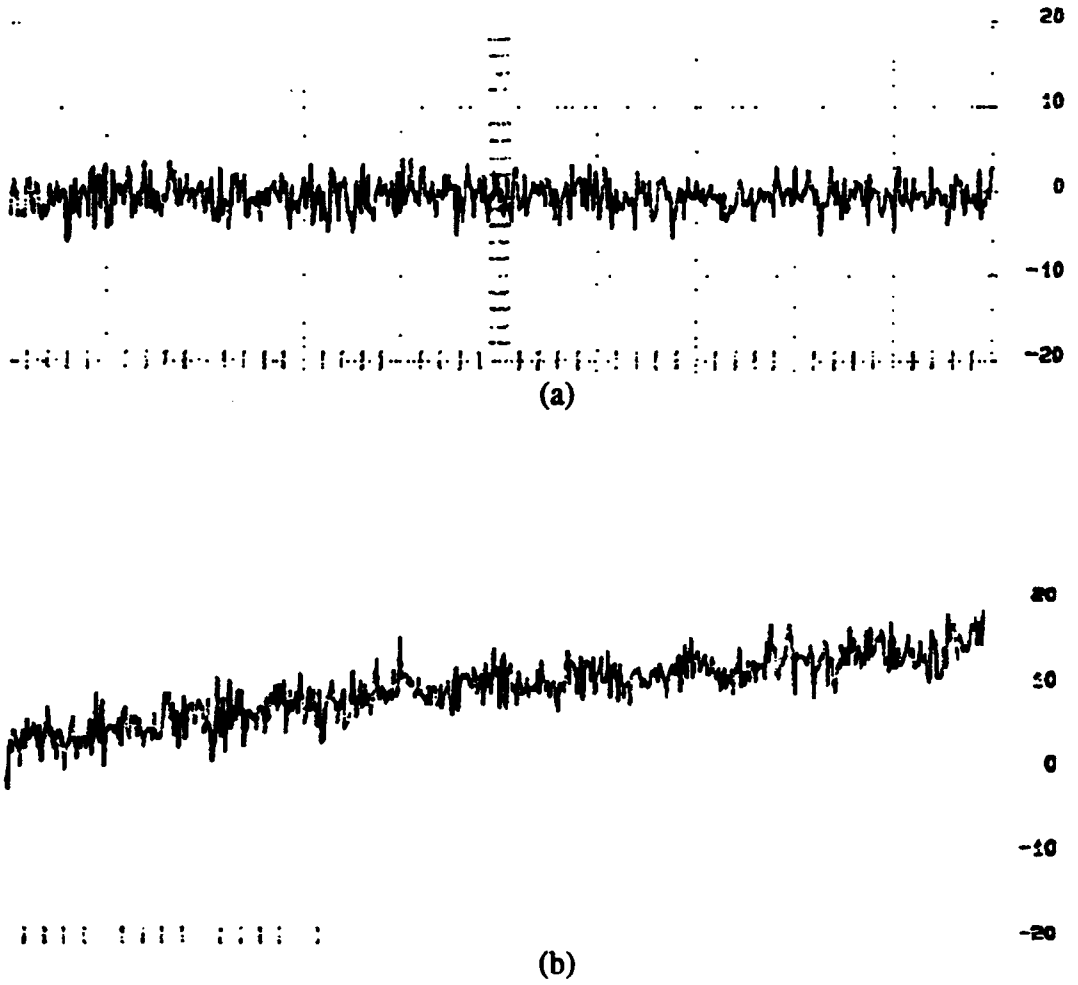

Fig. 3.5. Rear facet output power as measured by the spectrum analyzer (a) with feedback and (b) without feedback.

Therefore the above discussion is strictly valid only at for a specific pump current. For the CECL this means the phase for the modes will not be constant throughout the $L - I$ curve. For any point other than at 75 mA the external cavity phase cannot be known. This will be further examined at the end of this chapter.

Measurement of Effective Reflectivities

For small variations from P_1 and P_2 one can assume that

$$\begin{aligned} P &= P_1 + P_2, \\ P &= 2P_1 = 2P_2 = \text{constant} \\ &\text{when } R_1 = R_2, \end{aligned} \tag{3.10}$$

if the power goes as above. This leads to a solution for the change in effective reflectivity

$$\begin{aligned} R_1^{1/2} &= \frac{-P' \pm \sqrt{P^2 + 4}}{2}, \\ P' &= \frac{P_1}{P - P_1}\left(R_2^{-\frac{1}{2}} - R_2^{\frac{1}{2}}\right), \end{aligned} \tag{3.11}$$

which is plotted in Fig. 3.6. From this the coupling coefficient can be determined. If both powers are known this is an accurate method of determining the effective reflectivity at any point. This is particularly useful if the reflectivity is changing with intensity, which for photorefractives it will. For many laser diode packages the rear facet reflectivity is difficult or even impossible to obtain. As mentioned, the HLP1400 suffers from self-interference in that direction, and its mounting makes getting an objective lens close a problem. The coupling factor f can also be determined from the front facet power by measuring the reduction in threshold current. As shown by Seo [80], r_{eff} can be derived from the reduction in threshold gain, which in turn can be measured by the decrease in threshold current.

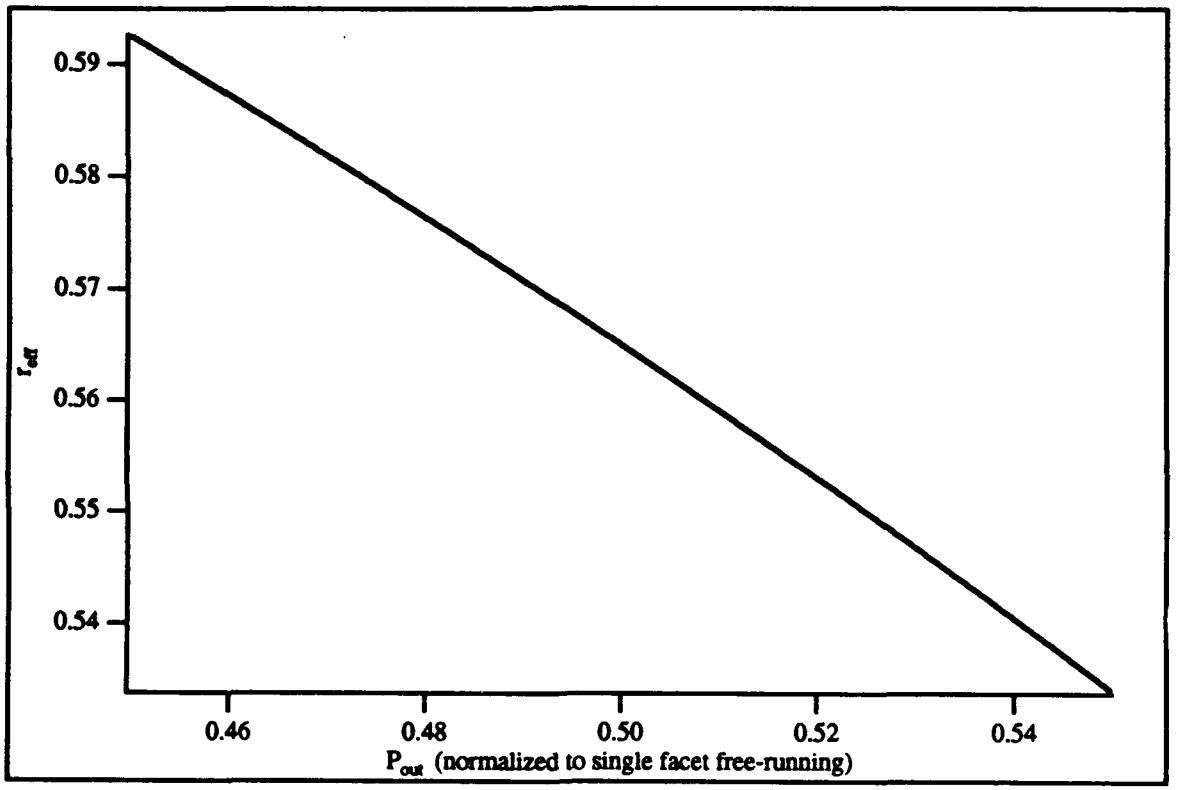

Fig. 3.6. **Effective reflectivity versus change in output power. Free running output power = 0.5.**

The threshold gain of a laser can be written

$$g_{th} = \beta I = -\frac{1}{2L}\ln\left(\frac{1}{r_1^2 r_2^2}\right)^2, \tag{3.12}$$

where β is a proportionality constant, I_{th} is the threshold current, L the length of the diode laser, and r_{eff} and r_2 the real effective and second facet amplitude reflectivities, respectively. The change in threshold gain can then be defined as

$$\delta = \beta(I_{FB} - I_{th}) = -\frac{1}{L}\ln\left(\frac{r_{eff}}{r_2}\right), \tag{3.13}$$

where I_{FB} is the threshold current with feedback. Let

$$\Delta I = I_{FB} - I_{th}, \tag{3.14}$$

and

$$L = \frac{v_g}{2f_d}; \quad \tau_p = \frac{1}{\beta I v_g}, \tag{3.15}$$

then

$$r_{eff} = r_2 \exp\left\{\frac{-\Delta I}{2f_d \tau_p I_{th}}\right\}, \tag{3.16}$$

here v_g is the group velocity, f_d is the mode spacing of the diode, and τ_p is the photon lifetime in the semiconductor laser. For $\tau_p = 2.1$ ps, $f_d = 135$ GHz, $I_{th} = 50$ mA (corresponding to the HLP1400), and $r_2 = 0.565$ the change in r_{eff} versus the change in threshold current is plotted in Fig. 3.7. Using the data from Fig. 3.4, the values in Table 3.2 are obtained.

Table 3.2. *Effective reflectives and coupling factors.*

$f_d = 135$GHz, $\tau_p = 2.1$ps

	URECL	CECL (Inc)	CECL (Dec)
I_{th} Δ I r_3	50 mA 1.5 mA 0.374	50 mA 1.0 mA 0.339	50 mA 2.0 mA 0.332
Power Method			
r_{eff} f	0.584 0.09	0.553 0 04	0.592 0.14
Current Method			
r_{eff} f	0.598 0.195	0.587 0.11	0.609 0.23

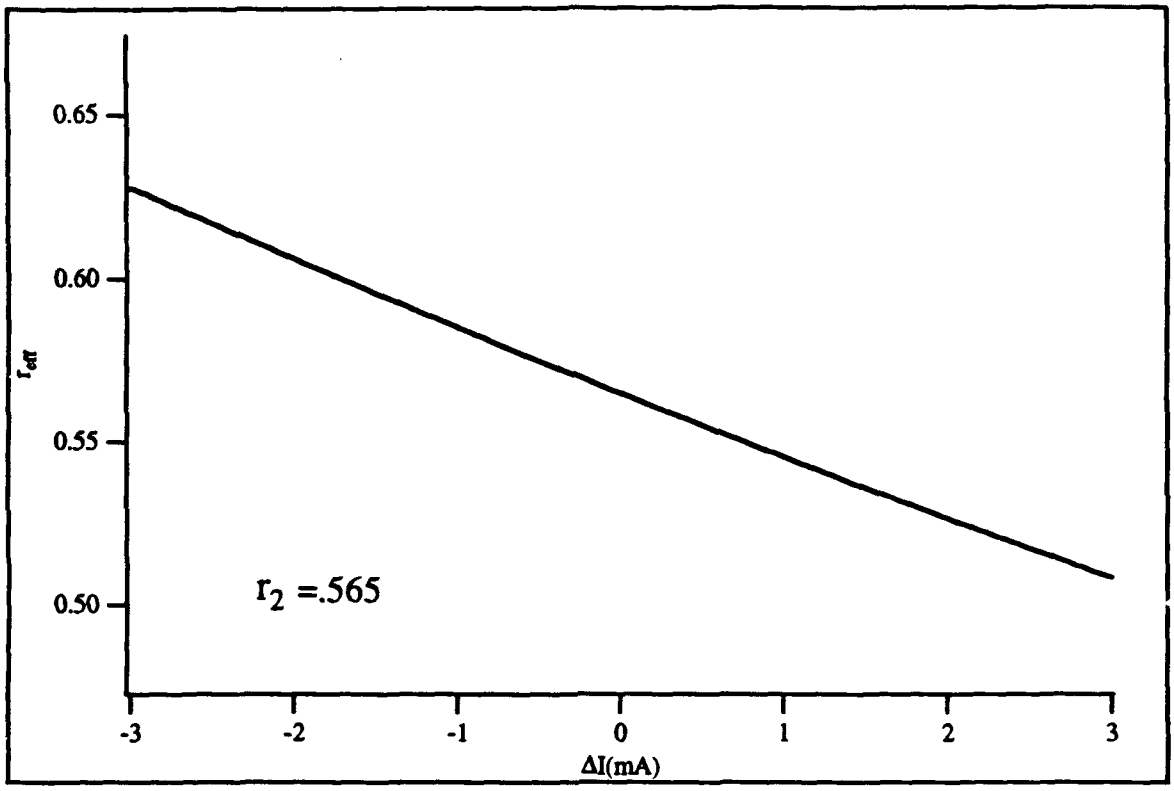

Fig. 3.7. Effective reflectivity versus change in threshold current.

As the results in that table indicate, the different techniques yield very different values for the effective reflectivities. This is due to several reasons. The assumptions that P_{tot} is a constant for any given current is not exact. Additionally, the phase conditions will change as the current is moved away from 80 mA. For the Ring PPCM, a multimode grating is written which can reflect many discrete laser frequencies, each with the same phase. But the relative intensities of the different wavelengths will change. For the conventional case only general conclusions can be derived without further information. The phases of the modes are completely undetermined for other than 80 mA pump current. These values provide an upper and lower bound to the parameters. One interesting point, though, in the case of increasing output power, using the change in current method to determine r_{eff} would suggest an increasing, not decreasing reflectivity, contrary to what one would expect. This, again, is due to the change in phase with different frequencies. Below threshold, the laser sees an external reflector of unspecified phase and thus can lase.

Coupling Factor

The coupling factor f can be derived from the expressions given for effective reflectivity in Chapter 2. With this included Eq. (2.34) becomes

$$r_{eff} = r_2 \left\{ 1 - \frac{(1-r_2^2)}{r_2^2} f \sum_1^\infty (r_2 r_3 e^{-i\omega\tau})^m \right\}. \tag{3.17}$$

Equation (2.21), the Ideal PCM effective reflectivity, becomes

$$r_{eff} = r_2 \left\{ 1 - \frac{(1-r_2^2)}{r_2^2} f \sum_0^\infty \left[\left(r_2 r_3 e^{i(\phi_{pc} - 2\phi_0)} \right]^{2m+1} + (r_2 r_3)^{2m} \right) \right\}. \tag{3.18}$$

And for the Ring PPCM

$$r_{eff} = r_2 \left\{ 1 - \frac{(1-r_2^2)}{r_2^2} f \sum_1^\infty \left[r_2 r_3 e^{(\omega\tau - \phi_R)} \right]^m \right\}. \tag{3.19}$$

When the boundary conditions are imposed in Eqs. (3.16) and (3.17) they are found to be equivalent, and equal to the conventional case for $\omega\tau = 2n\pi$. For comparison, the conventional case is evaluated at $\omega\tau = 0$ and π yielding

$$r_{\text{eff}} = \frac{r_2 + [r_2^2(1-f)+f]r_3}{1 + r_2 r_3} \quad \omega\tau = \pi(PC), \tag{3.20}$$

$$r_{\text{eff}} = \frac{r_2 - [r_2^2(1-f)+f]r_3}{1 - r_2 r_3} \quad \omega\tau = 0, \tag{3.21}$$

PC indicates phase conjugate solution. These equations can be manipulated to solve for f. This results in the following two equations for the conventional case and for the phase-conjugate cases

$$f = \frac{\pm(r_{\text{eff}} - r_2)(1 \pm = r_2 r_3)}{r_3(1 - r_2^2)} \quad \begin{array}{l} + : \omega\tau = \pi\ (PC) \\ - : \omega\tau = 0. \end{array} \tag{3.22}$$

Equations (3.20) and (3.21) are plotted in Fig. 3.8 for a range of effective reflectivities. Table 3.2 summarizes the values obtained using the above data. The variance from the previous method reflects the problem with the theory discussed previously. Unless otherwise noted $f = 0.1$ will be used in the rest of this work. This falls comfortably within the calculations and is consistent with previous work.

Linewidth Narrowing and Broadening

Line shape changes of an optical spectra are driven by the phase dynamics of the laser. Optical feedback can provide line narrowing or broadening for a semiconductor laser. In this instance the external cavity acts as a filter (or amplifier) for phase noise. The result is an increase or decrease in the self-coherence of the laser source. This effect is well known and has been studied by many authors [81-85]. Line narrowing of a single diode laser due to phase-conjugate

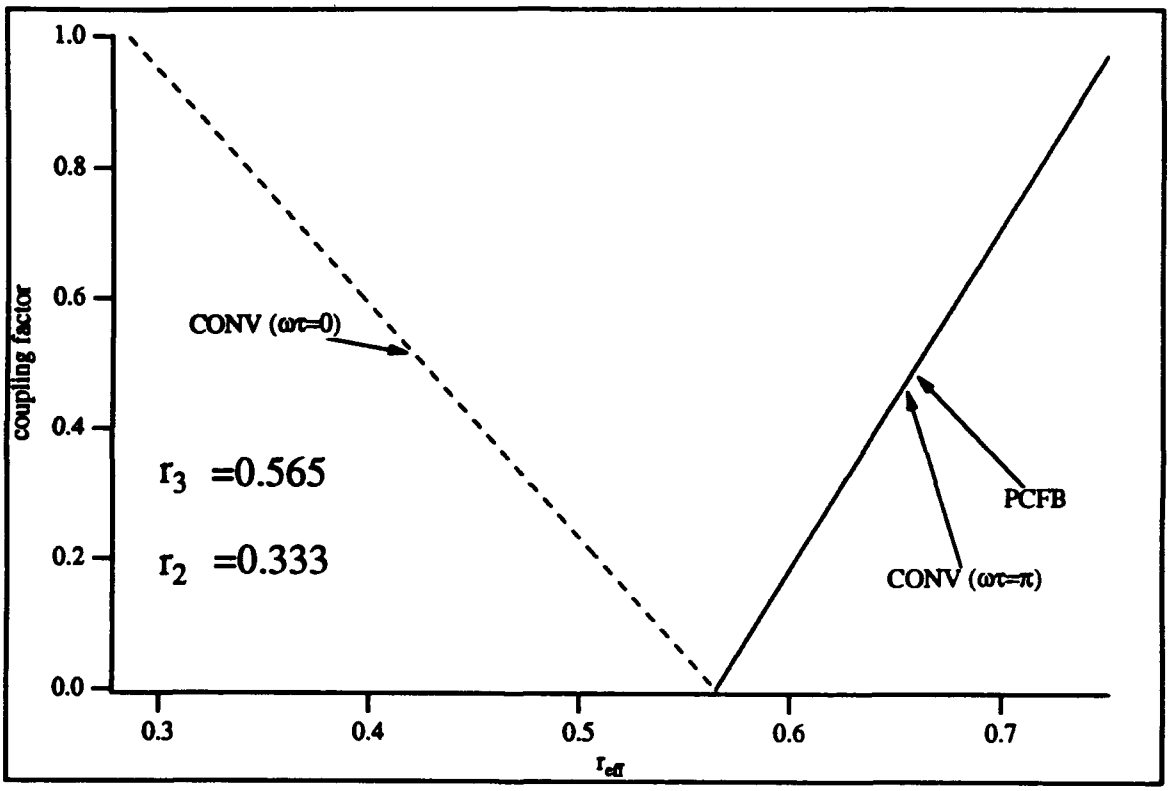

Fig. 3.8. Coupling factor "f" versus effective reflectivity.

feedback has been observed by two other groups [27, 86]. In the first case an anti-reflection coated laser diode was used. It emitted a broadband spectrum without the feedback. The PCM just lowered the threshold gain for a particular wavelength. In the second case Kerr type four-wave mixing produced the phase-conjugate beam. The narrowing was independent of the distance between the semiconductor lasers, as would be expected.

The amount of narrowing/broadening can be determined by defining a line-width reduction factor F^2 (F is called the chirp reduction factor). This is simply

$$F^2 = \frac{\Delta f_0}{\Delta f}, \tag{3.23}$$

where Δf_0 is the linewidth of the free running laser and Δf is the linewidth of the laser with feedback. F can be derived from the relation between Ω and ω

$$F = \frac{d\Omega}{d\omega}, \tag{3.24}$$

where Ω is the radial wavelength of the free running laser and ω is the radial wavelength of the laser with feedback [80].

Recall from Eq. (2.38) that, in the steady state, this relationship is

$$\Delta\omega = \omega - \Omega = \kappa\left(\frac{\alpha\cos\omega\tau - \alpha r_2 r_3 + \sin\omega\tau}{1 - 2r_2 r_3\cos\omega\tau + r_2^2 r_3^2}\right),$$
$$\text{where } \kappa = \frac{(1-r_2^2)r_3}{r_2}.\frac{f}{\tau_d}, \tag{3.25}$$

$$\Omega = \omega - \kappa\left(\frac{\alpha\cos\omega\tau - \alpha r_2 r_3 - \sin\omega\tau}{1 - 2r_2 r_3\cos\omega\tau + r_2^2 r_3^2}\right). \tag{3.26}$$

thus

$$F = \frac{d\Omega}{d\omega} = -(\tau)\kappa\Big[(1 - 2r_2 r_3\cos\omega\tau + r_2^2 r_3^2)(\cos\omega\tau - \alpha\sin\omega\tau)$$
$$- (2r_2 r_3\sin\omega\tau)(\alpha\cos\omega\tau - r_2 r_3 + \sin\omega\tau)\Big]$$
$$\times\left(\frac{1}{1 - 2r_2 r_3\cos\omega\tau + r_2^2 r_3^2}\right)^2. \tag{3.27}$$

Typically, this is evaluated at a specified value of $\omega\tau$. For $\omega\tau = 0, \pi$, the following result is obtained

$$F = \frac{d\Omega}{d\omega} = 1 \mp \frac{\kappa\tau}{(1 \mp r_2 r_3)^2} \quad \begin{matrix} - : \omega\tau = 0 \\ + : \omega\tau = \pi. \end{matrix} \tag{3.28}$$

From Eq. (2.53) F can be derived for the PCECL.

$$\Delta\omega = \kappa \left[\frac{\alpha \cos(\phi_{pc} - 2\phi_0) - \alpha r_2 r_3 - \sin(\phi_{pc} - 2\phi_0)}{(1 - r_2^2 r_3^2)^2} \right], \tag{3.29}$$

which leads to the interesting result

$$F_{pc} = \frac{d\Omega}{d\omega} = 1. \tag{3.30}$$

There is no narrowing or broadening with the Ideal phase conjugate mirror! This is to be expected. The Ideal PCM impacts the laser performance purely through the change in effective reflectivity. Linewidth phenomena are driven by changes in phase.

Line narrowing has been achieved using a four-wave mixing geometry [86]. Although phase-conjugation via four-wave mixing can be modeled by the Ideal PCM, that particular experiment used non-degenerate four-wave mixing, as is typical for semiconductor lasers [32-34]. Thus those results do not contradict the above model.

For the URECL, Eq. (2.64) shows the steady state phase

$$\Delta\omega = -\kappa \left[\frac{\alpha \cos(\omega\tau - \phi_R) + \alpha r_2 r_3 + \sin(\omega\tau - \phi_R)}{1 + 2 r_2 r_3 \cos(\omega\tau - \phi_R) + r_2^2 r_3^2} \right], \tag{3.31}$$

so that the chirp reduction factor is given by

$$\begin{aligned} \frac{d\Omega}{d\omega} = 1 - \Big\{ & \tau\kappa \Big[(1 + 2 r_2 r_3 \cos(\omega\tau - \phi_n) \\ & + r_2^2 r_3^2)(\alpha \sin(\omega\tau - \phi_R) - \cos(\omega\tau - \phi_R)) \\ & - (\alpha \cos(\omega\tau - \phi_R) + \alpha r_2 r_3 + \sin(\omega\tau - \phi_R)) \\ & \times (2 r_2 r_3 \sin(\omega\tau - \phi_R)) \Big] \\ & \times \left(\frac{1}{1 + 2 r_2 r_3 \cos(\omega\tau - \phi_R) + r_2^2 r_3^2} \right)^2 \Big\}. \end{aligned} \tag{3.32}$$

If the boundary conditions are imposed this becomes

$$F_{\text{ring}} = 1 + \tau\kappa\left[\frac{1}{(1+r_2r_3)^2}\right], \tag{3.33}$$

which is equal to the conventional case for $\omega\tau = (2n+1)\pi$, consistent with the derivations so far. Figure 3.9 plots F^2 for both geometries using the parameters for this experiment ($\tau = 5.3 \times 10^{-9}$, $\tau_d = 7.4 \times 10^{-12}$, $f = 0.1$, $\alpha = -4$, $r_3 = 0.333$, $r_2 = 0.565$). There is a π phase shift with between the conventional and ring equations which is consistent with previous calculations.

An interesting consequence can occur in the conventional case, but not with the ring. As Eq. (3.26) implies there is the possibility of

$$|F| < 1. \tag{3.34}$$

In this case, the laser will experience dramatic line broadening. If $|F| = 0$, it will become infinite. On the other hand, the URECL will never experience line broadening due to this effect. This phenomena is not to be confused with coherence collapse, which results from frequency beating in the laser itself. (Indeed, the URECL can experience coherence collapse. This is addressed in Chapter 4.) The line narrowing/broadening presented here is caused by a reduction in phase fluctuations due to the optical feedback. Figure 3.10 plots F^2 for small values.

If only a single round trip is considered the expression for line narrowing concurs with the result derived by Agrawal [83]. Starting with Eq. (2.43) for the steady state frequency change

$$\Delta\omega = \kappa(\alpha\cos\omega\tau + \sin\omega\tau). \tag{3.35}$$

Define

$$\alpha = \tan\beta; \quad \cos\beta = (1+\alpha^2)^{-1/2}, \tag{3.36}$$

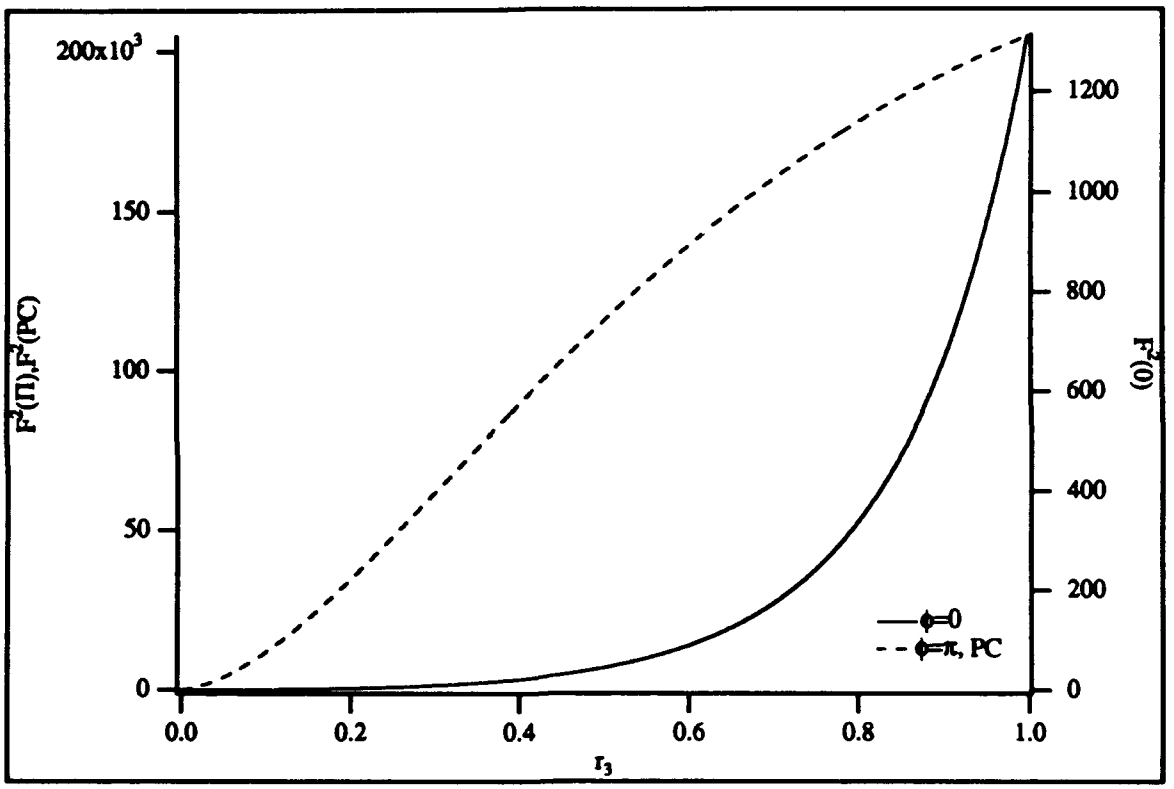

Fig. 3.9. Linewidth reduction factor versus effective reflectivity. Solid line – CECL; dashed line – URECL, CECL as noted.

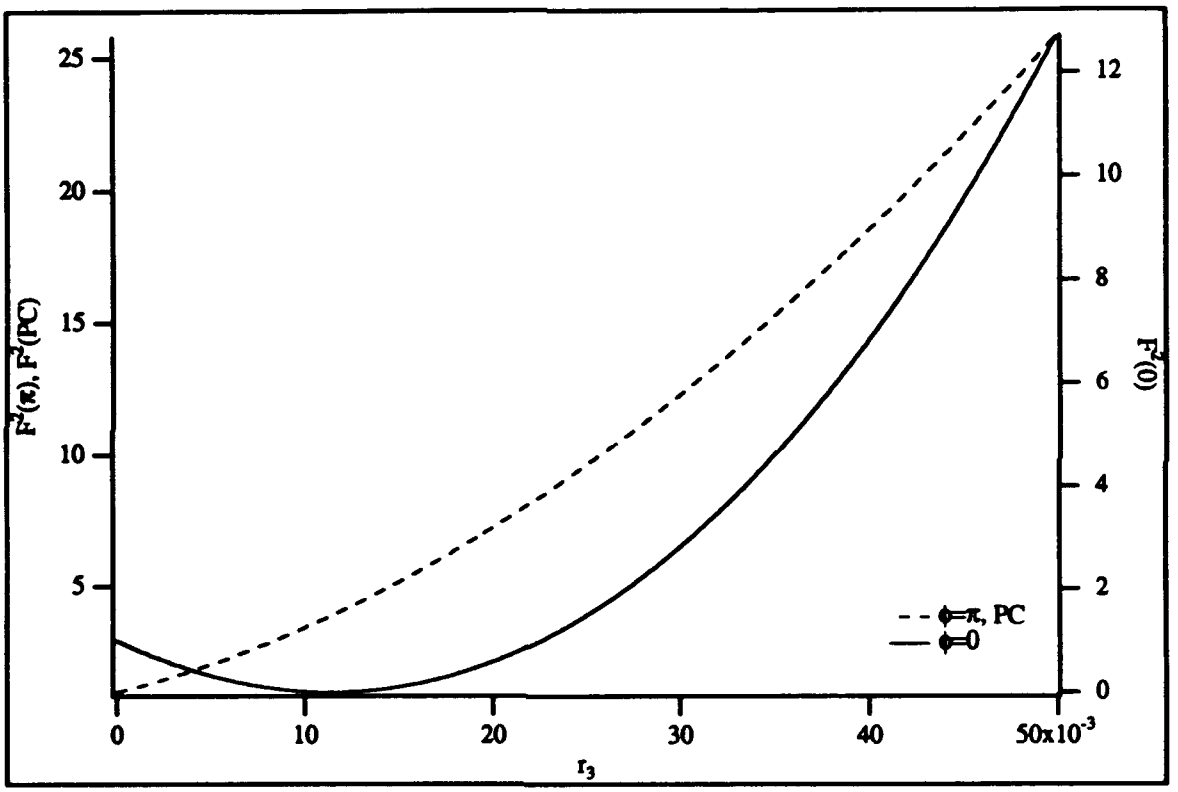

Fig. 3.10. Linewidth reduction factor versus effective reflectivity. Solid line – CECL; dashed line – URECL, CECL as noted.

to obtain

$$F_{\text{conv}} = \cos\beta \frac{d\Omega}{d\omega} = 1 - \kappa\tau[\cos(\omega\tau + \beta)], \tag{3.37}$$

which is Agrawal's result for linewidth change due to feedback. The factor $\cos\beta$ represents broadening in the free running laser due to antiguiding, not a consideration for this work. (To be exact, my F divided by this factor equals Agrawal's result for the laser with feedback.)

An inspection of Eq. (2.56) reveals, as for the multiple round trip case, that for Ideal phase conjugation

$$F_{\text{pc}} = 1. \tag{3.38}$$

Equation (2.67) gives the steady state solution for the URECL with one round trip

$$\Delta\omega = \kappa[\alpha\cos(\omega\tau - \phi_R) - \sin(\omega\tau - \phi_R)], \tag{3.39}$$

solving for F as above yields

$$F_{\text{ring}} = \cos\beta \frac{d\Omega}{d\omega} = 1 + \tau\kappa\{\cos[(\omega\tau - \phi_R) + \beta]\}. \tag{3.40}$$

By imposing the boundary conditions the solution for the ring becomes

$$F_{\text{ring}} = 1 + \kappa\tau[\cos(\arctan\,\alpha)]. \tag{3.41}$$

Equations (3.35) and (3.39) are plotted against $\omega\tau$ in Fig. 3.11. In that figure $r_2 = .565$, $r_3 = 0.010$, $\tau = 5.3 \times 10^{-9}$, $\tau_d = 7.4 \times 10^{-12}$, $\alpha = -4$, and $f = 0.1$. These equations are only valid for small values of the product $\kappa\tau$. Agrawal gives an upper limit of 10 for this number. He also mentions that the magnitude of this approximate reduction is always less than the rigorous result [83]. The main difference between including multiple round trips or a single round trips is in the antiguiding factor α. In the former, α is included implicitly. For large F^2, the "phase" shift introduced by its inclusion is not as important. However, for small F^2, it does become significant and the latter approach was used for analysis.

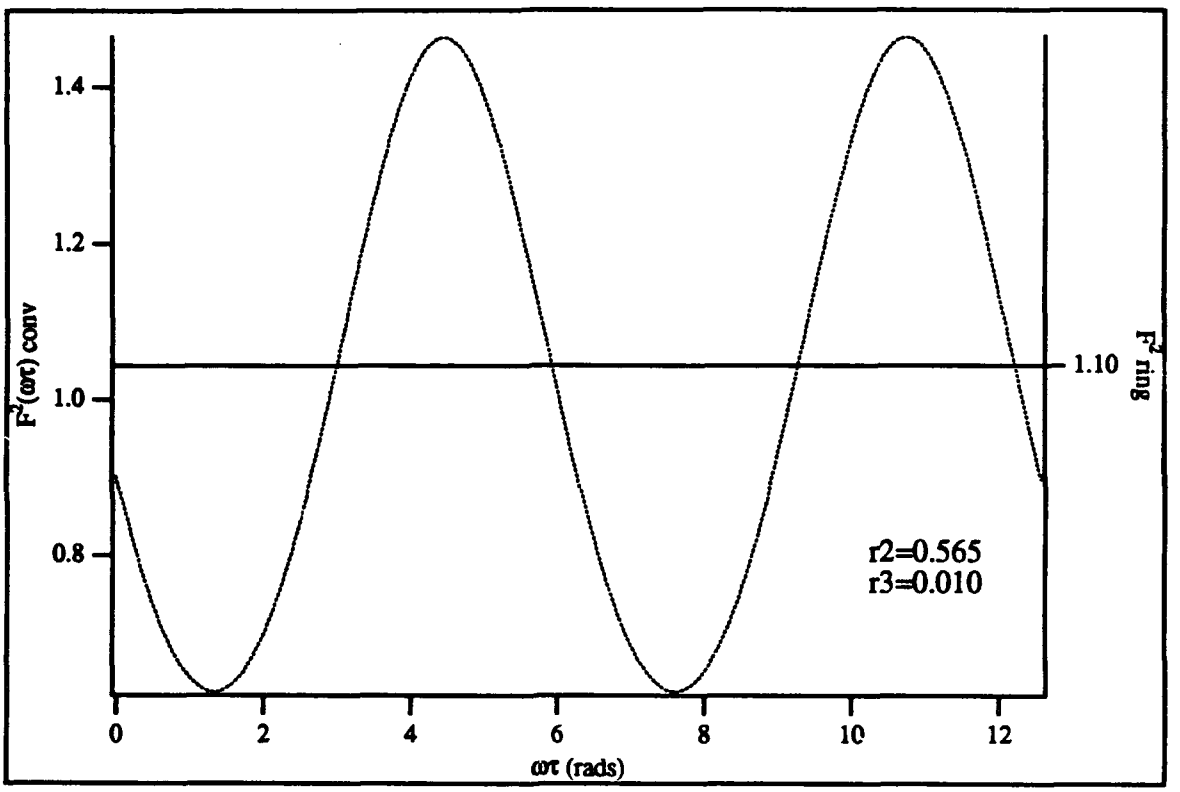

Fig. 3.11. Linewidth reduction factor versus $\omega\tau$. Dotted line – CECL; solid line – URECL.

For small amounts of feedback, linewidth narrowing with the URECL has been observed. The reflectivity of the Ring PPCM was difficult to measure at these feedback levels, due to the limitations of the detectors. In Fig. 3.12, the linewidth (FWHM) with feedback (Fig. 3.12a) is approximately 20% (THAT) of the free running laser (Fig. 3.12b) for an external amplitude reflection of 0.045. The calculated reduction is 27%. In Fig. 3.13 the measured value is 50%, the calculated value 40%, for an external reflectivity of 0.0136. The error represents the difficulty in measuring f, and the ill defined α. Note that the phase delay was assumed to be zero for these values. (The spectra were taken with FP-2.) The horizontal scale was not measured for these experiments. Later calibration indicated a scale of from 75-100 MHz/Div.

In addition to line narrowing, frequency stabilization was observed. Though not obvious from the above data, the spectra are stable: they do not shift in frequency with respect to time. This will not be obtained for arbitrary conventional feedback, special effort must be made for that. For phase-conjugate feedback from the ring PPCM it will always be obtained because the external cavity will be resonant, by definition, with the diode laser. This has been shown to stabilize the frequency [87]. This is true for the static hologram as well since any "jitter" off of the resonant frequency will not reflect unless it is within the bandwidth of the photorefractive grating, which is $\sim$ 1 Hz. (It can, of course, hop to a different lasing line, but that is a different phenomena.)

Multimode Spectra

A full multimode analysis of a semiconductor laser with feedback would be quite an undertaking and is beyond the scope of this work. However, there is a consistent and distinct behavior for the different geometries. Some generalizations can be made to qualitatively describe what has been observed.

The spectra for the free-running laser, Fig. 3.14, are typical for semiconductor lasers. The spectra were taken at 5% above threshold current, 10% above,

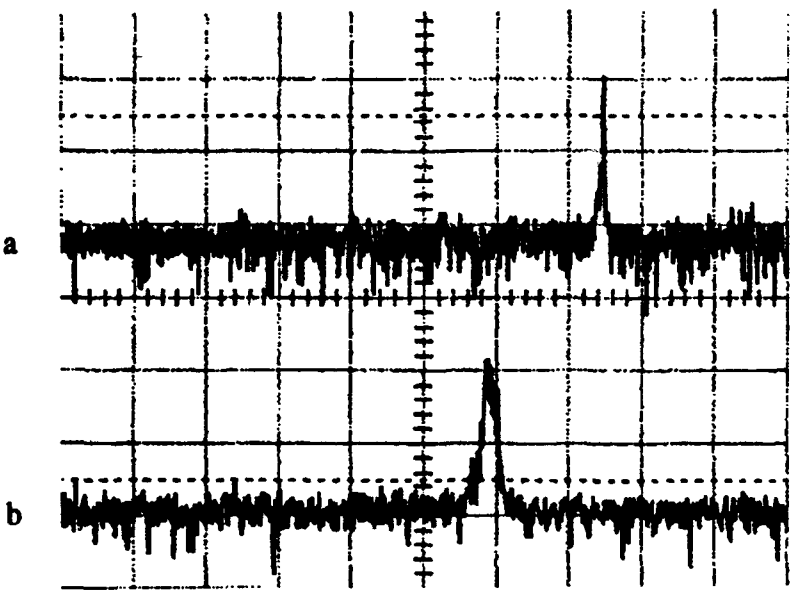

Fig. 3.12. Linewidth narrowing for $r_3 = .045$. (a) with feedback and (b) without feedback.

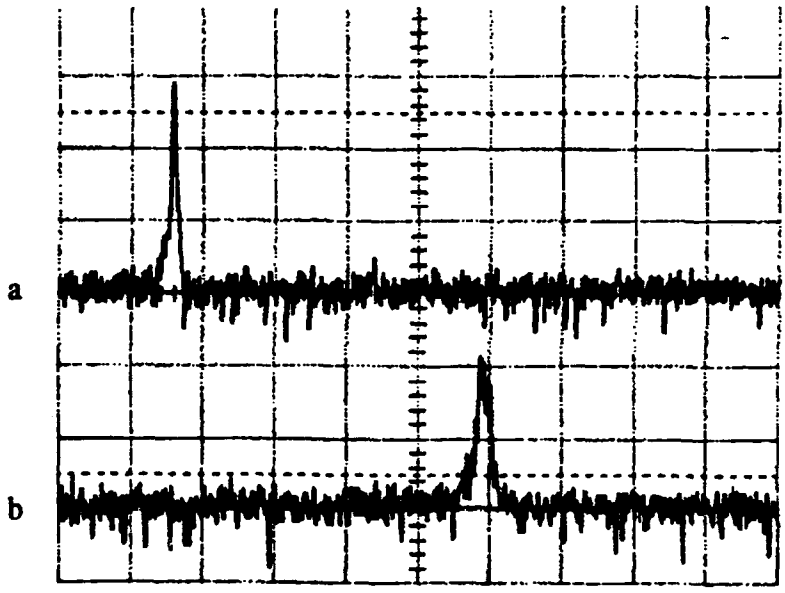

Fig. 3.13. Linewidth narrowing for $r_3 = .0136$. (a) with feedback and (b) without feedback.

and then in increments of 10% until the current was 150% of threshold current. The free running laser starts out multimode (Fig. 3.14a) and gradually becomes single mode (Fig. 3.14g). The gain peak shifts with increasing current and the gain curve appears asymmetric.

The CECL spectra are taken the same way (Fig. 3.15). The power reflectivity, measured at 75 mA, was 4.5%. The laser starts out multimode and stays that way due to the optical feedback. The mirror does not discriminate, all wavelengths are reflected equally. But the longitudinal modes can have different phase delays, specified by their frequency and the external cavity length. External cavity modes are also present with a spacing of $c/2L$, where c is the speed of light and L is the length of the external cavity. The length of the CECL was kept at half the length of the URECL so that the external cavity modes would have the same frequency spacing. Note the structure of the spectra: the modes seem to be alternating in intensity. This feature was common for any reflectivity.

When the external cavity mirror is adjusted at a particular pump current, it sets the phase delay for each mode at that current only. As the current is changed, the lasing frequencies can change. If only the relative intensities of the modes shift, the phase delay $\omega\tau$ will remain constant for each individual mode. If the individual frequencies of the modes vary, then they will experience a change in delay phase with every change in current. Either way, each line of the multimode spectra will have a different phase delay for conventional feedback.

The URECL spectra were recorded in a similar fashion (Fig. 3.16). The power reflectivity, measured at 75 mA, was 5%. This is about 40% above current threshold. Again the laser is multimode throughout. In this case the mirror is a phase conjugator or static hologram, as discussed. As the current changes, the gain peak shifts. The intensity of the modes taper off from the highest gain lasing mode with no evidence of alternating intensity peaks (or other structure).

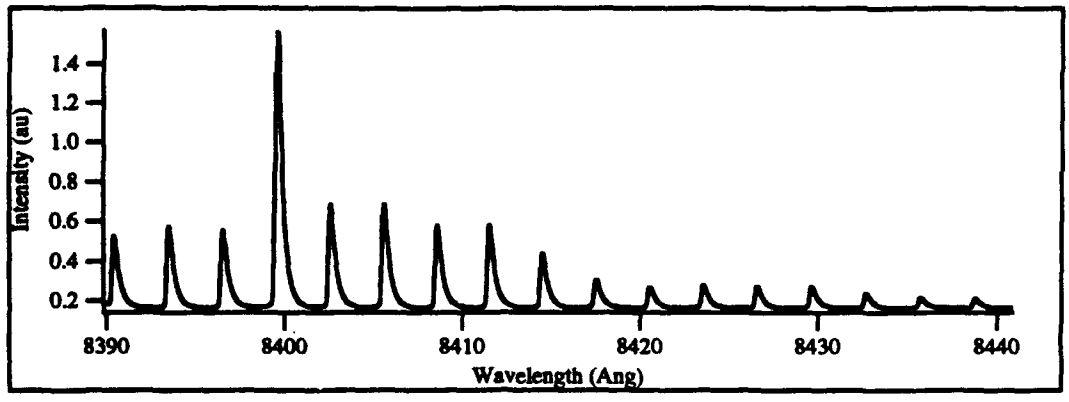

(a)

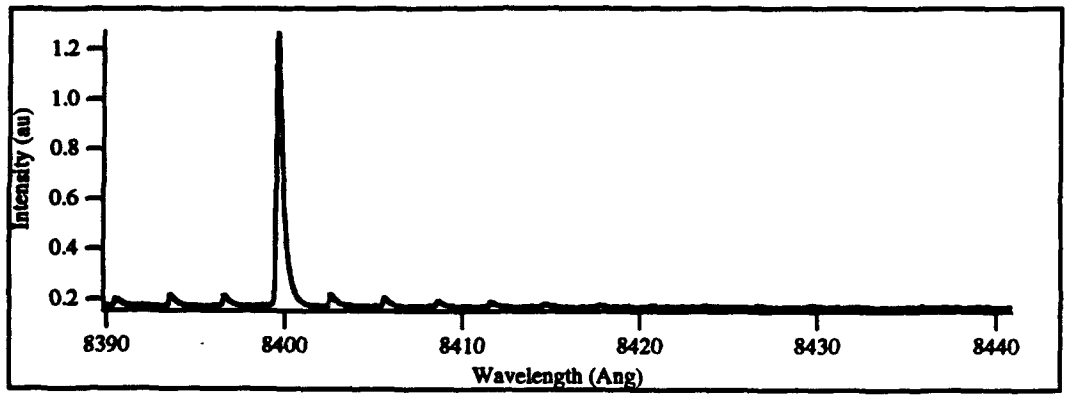

(b)

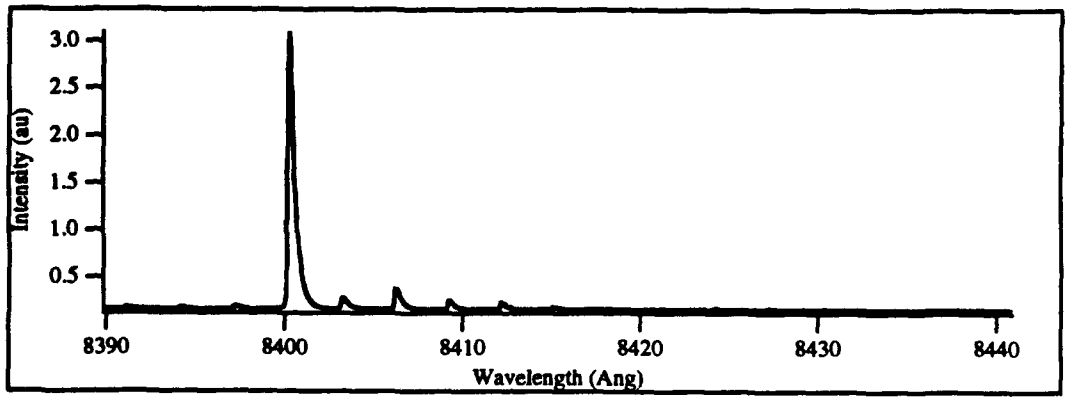

(c)

Fig. 3.14. Free running laser. (a) 105% current threshold, (b) 110% current threshold, and (c) 120% current threshold.

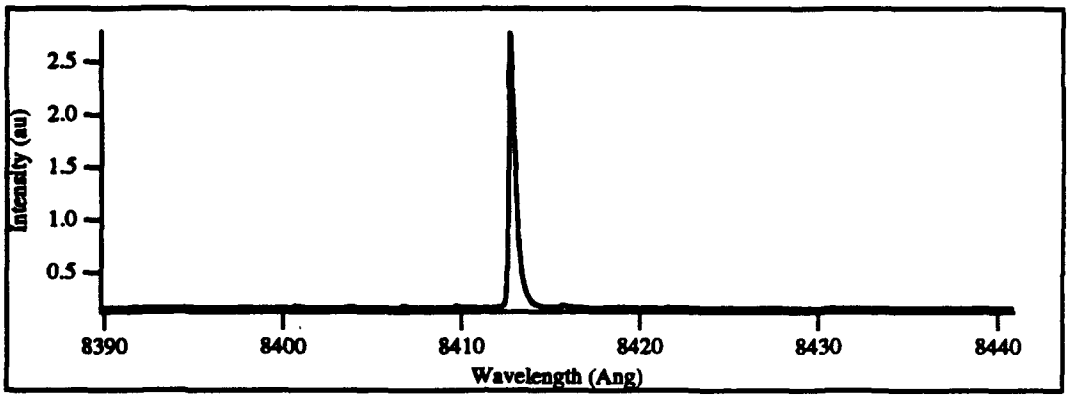

(d)

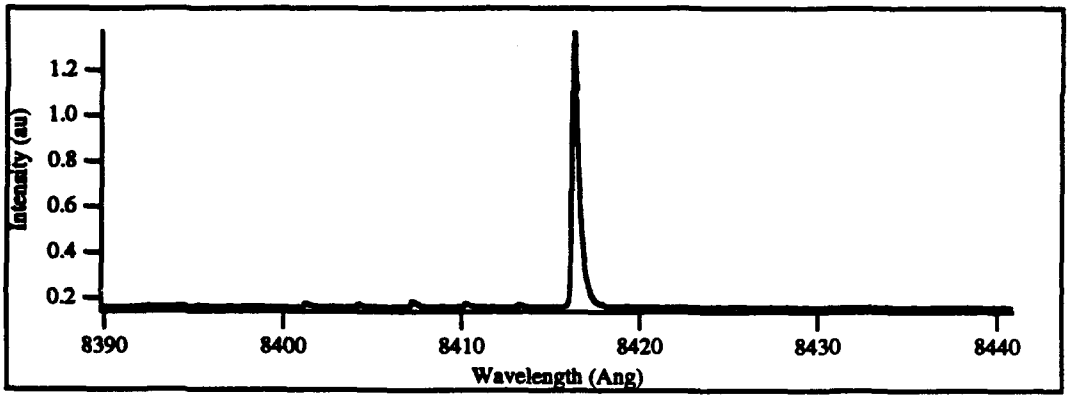

(e)

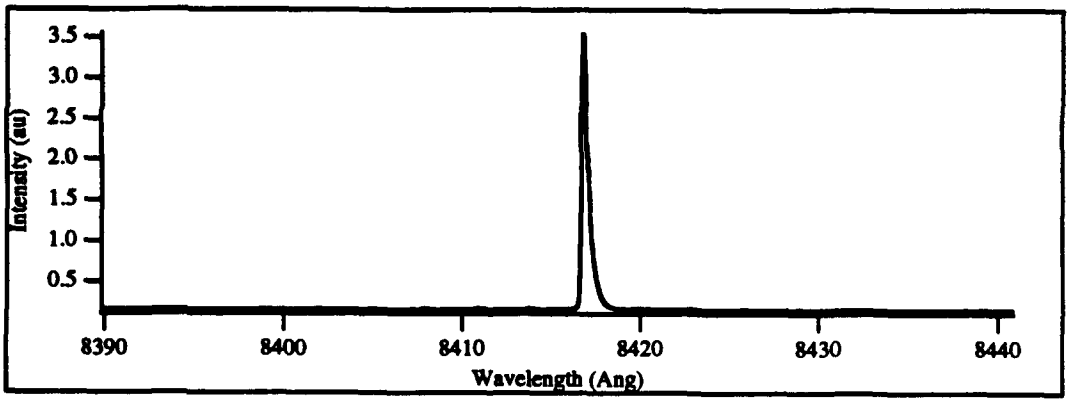

(f)

Fig. 3.14. Continued ... (d) 130% current threshold, (e) 140% current threshold, and (f) 150% current threshold.

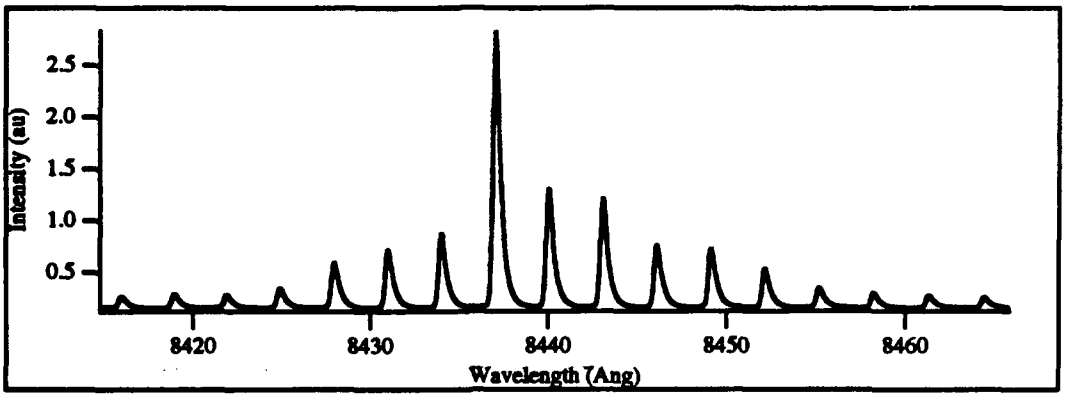

(a)

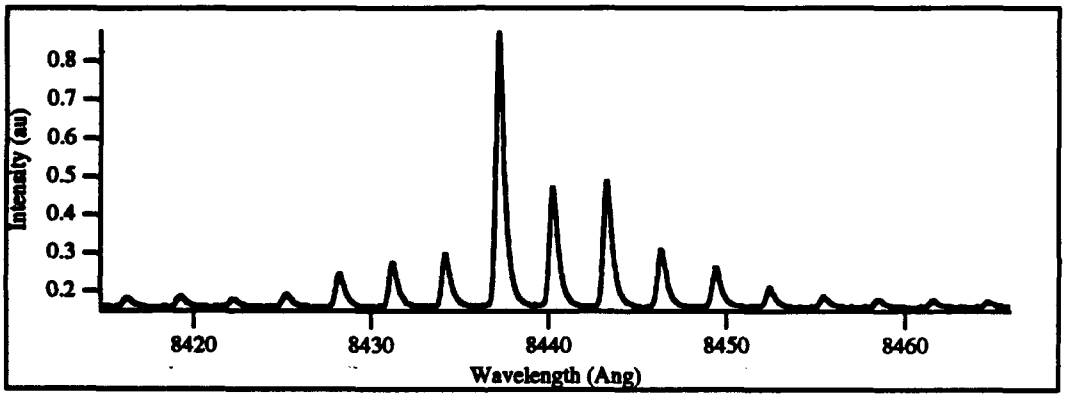

(b)

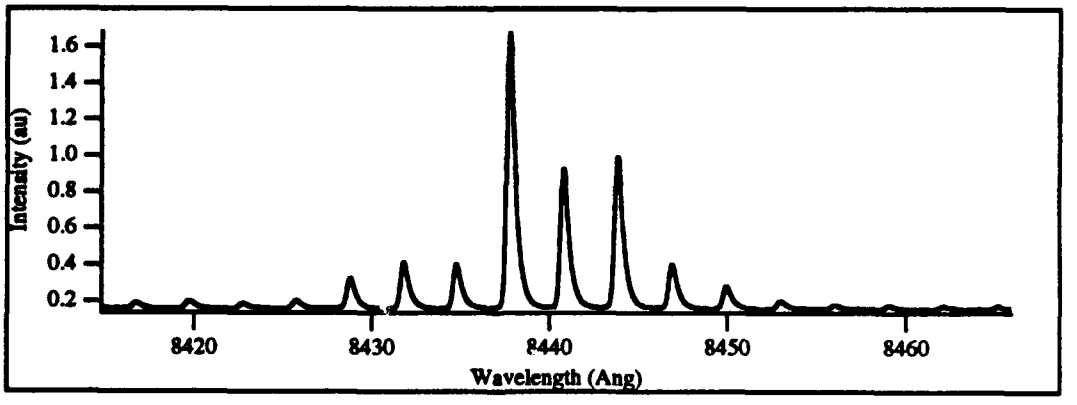

(c)

Fig. 3.15. Laser with conventional feedback. (a) 105% threshold current, (b) 110% threshold current and (c) 120% threshold current.

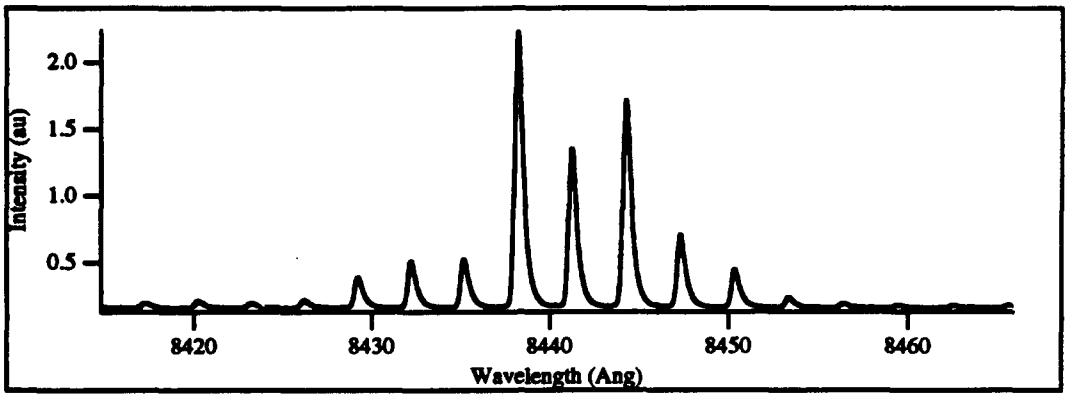

(d)

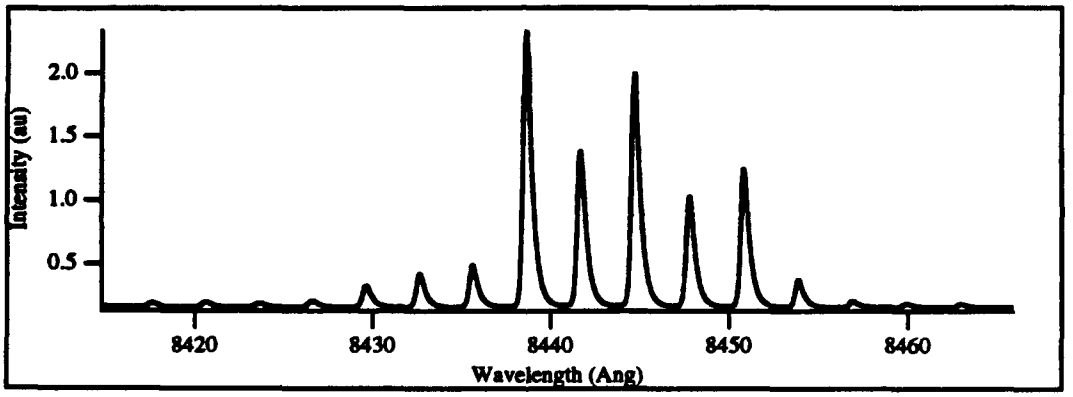

(e)

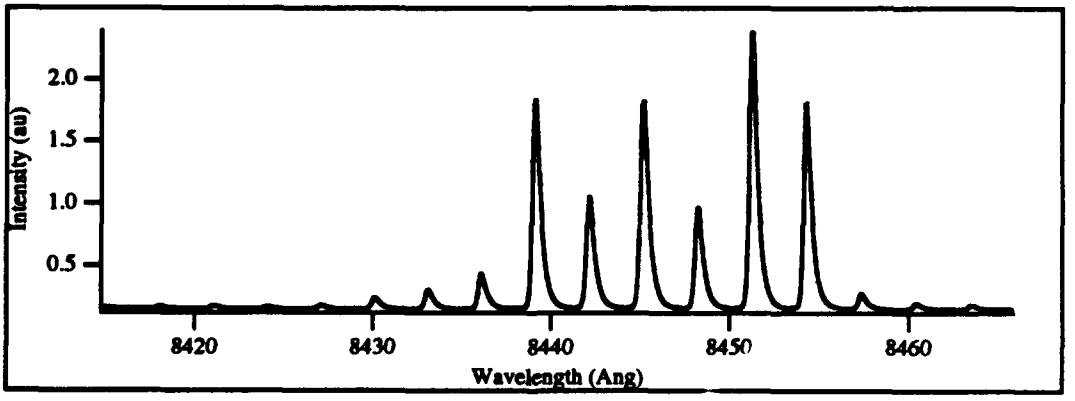

(f)

Fig. 3.15. Continued ... (d) 130% threshold current, (e) 140% threshold current and (f) 150% threshold current.

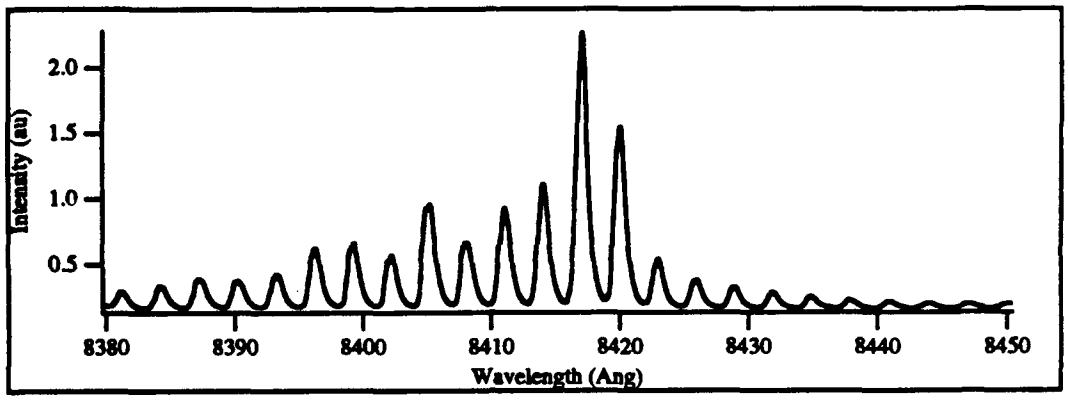

(a)

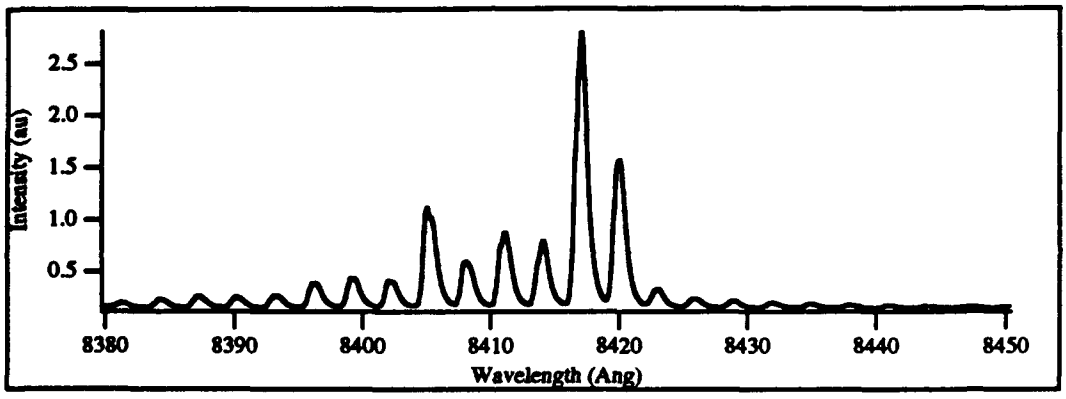

(b)

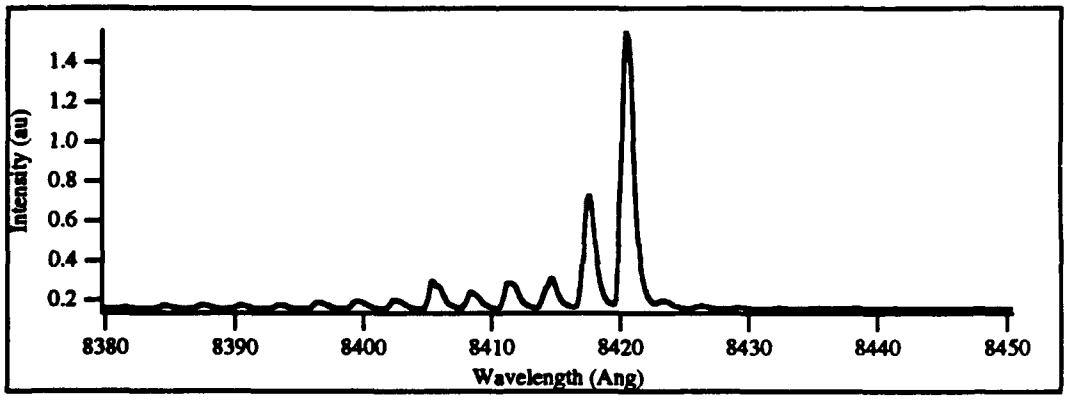

(c)

Fig. 3.16. Laser with phase-conjugate feedback. (a) 105% threshold current, (b) 110% threshold current and (c) 120% threshold current.

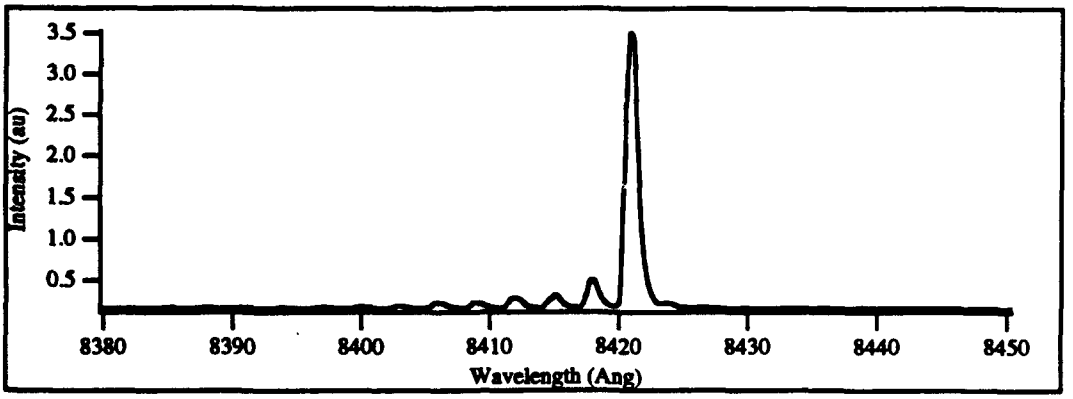

(d)

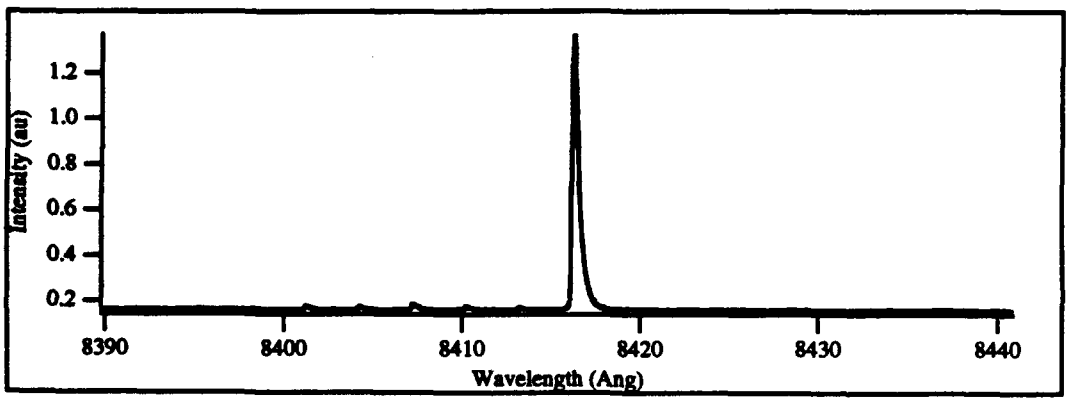

(e)

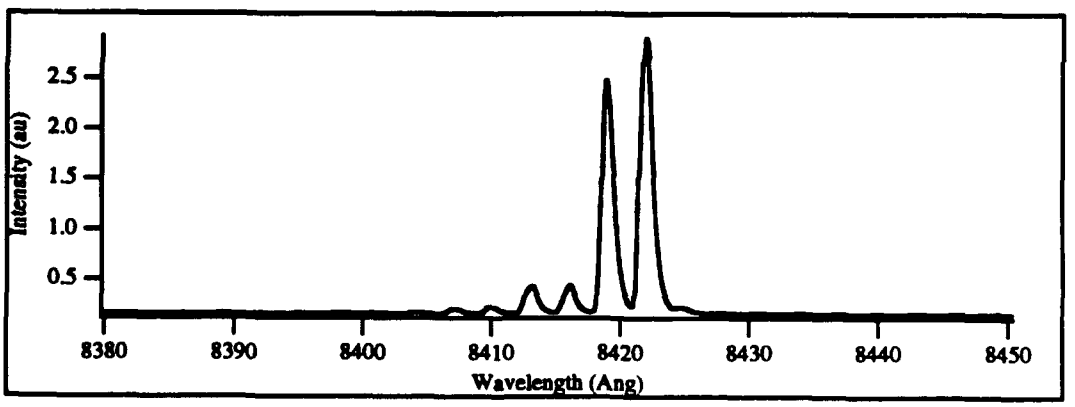

(f)

Fig. 3.16. Continued ... (d) 130% threshold current, (e) 140% threshold current and (f) 150% threshold current.

This feature is consistent for all reflectivities, although more side modes may be present. External cavity modes are present, corresponding to the c/L spacing of the ring cavity (see Chapter 4).

In the Barium Titanate crystal there is a collection of gratings; one grating for each lasing frequency in this geometry. If, as the current is varied, only the relative intensity of the modes change, the phase delay for each mode will remain constant at the value determined by the grating determined by the grating ($2n\pi$). If the frequency of the individual modes change, then the PCM will act as a static hologram. (Remember: $BaTiO_3$ is too slow to account for quick changes in frequency.) However, since no new gratings will be written the laser modes will be driven by the phase matching conditions of the static gratings. Thus the phases will not be free to vary arbitrarily, and will be equal to $2n\pi$, just as for the phase-conjugate case. Unlike the phase conjugate case, there will be a phase bandwidth for each mode. In $BaTiO_3$, the allowable phase mismatch is on the order of 1 Hz.

The structure that is exhibited by the CECL and absent in the URECL can be simply explained. The external cavity will impart a different delay phase to each longitudinal mode since $\omega\tau$ will be different for each. If the main peak of the spectra has a phase $\omega\tau$ then the delay phase of the other modes can be expressed as

$$\omega_n\tau = \omega_0\tau + n\Delta\omega\tau, \tag{3.42}$$

where n is any integer, ω_n is the radial frequency of the Nth mode, τ the round trip time in the external cavity, and $\Delta\omega$ is the radial frequency spacing of the laser. The peak with the greatest intensity is assumed to have $2n\pi$ phase delay. The optical feedback allows other modes to lase that normally would not. However, the losses will be different for each mode [70]. The coupled external cavity can be thought of as an effective facet with a phase dependent loss. If this is

modeled by a cosine function and the expression in Eq. (3.42) is its argument, then the intensity of the longitudinal modes will vary as

$$I(\omega_n \tau) \sim g(\omega_n \tau) \cos^2(\omega_n \tau), \tag{3.43}$$

where $g(\omega n \tau)$ describes the gain curve. In principle one could measure the mode spacing and delay time and fit the model to this. Unfortunately this requires a knowledge of the product $\omega\tau$ to better than one part in twc thousand. Fortunately, the external cavity is long enough to support almost any mode spacing chosen. Thus if

$$\Delta\omega\tau = s\pi, \tag{3.44}$$

where the arbitrary constant s is fitted to the data, Fig. 3.17a is obtained. This plot demonstrates how well this approximation works.

For the ring PPCM the boundary conditions require that the phase delay be equal to $2n\pi$. Thus the additional modes will have no frequency dependent facet loss and the intensity will go as

$$I(\omega_n \tau) \sim f(\omega_n \tau) \cos^2(2n\pi). \tag{3.45}$$

This is shown in Fig. 3.17b.

In Figs. 3.18 and 3.19 further confirmation is presented. Figures 3.18 and 3.19 both show the longitudinal spectra of a semiconductor laser with phase-conjugate feedback. The difference between the two is that in the former case the alignment of the beams is intentionally skewed so that the four beams are no longer co-planar. Thus the return beam will have an additional phase component as can be seen from the the analysis in Chapter 2. The return beam will not be phase conjugate to the pump beam, as the phase conjugate beam would be out of the plane. The laser sees reflection off a static hologram that is out of phase .

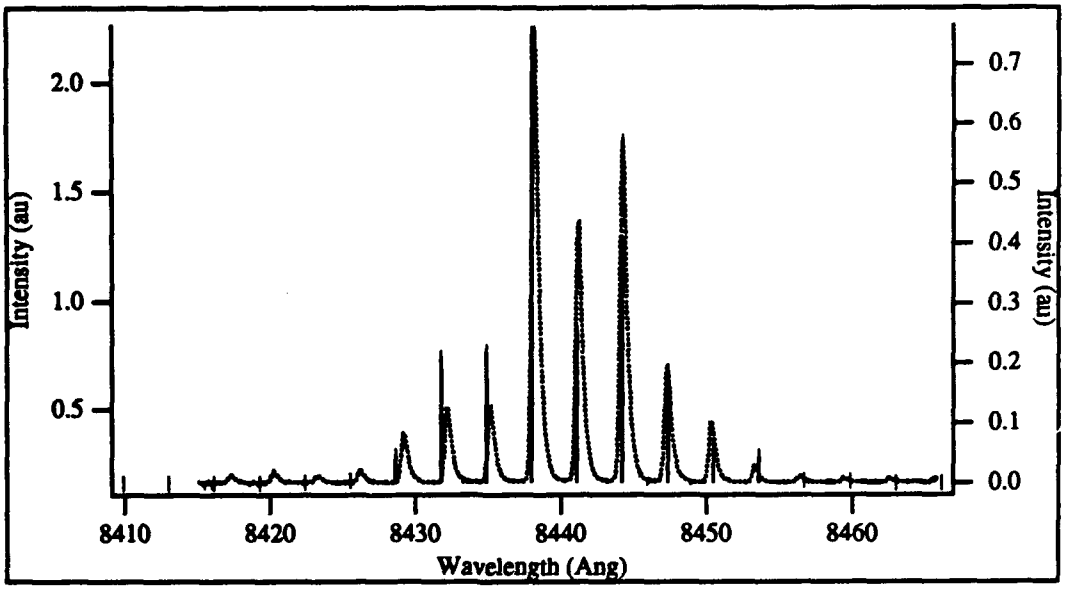

(a)

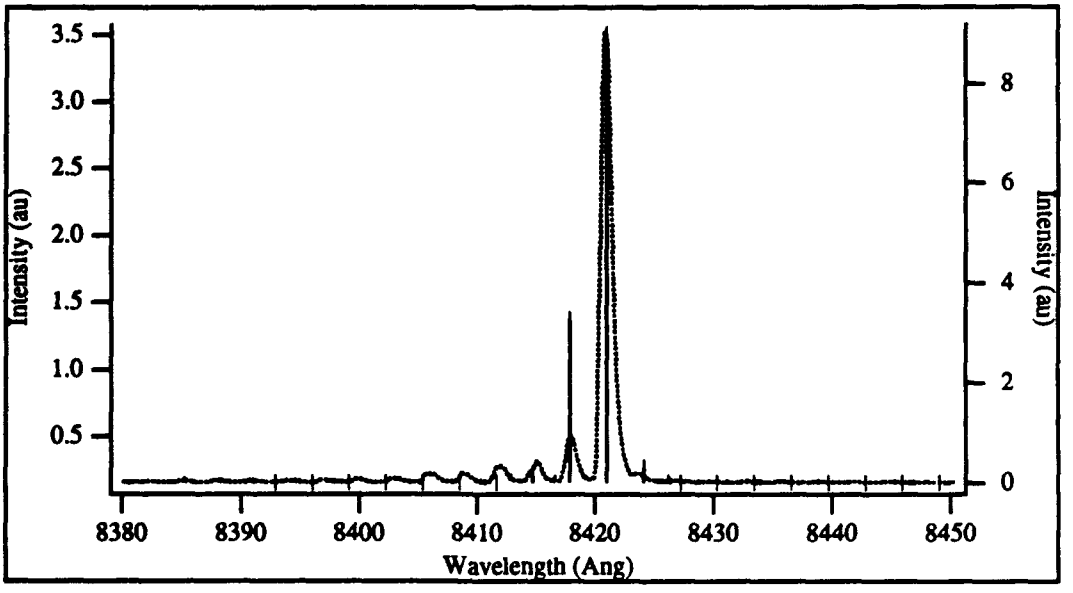

(b)

Fig. 3.17. Model of multimode spectra. (a) CECL and (b) URECL. Dotted line – experimental, solid line – model.

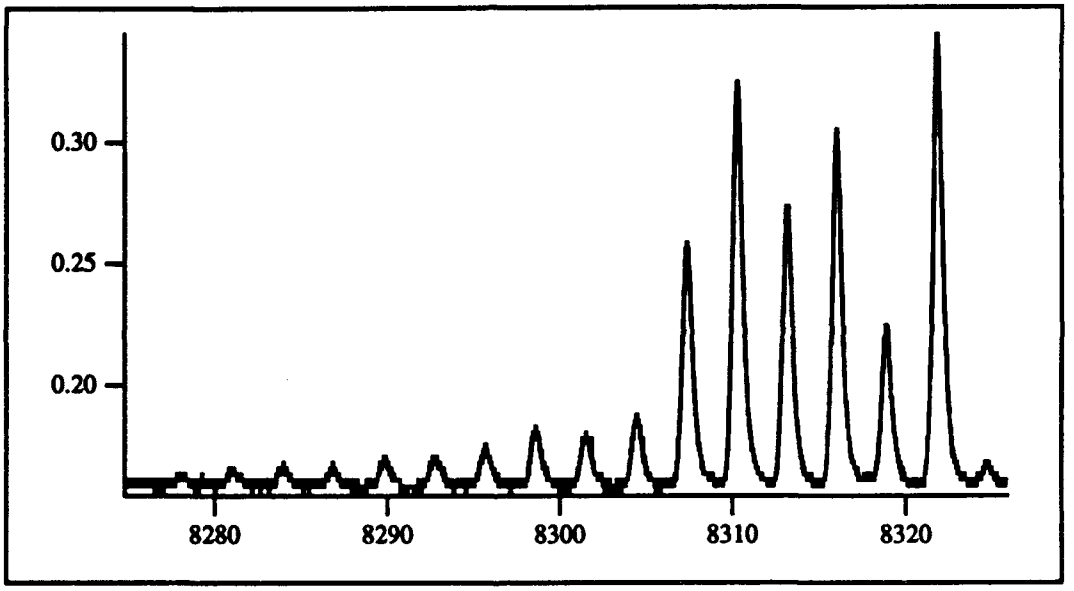

Fig. 3.18. Poor quality feedback from ring.

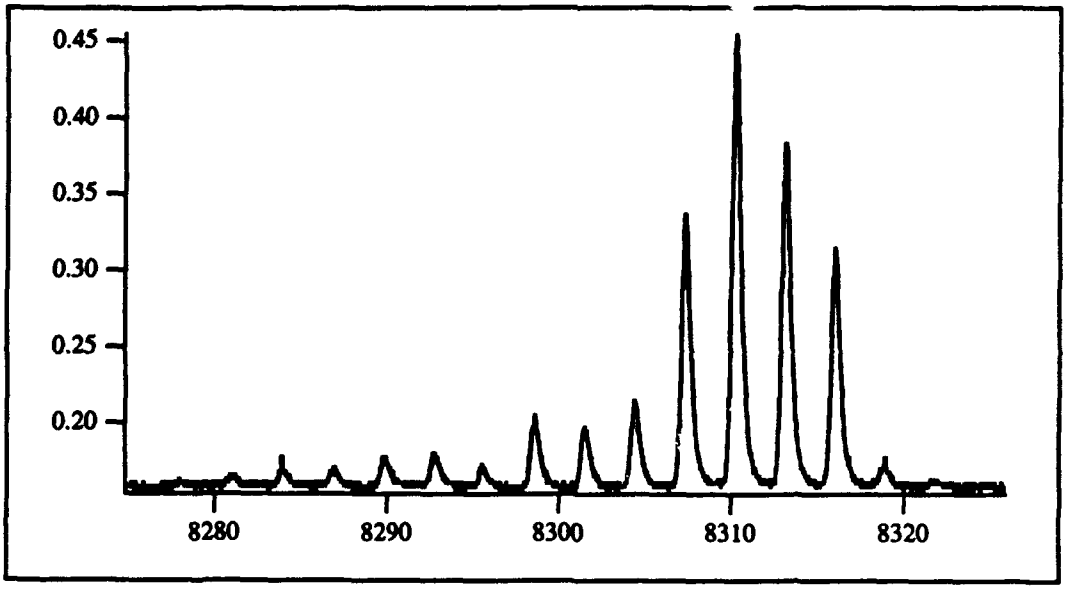

Fig. 3.19. Good quality feedback from ring.

The alignment in the latter case is quite good. Phase matching is preserved and the results indicate uniform phase delay for all longitudinal modes.

This theory has serious limitations: gain competition, mode spacing shifts, mode coupling and other effects are ignored. A full dynamical treatment, allowing for a change in pump current, would have to take those factors into account. But the $2n\pi$ phase delay concept for the ring PPCM is shown to be viable, and this phenomenological explanation may suffice for other properties as well.

Summary

In this chapter the static properties of the Ideal PCM and the Ring PPCM external cavities have been examined and compared to the conventional external cavity. Following a detailed description of the experimental set-up the boundary conditions for the PCECL and URECL were derived. These cavities were found to have a $2n\pi$ phase delay. This was supported by an examination of the L-I characteristics of the URECL. The effective reflectivities were discussed in depth and the coupling factor f was defined and derived. The chirp reduction factor F was derived for all cases, with the interesting result that $F = 1$ for the PCECL. The linewidth reduction factor was compared for all geometries. Linewidth narrowing compared well with the data (further supporting the $2n\pi$ phase delay theory). Multimode spectral phenomena were displayed and an empirical explanation of their behavior provided.

CHAPTER 4

DYNAMIC PHENOMENA: COHERENCE COLLAPSE

Coherence collapse is the term used to describe the dramatic linewidth broadening of a semiconductor laser due to optical feedback [88]. In this chapter the first evidence of this phenomena with a phase-conjugate external reflector is presented. The discussion begins with a description of the experimental geometry and technique. This will be followed by the presentation of the data, clearly showing coherence collapse for the semiconductor laser with feedback from the ring PPCM. Then some data demonstrating external cavity mode suppression at low levels of phase-conjugate feedback, a result previously unseen for even the conventional case, will be presented. The chapter will close with a discussion of the rate equations for the conventional external cavity laser (CECL), Ideal phase-conjugate external cavity laser (PCECL), and the unidirectional ring passive phase-conjugate external cavity laser (URECL).

Experimental Set-Up

The experimental geometry used for this study was essentially the one described in Chapter 3. The diagnostics consisted of the spectrum analyzer (SA), monochromator (MONO), and Fabry-Perot 2 (FP2) as shown in Fig. 4.1. The Fabry-Perot has a free spectral range of 16.5 GHZ. An etalon was inserted between the attenuator and crystal to ensure that the laser ran in single longitudinal mode. This is important because coherence collapse is a single mode phenomenon. The round trip length of the external cavity was 169.5 cm. The

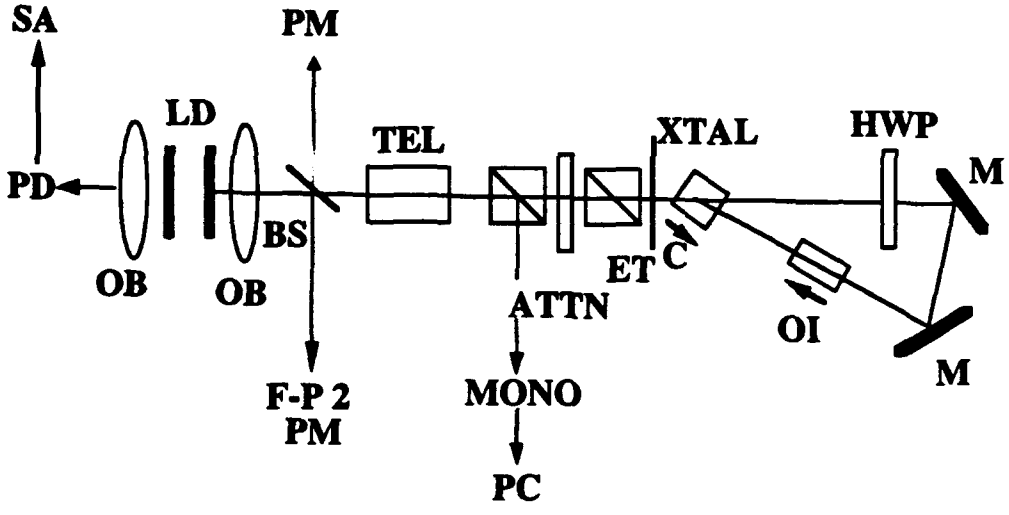

Fig. 4.1. Coherence Collapse Geometry.

maximum power reflectivity of the ring PPCM was typically 14.5%. The attenuator is capable of nearly 0-100% transmission but the power meters are only able to discern to the microwatt range. This, coupled with the background levels, made low reflectivities difficult to measure. The configuration allowed for the simultaneous recording of the noise spectra, the FP2 spectra, longitudinal spectra, and the F-P spectra.

Experimental Technique

The laser was operated at a constant pump current throughout each run. Several runs were performed and the data was easily reproducible. The gratings would be written at particular intensity (corresponding to a particular pump current) for 15-20 minutes with the attenuator set for maximum through-put. Then it would be turned down to the desired reflectivity and the data taken. The crystal would again be illuminated at previous writing intensity while the data was recorded and preparations made for the next point. This was done to insure that the gratings remained constant in strength and frequency throughout the experiment.

Results

The effects of the self-pumped phase conjugate feedback are seen in Fig. 4.2, the FP2 spectra, Fig. 4.3, the noise spectra taken from the spectrum analyzer, and Fig. 4.4, the monochromator (longitudinal mode) spectra. For these experiments r_3 varies from 0 to 5.2×10^{-2}.

The onset of coherence collapse is clearly seen in Fig. 4.2. The vertical scale is in linear arbitrary units and is consistent throughout. The free running laser is plotted in Fig. 4.2a. The laser is stable and single mode, with no observable external cavity modes or longitudinal sidebands. As soon as feedback is observed,

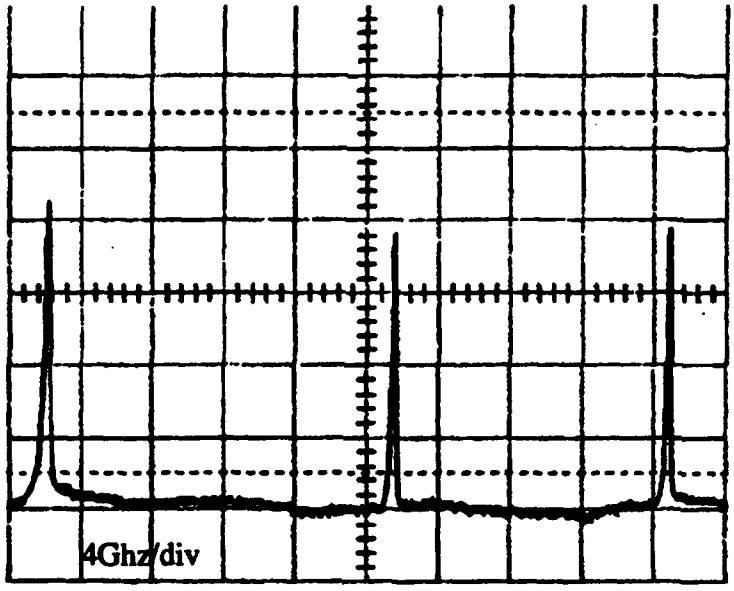

(a)

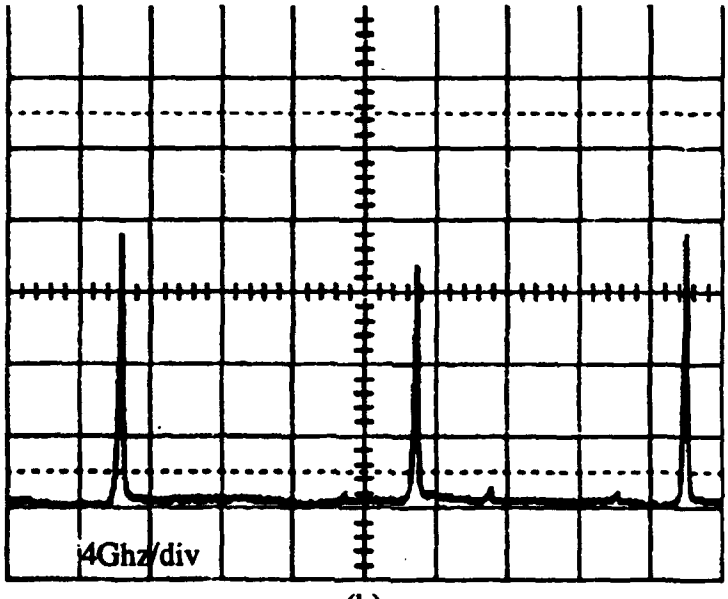

(b)

Fig. 4.2. Fabry-Perot spectra of laser with feedback. (a) free running, and (b) $r_3 < 0.0141$.

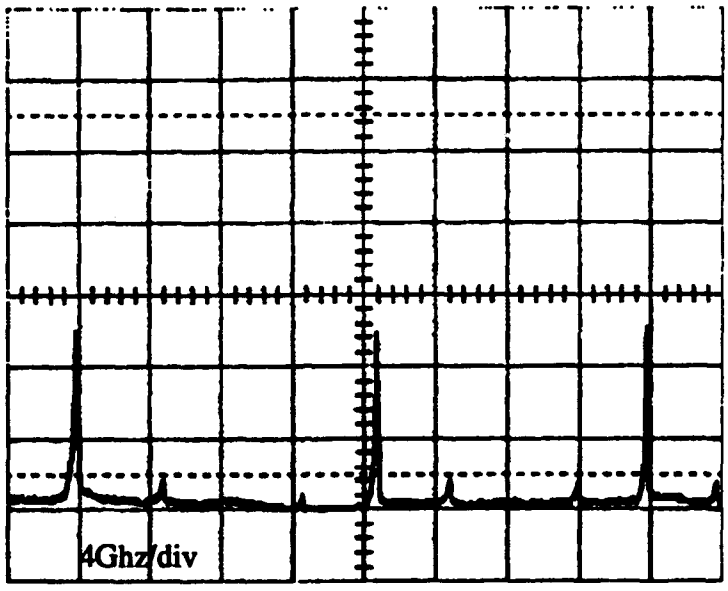

(c)

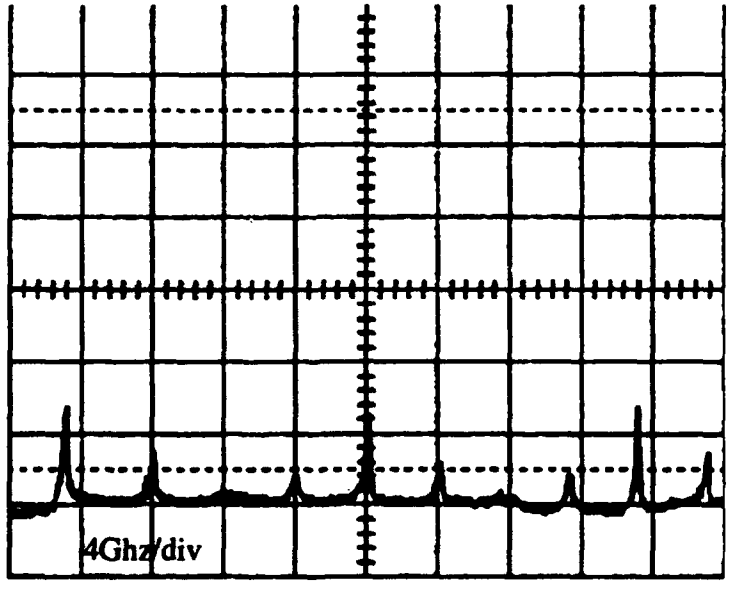

(d)

Fig. 4.2. Continued – (c) $r_s < 0.0141$, and (d) $r_s = 0.0265$.

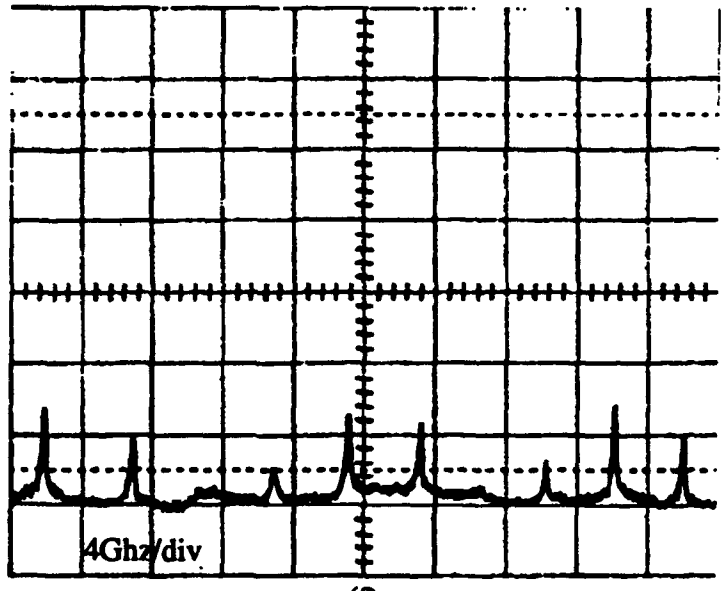

(f)

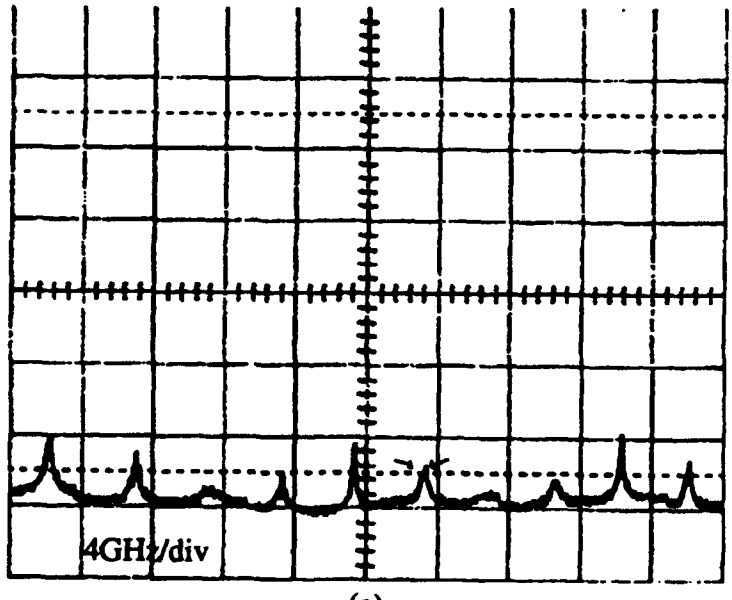

(e)

Fig. 4.2. Continued – (e) $r_s = 0.0300$, and (f) $r_s = 0.0316$.

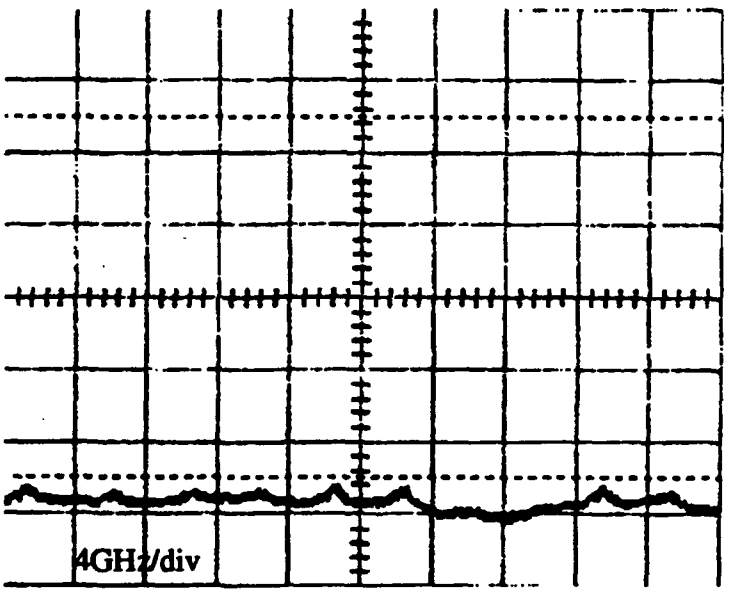

(g)

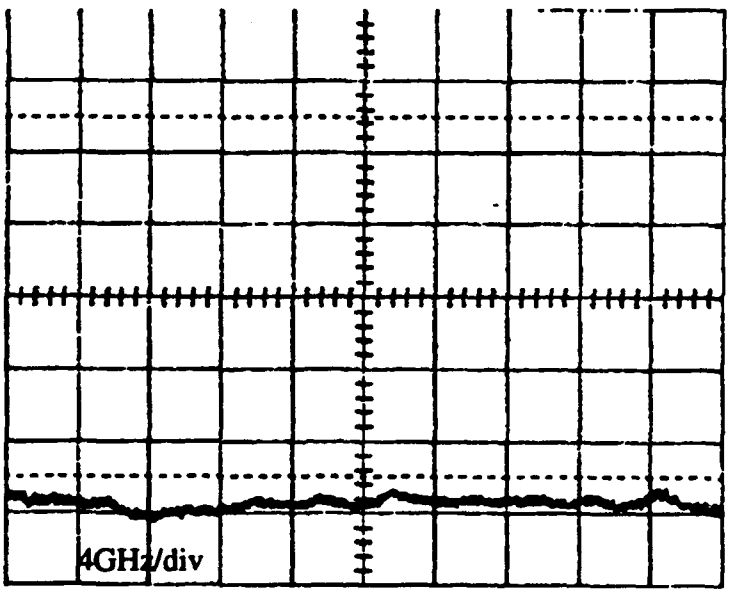

(h)

Fig. 4.2. Continued - (g) $r_s = 0.0458$, and (h) $r_s = 0.0520$.

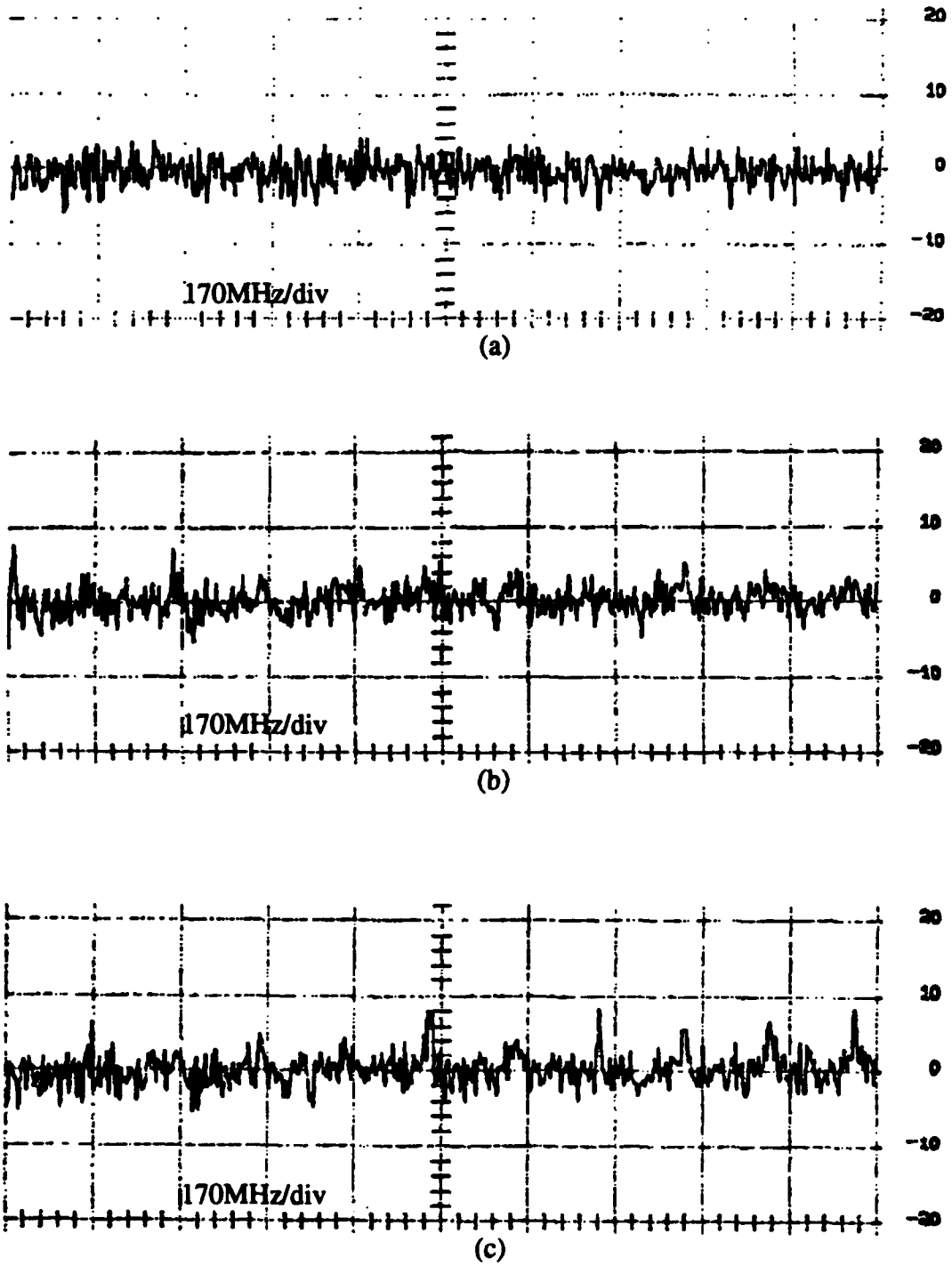

Fig. 4.3. Noise spectra of laser with feedback. (a) $r_3 < 0.0141$, (b) $r_3 = 0.0265$, and (c) $r_3 = 0.0300$.

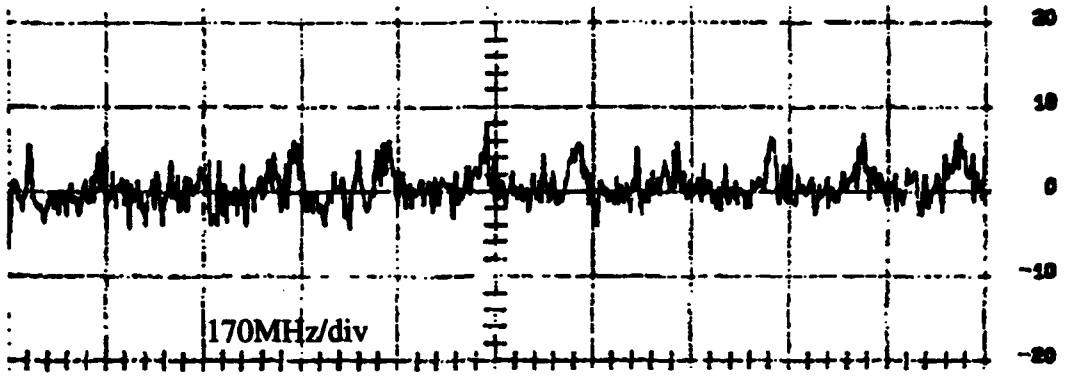

(d)

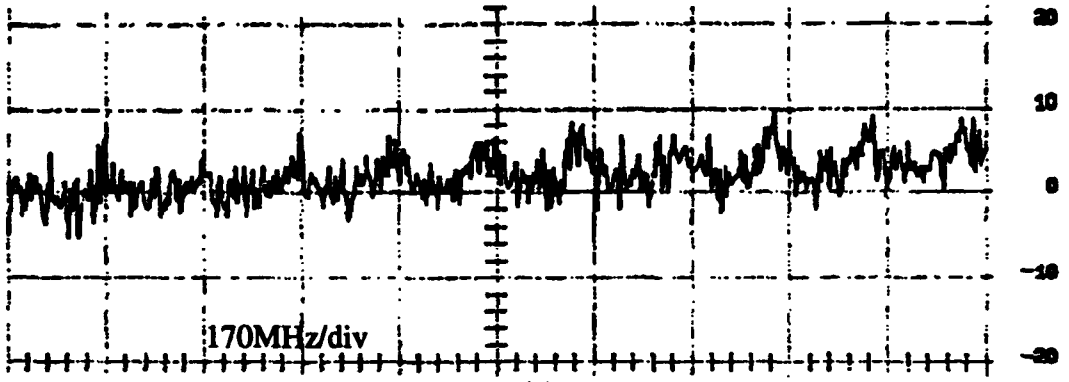

(e)

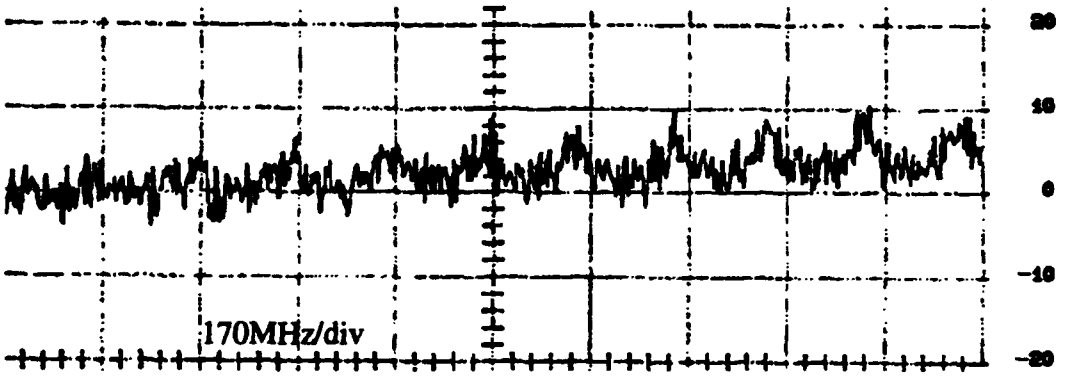

(f)

Fig. 4.3. Continued – (d) $r_s = 0.0316$, (e) $r_s = 0.0458$, and (f) $r_s = 0.0520$.

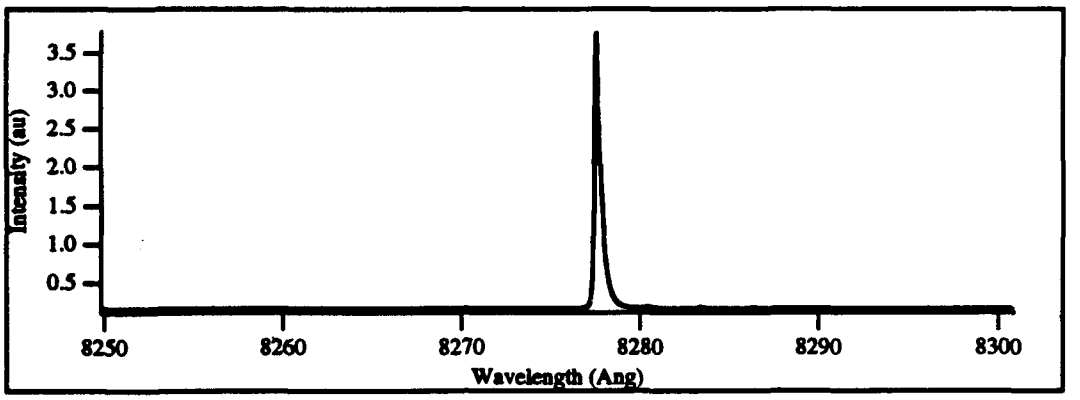

(a)

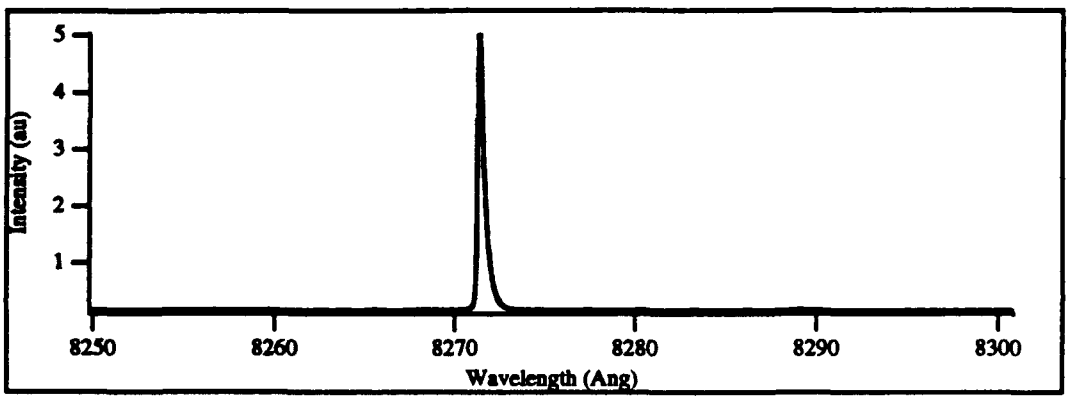

(b)

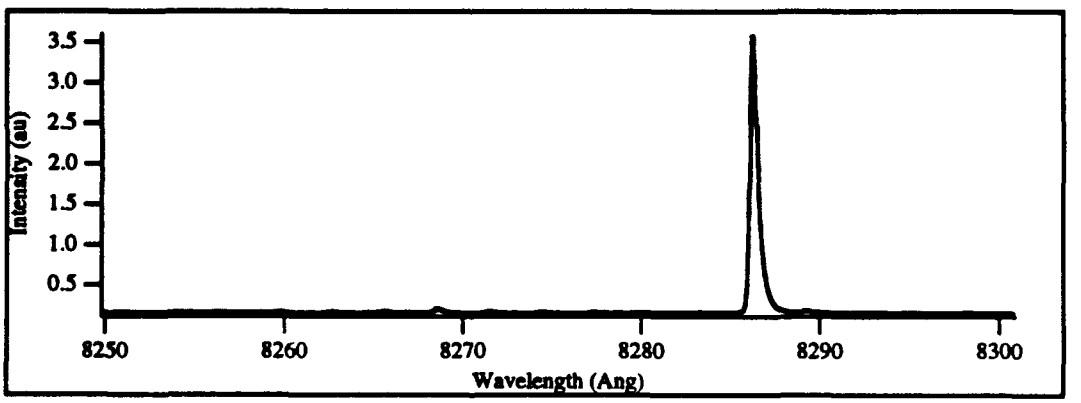

(c)

Fig. 4.4. Longitudinal spectra during coherence collapse. (a) Free running laser, (b) $R < 2 \times 10^{-4}$, and (c) $R = 7 \times 10^{-4}$ and above.

Fig. 4.2b, lasing at the relaxation oscillation frequencies takes place, 4.4 GHZ on either side of the main lasing mode. The feedback is to low to accurately measure at this point, except to say that the external amplitude reflectivity, $r_3 < 0.0141$. This corresponds to a coupling coefficient $\kappa = 2.3 \times 10^8$ sec^{-1}. Although the reflectivity is increased (Fig. 4.2c), it is still to low to be measured. Suffice it say that it is still below 0.0141. But even a small increase gives rise to higher intensities at the relaxation oscillations.

As the external reflectivity is increased to 0.0265 (Fig. 4.2d) the main lasing peaks are beginning to broaden. $\kappa = 4.31 \times 10^8$ sec^{-1} at this point. A slight increase in r_3 has a significant impact (Fig. 4.2e, $r_3 = 0.0300$, $\kappa = 4.9 \times 10^8$ sec^{-1}). When the reflectivity has reached 0.0316, $\kappa = 5.1 \times 10^8$ sec^{-1} (Fig. 4.2f), the linewidth of the laser has greatly broadened; the main lasing peak is barely discernible from the undamped relaxation oscillations. The arrows point to structure within the peak that although observable is beyond the resolution of the instrument. At $r_3 = 0.0458$, $\kappa = 7.5 \times 10^8$ sec^{-1} (Fig. 4.2g) the lasing mode is so broad that it can be seen, but not resolved by the instrument. Finally, as seen in Fig. 4.2h complete coherence collapse has taken place. The reflectivity is 0.0520; $\kappa = 8.5 \times 10^8$ sec^{-1}. Any further increase in the feedback level has no discernible effect on the FP2 spectra.

The noise spectra are revealing as well. The vertical scale is in decibels. Until the external reflectivity reaches 0.0265 (Fig. 4.3b) the spectra of the laser with low feedback (Fig. 4.3a) is indistinguishable from the free running laser. In the former case, external cavity modes corresponding to 169 MHz are just visible. This is slightly more than would be calculated, 177 MHz, for a cavity of this length, 1.695 m. This relates to the error in estimating the optical path length of some of the optics.

The initial modes that appear are unstable in intensity, bouncing up and down in time with no apparent pattern. They occur at the frequencies expected

for the external cavity (given the above caveat). Suppression of alternate modes can take place as the reflectivity increases. This takes place just before stable, normally spaced modes appear and is discussed later in the chapter.

An increase of the external reflectivity to 0.0300 brings about discernible modes at the ring cavity spacing c/L (Fig. 4.3c). The modes are noisy, as can be seen. This was not always the case, sometimes they were quite distinct. They become somewhat clearer with an increase of r_3 to 0.0316 (Fig. 4.3d). At $r_3 = 0.0458$ there is a gentle rise in the baseline of the spectra (Fig. 4.3e). This is an indication of increased power output from the rear facet. As seen above, this is at the coherence collapsed state. A further increase in reflectivity increases this rise (Fig. 4.3f). Coherence collapse is now complete ($r_3 = 0.0520$). Additional increase in feedback cause a continued rise in the baseline and a blurring of the external cavity modes.

The longitudinal spectra undergoes little change throughout this process. It begins single mode and stays that way. Even the slightest amount of feedback causes the line to jump. The free running spectra is shown in Fig. 4.4a. The slightest amount of feedback causes the laser line to jump as shown in Fig. 4.4b, corresponding to Fig. 4.2b above. The remains stable in both frequency and intensity at this reflectivity and above until the external reflectivity reaches 0.0265. Then it jumps again as seen in Fig. 4.4c. It is still stable in intensity and there is no jitter. This is the wavelength at which the photorefractive gratings were written. Any further increase does not cause a shift or hopping. The laser remains at the wavelength. No instabilities are observed. The slight sidebands towards the blue do not grow throughout the coherence collapse process.

Discussion of the Coherence Collapse Data

The behavior of the URECL corresponds exactly to what is now commonly called coherence collapse: small amounts of feedback cause a dramatic linewidth

broadening in a single mode laser [74]. As the Fabry-Perot spectra show, the relaxation oscillations become undamped. Since the laser is a nonlinear medium they can beat with the lasing line and the external cavity modes. In principle the beat frequencies can be measured [74]. The structure visible in the frequency peaks strongly suggest that such beating is going on within the laser.

The observation of external cavity modes illuminate the difference between a self-pumped PCM and an Ideal PCM; they would not be present in the latter case. Their onset occurs after the relaxation oscillations become undamped. Thus this phenomena should still occur in the PCECL as long as the external PCM can reflect at the relaxation oscillation frequency.

The longitudinal spectra corroborate an problem mentioned earlier in Chapter 3: the nature of the coupling at extremely low reflectivities. Previously this gave rise to error in the calculation of the coupling factor f. Here it is a demonstration that crystal is behaving, initially at least, as a static hologram. The ring PCM can only reflect at certain discrete wavelengths that will support the initial boundary condition. There were no other wavelengths present during the writing phase at the higher intensity. The phase matching conditions are not relaxed.

Even when the laser operates at the grating writing wavelength it can still act as a static hologram. The time scale of phase fluctuations in the laser diode is on the order of microseconds. This is seven orders of magnitude faster than the response time of Barium Titanate. If this was not so there would be no line narrowing (Chapter 3). The consequence for coherence collapse is that although the phase delay of the cavity may not be arbitrary, it acts in every other respect as a conventional external cavity. So the similarity to previous work is not surprising [74].

Unlike the PCECL, the URECL, static hologram or not, retains phase delay information. It has been suggested [74, 91] that the process of coherence collapse

is dependent on the product $\kappa\tau$, where κ is the coupling factor and τ is the delay time. The values for κ derived in this experiment are an order of magnitude less than that of earlier work [74]. The external cavity length used here is an order of magnitude longer. This suggests just such a correlation.

Increasing the reflectivity past the coherence collapsed state was difficult because the maximum power reflectivity of the ring PCM was only 14.5%. If the ring was allowed to be bidirectional, this could be increased to approximately 50% power reflectivity. For conventional lasers single mode behavior will return at high reflectivities. Some signs of this were apparent with the ring. As seen in Chapter 3, the multimode longitudinal spectra would tend towards single mode as the feedback level was increased. Occasionally, but not routinely, external cavity modes would re-appear out of the noise as the reflectivity was increased. No indication of linewidth narrowing, or even a reduction in linewidth from the coherence collapsed state was ever observed, though, again, this could be due to the limitations of the reflector.

It has been suggested that chaos plays a role in the onset of coherence collapse [74]. In that work, the route to chaos was chartered as "f_1 – f_2 – chaos," where f_1 is the relaxation oscillation frequency, and f_2 was loosely defined as corresponding to a beat frequency within the laser. The structure observed in our spectra fits with that behavior. If, indeed, there is a route to chaos mechanism for conventional feedback, feedback from the ring should be susceptible to it as well. This mechanism may be quite different for an Ideal PCM [63]. Although in that work it was shown that instabilities due to the undamping of the relaxation oscillations can take place, there are no external cavity modes, thus no beating with them.

This point warrants further consideration. Conventional wisdom has held that coherence collapse is caused by the frequency beating (within the gain

medium) of the lasing line, external cavity modes, and the relaxation oscillators. This is chaotic, thus the linewidth will be broadened due to phase instabilities. The problem cannot simply be solved by increasing the signal-to-noise ratio. The theory proposed by Agrawal and Klaus suggest there may be a different mechanism. It is not clear that this is coherence collapse. Further work in this area is ongoing.

External Cavity Mode Suppression

A curious phenomena was observed during the experiments: at extremely low reflectivities alternate external cavity modes would be suppressed. This behavior was seen repeatedly and occurred with the URECL, not the CECL. The absence or presence of the etalon made no difference so it is not necessarily a single mode phenomena. The mode suppression was seen in both the transient case and steady state. The former is shown in Figs. 4.5a and 4.5b. In that experiment the spectral behavior of the URECL was tracked as the gratings built up in the crystal. The laser started out free running and ended up in the steady state feedback condition. As the gratings became strong enough to reflect, external cavity modes would appear. At first they were unstable as described above. During the transition from unstable random modes to stable normally spaced modes, mode suppression would occur. This is at an amplitude reflectivity of 0.017 and is shown in Fig. 4.5a. A slight increase to 0.024 results in normal behavior, although the intensity of the initial modes remains high until more feedback is provided (Fig. 4.5b).

If the gratings have been previously written the same behavior can still be observed. This is seen in Figs. 4.6a and 4.6b. In that case a static hologram has been written in the crystal. By adjusting the attenuator, the mode suppression can be produced at a reflectivity of 0.014. Below a certain minimum reflectivity

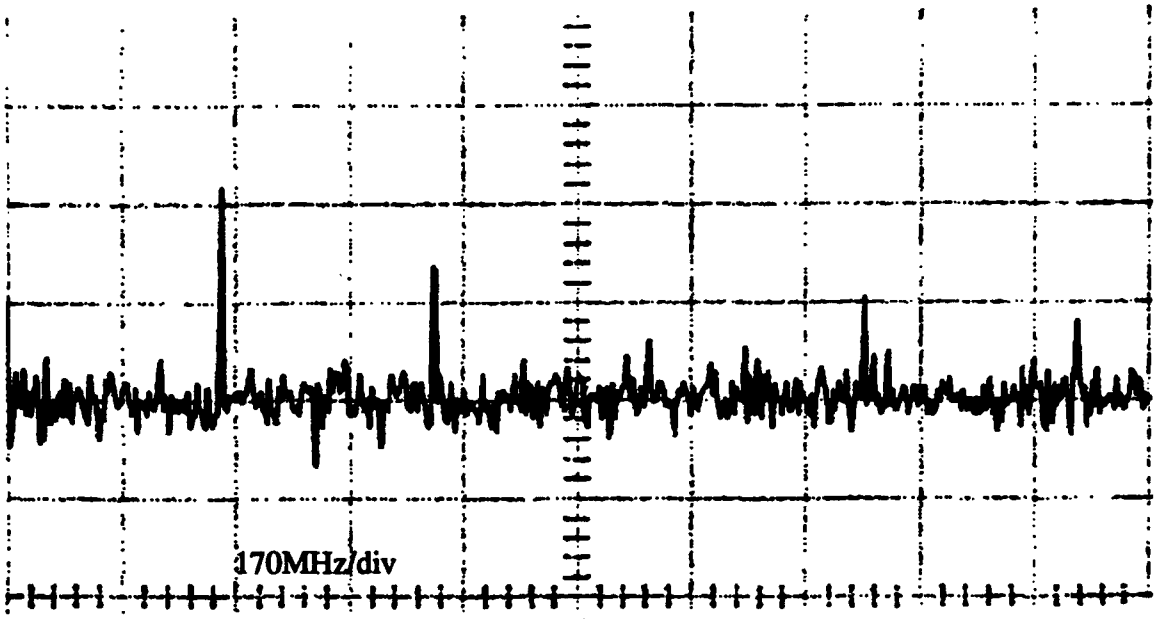

(a)

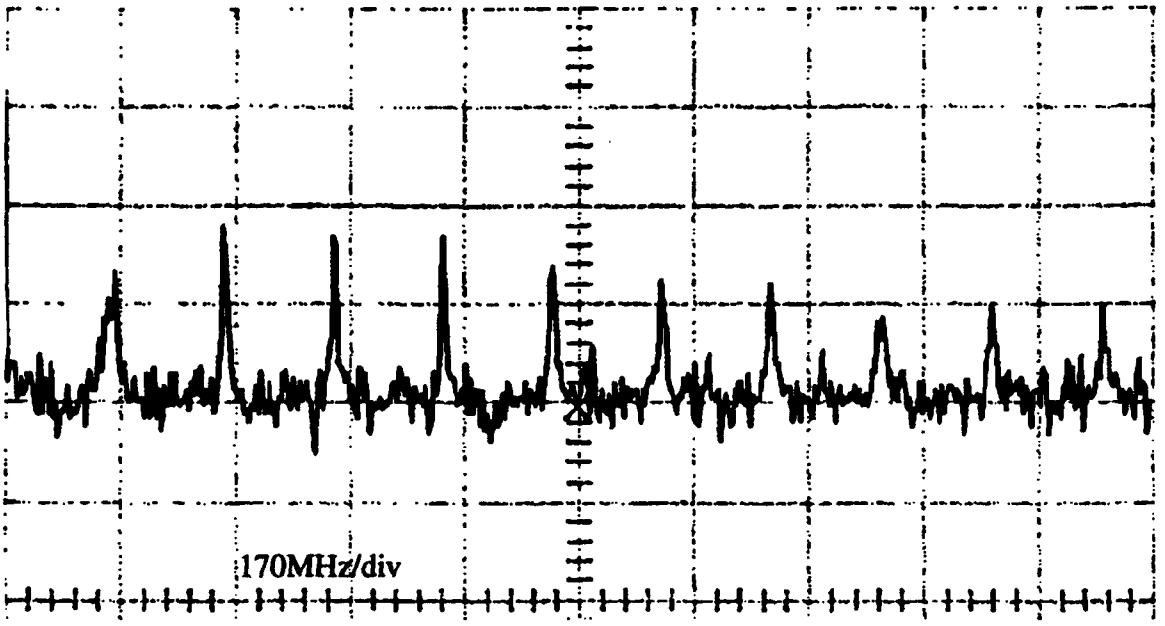

(b)

Fig. 4.5. Noise spectra showing alternate cavity mode suppression.

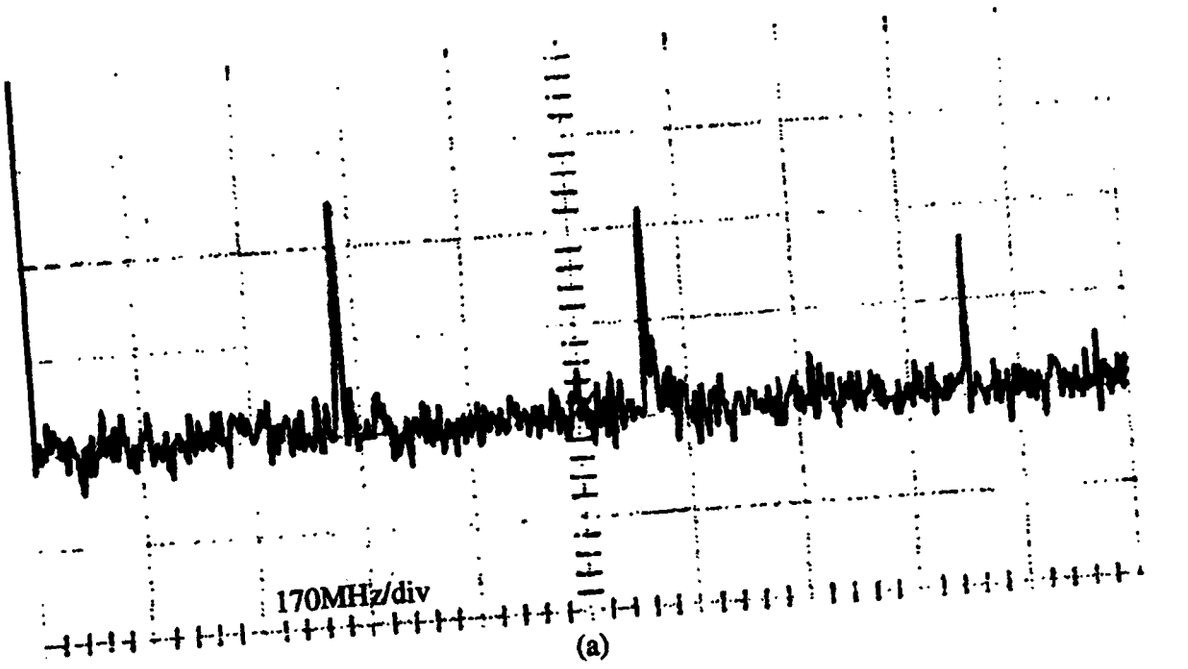

(a)

Same scale as above

(b)

Fig. 4.6. Noise spectra showing external cavity mode suppression.

(Fig. 4.6a) modes are suppressed. An increase to 0.017 in feedback leads to normal spacing (Fig. 4.6b). In this case, and it was unusual, every third mode experienced gain and the intermediate modes were suppressed. In general only alternate modes were suppressed for both the static hologram and the PCM.

In the first case the crystal was acting as a phase conjugator. In the second case as a static hologram. The behavior of both was the similar. Frequency suppression was never observed with the conventional reflector. This supports the assumption that the static hologram will only reflect a beam that matches the phase matching conditions set when the gratings were written. If it did not, it would just act like a conventional mirror and this behavior would be unexpected.

Even if the specific phenomena shown in Fig. 4.6 is considered an anomaly, alternate mode suppression was fairly common. Reflection gratings [6] in the crystal are ruled out because the frequency spacing does not correspond. There is no obvious mechanism that would cause low feedback levels to mimic halving the length of the external cavity. At present there is no theory to explain this behavior; further work is ongoing.

Rate Equations: Multiple Round Trips

The effects of optical feedback on semiconductor laser have attracted considerable attention [15-19]. Of particular interest are the instabilities that arise from such conditions [74, 88, 89-93]. In the next sections the methods of previous analysis are followed [62-63, 74].

The dynamic rate equations for the CECL, PCECL, and URECL can written down from Chapter 2. Instead of solving for the steady state all the dynamic phase terms are kept. With this substitution Eq. (2.33) becomes

$$\dot{A} = \frac{1}{2} gnA(t) - \kappa \sum_{1}^{\infty} (r_2 r_3)^{m-1} A(t - m\tau) \cos(\phi(t - m\tau) - \phi(t) - m\Omega\tau), \quad (4.1)$$

$$\dot{\phi} = \frac{1}{2}\alpha g n - [A(t)]^{-1}\kappa \sum_{1}^{\infty} (r_2 r_3)^{m-1} A(t-m\tau)\sin(\phi(t-m\tau)-\phi(t)-m\Omega\tau). \quad (4.2)$$

The equation for the carrier density, Eq. (2.45), is unchanged

$$\dot{n} = R_0 - (G_0 + gn)|A(t)|^2 - \frac{n(t)}{\tau_s}. \quad (4.3)$$

The equations for the PCECL can be attained the same way. In this case the boundary conditions are explicitly included in the equations. From Eq. (2.50)

$$\dot{A} = \frac{1}{2} g n A(t) + \kappa \sum_{1}^{\infty} (-r_2 r_3)^{m-1} A(t-m\tau). \quad (4.4)$$

$$\dot{\phi} = \frac{1}{2}\alpha g n. \quad (4.5)$$

The carrier density is unchanged and given in Eq. (4.3). Finally, Eq. (2.60) leads to the result for the URECL. The inclusion of the boundary conditions in this case leads to an interesting result. When the ring PPCM acts as a phase-conjugator, the return phase is set at $2n\pi$, where n is an integer. In that case the rate equations become

$$\dot{A} = \frac{1}{2} g n A(t) + \kappa \sum_{1}^{\infty} (r_2 r_3)^{m-1} A(t-m\tau), \quad (4.6)$$

$$\dot{\phi} = \frac{1}{2}\alpha g n. \quad (4.7)$$

As expected, the phase conjugate cases do not contain any phase information beyond phase shifts in reflectivity due to fresnel reflection. But the nature of this process is different for the PCECL and URECL. The former is actually undoing any external cavity phase effects.

When the ring PPCM acts as a static hologram, it can only reflect frequencies that match the boundary conditions. Thus the return phase must be equal

to $2p\pi$, where p is any integer. This can be expressed with the dirac delta as follows:

$$\dot{A} = \frac{1}{2}gnA(t) + \kappa \sum_{m=1}^{\infty} (r_2 r_3)^{m-1} A(t - m\tau)\cos(\phi(t - m\tau) - \phi(t) - m\Omega\tau + m\phi_R)$$
$$\times \delta(\phi(t - m\tau) - \phi(t) - m\Omega\tau - +m\phi_R - 2p\pi), \tag{4.8}$$

$$\dot{\phi} = \frac{1}{2}\alpha gn - \kappa \sum_{1}^{\infty} (r_2 r_3)^{m-1} A(t - m\tau)\sin(\phi(t - m\tau)$$
$$- \phi(t) - m\Omega\tau + m\phi_R)$$
$$\times \delta(\phi(t - m\tau) - \phi\tau) - m\Omega\tau + m\phi_R - 2p\pi). \tag{4.9}$$

The bandwidth of the hologram is implicitly assumed in the delta function. As it is on the order of several Hz for $BaTiO_3$, the use of the delta function in this case is justified. Again the carrier density is given in Eq. (4.3).

Rate Equations: One Round Trip

The single round trip approximation falls directly out of the above equations; simply keep only one feedback term. For the CECL this reduces to

$$\dot{A} = \frac{1}{2}gnA(t) - \kappa A(t - \tau)\cos(\phi t - \tau) - \phi(t) - \Omega\tau), \tag{4.10}$$

$$\dot{\phi} = \alpha gn - \frac{\kappa A(t - \tau)}{A(t)}\sin(\phi(t - \tau) - \phi(t) - \Omega\tau), \tag{4.11}$$

and the carrier density has the same form as before. These equations are in agreement with previous work [74]. The PECL rate equations take the following form

$$\dot{A} = \frac{1}{2}gnA(t) + \kappa A(t - \tau), \tag{4.12}$$

$$\dot{\phi} = \alpha gn. \tag{4.13}$$

This also agrees with previous efforts [63] except that the boundary conditions are not defined in the earlier work. When the PCM of the URECL acts as a phase conjugator, the rate equations reduce to

$$\dot{A} = \frac{1}{2} gnA(t) + \kappa A(t-\tau), \tag{4.15}$$

$$\dot{\phi} = \alpha gn. \tag{4.16}$$

In a similar fashion to the round trip case, the rate equations for the URECL with a static hologram are

$$\begin{aligned} \dot{A} = {} & \frac{1}{2} gnA(t) + \kappa A(t-\tau)\cos(\phi(t-\tau) - \phi(t) - \Omega\tau + \phi_R) \\ & \times \delta(\phi(t-\tau) - \phi(t) - \Omega\tau + \phi_R - 2p\pi), \end{aligned} \tag{4.17}$$

$$\begin{aligned} \dot{\phi} = {} & \frac{1}{2}\alpha gn - \kappa \frac{A(t-\tau}{A(t)} \sin(\phi(t-\tau) - \phi(t) - \Omega\tau + \phi_R) \\ & \times \delta(\phi(t-\tau) - \phi(t) - \Omega\tau + \phi_R - 2p\pi). \end{aligned} \tag{4.18}$$

Discussion of the Rate Equations

The differences between the rate equations was examined in Chapter 2; a few further comments are warranted here. The phase-conjugate terms become single valued. This would be true even if the boundary conditions were not imposed [63] because the phase of the feedback would not be arbitrary. (As shown in Chapter 3, the laser sets the boundary conditions.) The ring and Ideal PCM's are not identical, even when the ring is acting as a phase conjugator. This is one of the subtle differences between self-pumped and externally pumped PCM's that show up in the phase. The integer value of π for the static hologram does not need be equal to that which wrote the grating.

The implication for laser coupling is significant. Unlike lasers coupled via conventional optics, those coupled with self-pumped PCM's will have as specified

phase. However, they will still have a dependence on the length between the resonators, so not all problems plaguing coupled cavities [45] can be cured with passive phase conjugation.

Summary

In this chapter the experimental demonstration of coherence collapse due to feedback from a ring PPCM has been shown. The behavior is seen to be quite similar to the case of conventional feedback. The observation of mode suppression at low was discussed. The rate equations for all geometries were presented and compared. The hybrid nature of the URECL is seen in the equations.

CHAPTER 5

BEAM QUALITY ASPECTS OF THE URECL

There have been a number of experiments performed on the aberration correction properties of phase conjugators. Early work featured kerr media devices and this work continues [94-95]. As soon as photorefractives were used to generate phase conjugate beams their ability to correct for aberrations became an issue [7, 52, 96-98]. Although problems remain, as this work shows, photorefractives have been employed in devices for beam cleanup [99, 100]. To date, no work has been done on the PCM as an element of an external cavity. This chapter investigates these aspects.

The most striking difference between the Conventional External Cavity Laser (CECL) and the Unidirectional Ring External Cavity Laser (URECL) is the latter's ability to correct for aberrations in the beam. In this respect, the URECL behaves much as a Phase Conjugate External Cavity Laser (PCECL) would be expected to act. This profoundly affects any device application for which an

external cavity laser might be employed. Thus a discussion of the beam quality is imperative. The modeling of this behavior is quite complex. This chapter is only intended to examine several pertinent issues, so the results will be purely experimental and the discussion empirical. The work presented here looks at properties that would have an impact on cavity coupling and, by analogy, laser coupling. Following a discussion of the set-up and technique the quality of the return beam is compared for a conventional mirror and ring PPCM. Time

dependent effects are considered and turn out to be extremely important. The output of the the laser with feedback is documented. The return beams are compared to the conventional case. Finally, the buildup of the phase-conjugate return is chronicled with video.

Experimental Geometry #1

The first experimental set-up shown in Fig. 5.1. This was used to collect the quantitative data presented first. It is essentially the same as the previous geometries. In this configuration, an aberrator can be inserted before the crystal. Several types of aberrators were tried, finally a thin piece of polypropelene was selected. (The same material as might be found in a clear plastic bag.) The aberrator was chosen so that it would distort the phase front of the beam while having minimum impact on the intensity. There was still a significant reduction in intensity, however. This was due to absorption and scattering by the plastic.

The beams were analyzed in a different fashion than from before. In the first set of measurements, the return beam was deflected by the beam splitter and set to a second 50/50 beam splitter. The throughput was sent to a power meter. The reflected beam was focused through a slit on route to a second power meter. The width and height of the slit (essentially a rectangle) were set to correspond to the minimum focused spot size for a gaussian beam of the incident dimensions. The height and width of the beam incident on the lens are 8.8 mm vertical and 4.0 mm horizontal. This requires a slit size of 141 microns vertical and 311 microns horizontal, respectively. The intensities off the beam splitter were measured and the intensity of the focused beam was divided by that of the unfocused beam. This ratio was called the beam quality, it can range from zero to one.

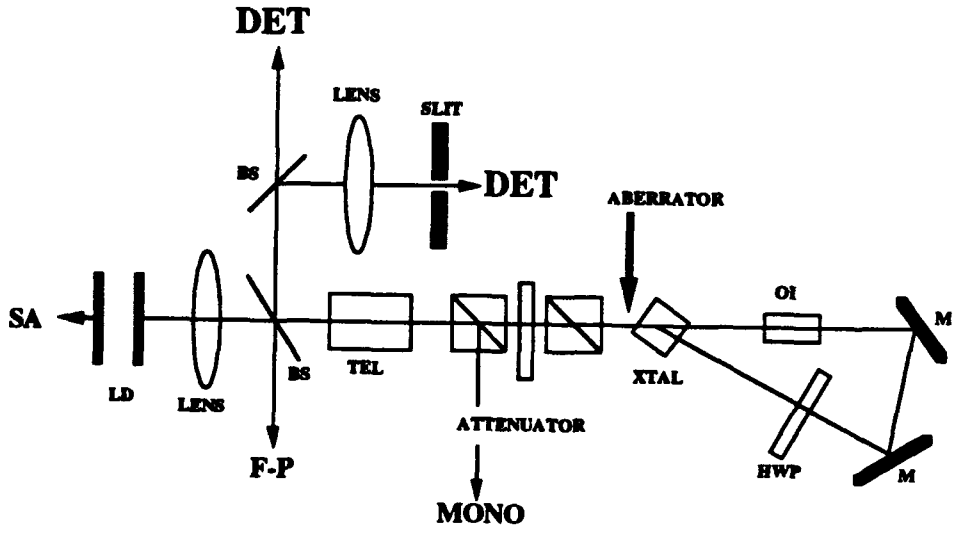

Fig. 5.1. Experimental Geometry #1.

Time Response

The time response of the media is shown in Fig. 5.2. Both the reflectivity and the beam quality are plotted against time. Throughout this work, the claim for a steady state coupling constant was made due to the slow response of Barium Titanate at this wavelength. . This is clearly seen in Fig. 5.2. Measurements taken on short time scales, a few seconds, will experience virtually no change in reflectivity as the gratings grow. After 15-25 minutes, there will be no change in reflectivity on this time scale and longer. The error in measurement is to small to show up on this scale.

This type of measurement has been taken before [101]. What has not been considered was the time response of the beam quality. The implicit assumption was that it tracked the reflectivity. Note that the beam quality initially lags the reflectivity. Indeed the reflectivity is at almost half its maximum value before the beam quality begins to rise. After four minutes this condition reverses itself and the beam quality now leads the reflectivity for a few minutes until they both begin to taper off to tneir steady state values.

After ten minutes the beam quality starts to drop off even as the reflectivity is slowly increasing. It is not clear why the beam quality should decrease. The light from the gratings no longer scatters entirely into the phase-matched direction. It seems that as the gratings get strong enough some light can be scattered into the higher order diffraction terms. Additionally, the writing beams and gratings are multimode, thus nondegenerate four-wave mixing can take place. The different modes can diffract off other gratings if they satisfy the phase matching conditions. This scattering will be weak compared to the degenerate case, but can take place.

The above behavior was fairly typical for all the runs performed. This indicates that for any application in which rise time is important it is not enough

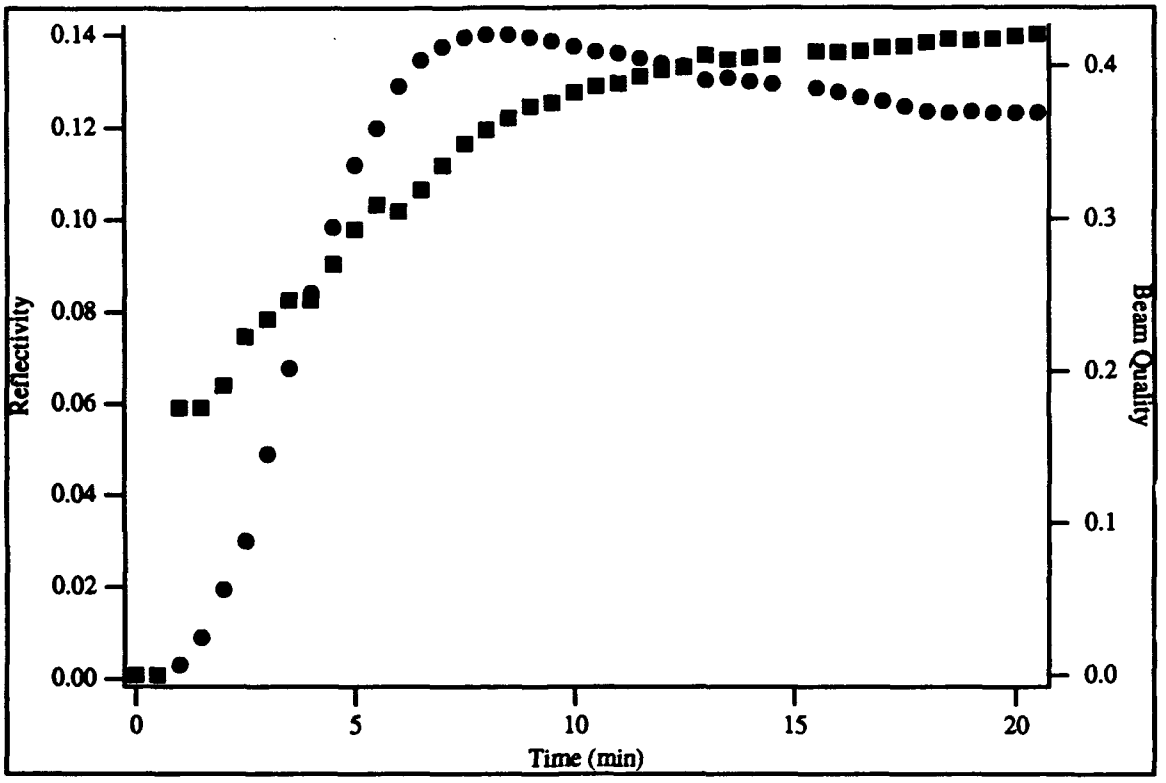

Fig. 5.2. Time Response of Barium Titanate. Squares – reflectivity, and circles – beam quality.

to just consider the reflectivity. Changes in the steady state can not be treated as mere permutations. They can lead to a new set of parameters as the coupling can change as well.

Beam Quality

Beam quality is the unit of interest for the first part of this chapter. Whether considering the coupling of a laser to itself via an external cavity, or the coupling of independent resonators, the beam quality is of primary importance. It has already been implicitly considered in this dissertation by the empirical coupling factor f, derived in Chapter 3. The work presented here attempts to explain why f is less than one.

The ring PPCM compares well to the conventional plane mirror in terms of beam quality as seen in Fig. 5.3. This data was taken by simply adjusting the attenuator and recording the values. For the conventional mirror the steady state is instantly attained. For the unidirectional ring PPCM the gratings were allowed to write for 20 minutes and then the attenuator was quickly turned down as the data was taken. A slight increase in beam quality seems to be effected with increasing reflectivity, however, this increase was within experimental error. The beam quality of the PCM is always slightly higher than for the dielectric reflector. The ring is known to have poor beam quality compared to other phase-conjugate devices. Additionally, the ring cannot return better beam quality than the laser emits. With no intentional aberrations and good quality optics, the conventional case only suffers from divergence. The PCM should correct for this, but do no better. Thus a large increase in beam quality is not expected.

The good beam quality throughout the reflectivity range argues that the ring PPCM keeps the return phase constant regardless of the incident light. If this were not so the gratings would reflect light off axis and the beam quality should be quite poor.

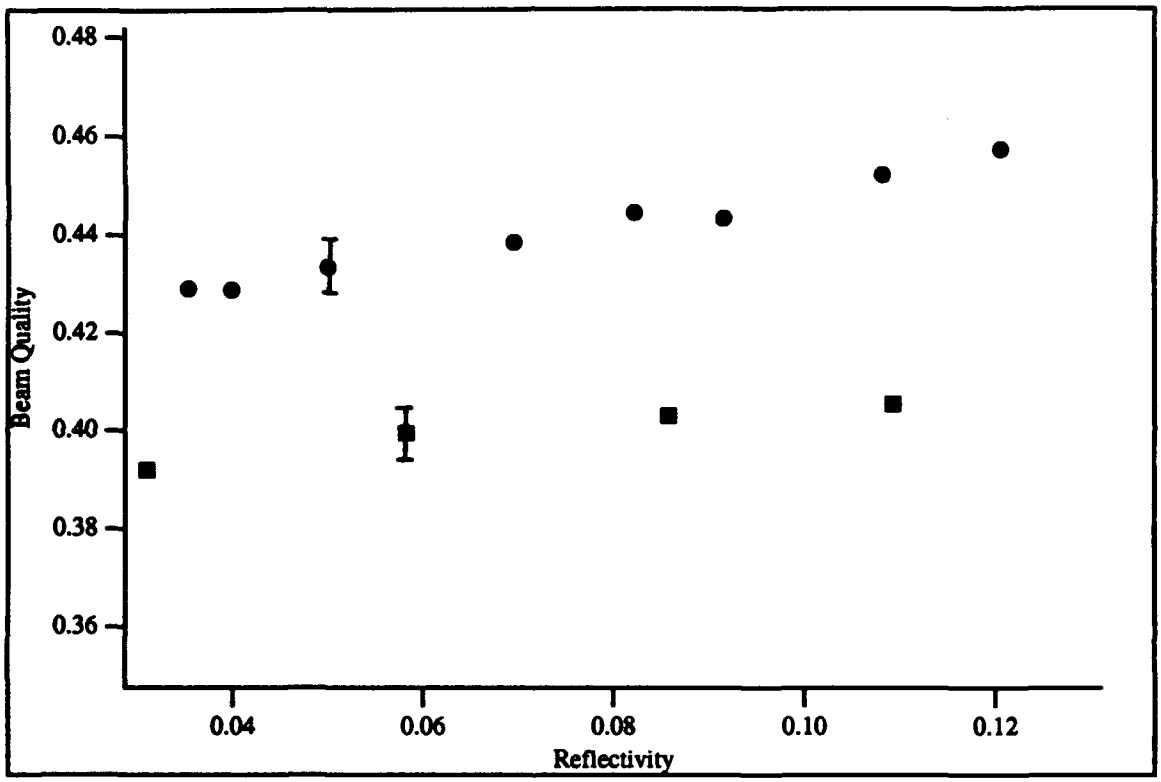

Fig. 5.3. Beam quality versus reflectivity. Squares – conventional mirror, and circles – phase conjugate mirror.

The aberration correction, or *beam cleanup*, properties of the ring PPCM are evident in Fig. 5.4. In that case the ring was allowed to act as both a phase conjugator and as a static hologram. The conventional data was taken simply by inserting the aberrator in the beam path as shown in Fig. 5.1, and reading the data. It will not change in time. For the phase conjugate case, the aberrator was put in front of the crystal and the gratings were allowed to write until maximum reflectivity was attained. The reflectivity was set by the attenuator. For the static hologram, the gratings were allowed to write at a specific reflectivity and then the beam was aberrated. The values were measured and the aberrator removed before the gratings could adjust and rewrite.

Due to the aberrator itself, the reflectivity is lower than before, with a maximum of just over 5%. Not as much light will get through to write the grating or reflect off of them, or the conventional mirror. The conventional case suffers from a significant decrease in beam quality; it is reduced an average of 50%. The phase conjugator does a good job of preserving beam quality. That parameter is reduced by about 20%. The reduction for the static hologram is measured between that of the phase conjugate without aberration and the static hologram with aberration. The reduction in beam quality is 48%, which is in line with the conventional case. This is expected, as it acts only as a reflection grating. The aberrator not only degrades beam quality, it prevents the beam from being phase matched to the ring PPCM.

Other Considerations

As Fig. 5.1 shows, the geometry allowed for the measurement of spectral data as well. In this respect the aberration had no discernible effect other than to reduce the feedback intensity. The spectral structure would change with the insertion of the aberrator, but no consistent behavior that indicated that distortion of the wave front had any great affect. This is in keeping with the model

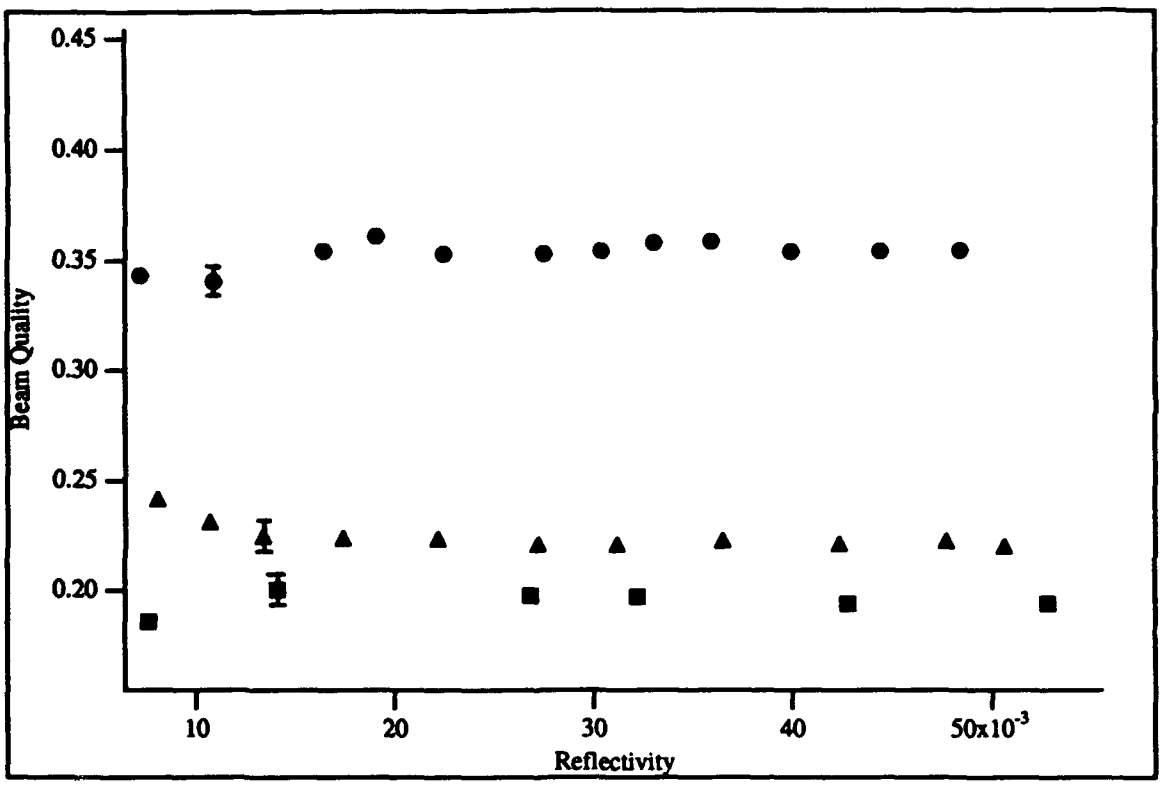

Fig. 5.4. Beam quality versus reflectivity with aberration. Squares – conventional mirror, circles – phase conjugate mirror, and triangles – static hologram.

developed in earlier chapters. The longitudinal behavior of the laser can be considered independent of the transverse structure, at least for the HLP1400. If the laser had been induced to run in higher order transverse modes this certainly would not be the case. At any rate, the main effect of the aberrator was to reduce the coupling factor f; not an insignificant result.

Experimental Geometry#2

The second experimental geometry, shown in Fig. 5.5, was designed to allow video recording of the output and return beams of the external cavity. The slit has been replaced by lens and a screen upon which the return beam was imaged. This was recorded on video tape. A clock in the background kept running time. Although the Fabry-Perot's could still be accessed on the output beams, they were not for the reasons given above. Instead, the output was imaged on a screen and could be recorded as well. (This was not done simultaneously, the camera was moved as necessary). The resolution of the images has been degraded in their transfer to print. They where originally recorded on video tape, then digitized from that media, and printed on film. The film was not suitable for publication so those images were digitized again and printed on paper. For most of what is to be presented this is not a serious limitation as only the gross behavior is being examined. However, the lack of resolution makes any quantitative measurements difficult.

Beam Profile

The beam profile of the laser output was considered first. There was no great effect observed on the output of the laser. Figure 5.6 demonstrates this. Figure 5.6a is the beam profile of the laser without feedback. Figure 5.6b is of the laser with feedback from the unidirectional ring PPCM. No change in structure

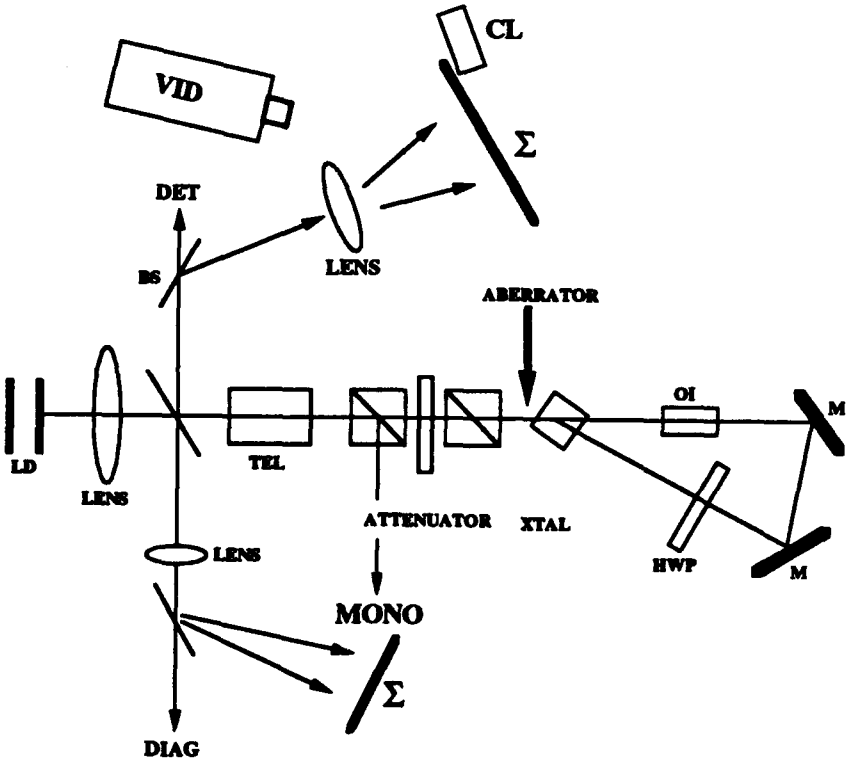

Fig. 5.5. Experimental Geometry#2.

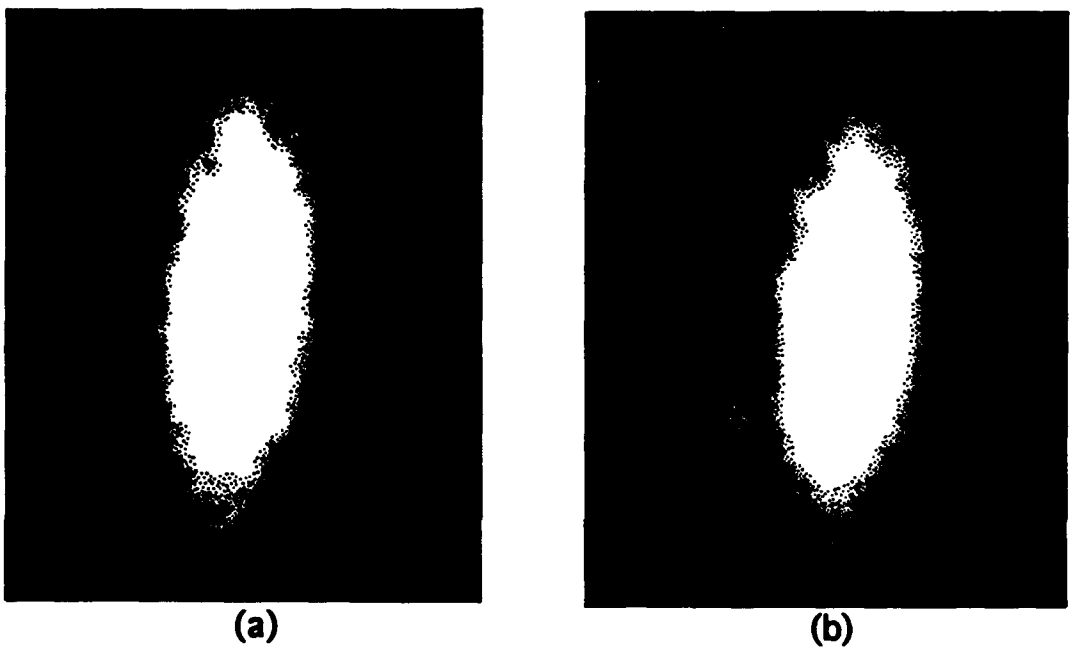

Fig. 5.6. Output profile of laser. (a) Free running, and (b) with feedback.

is seen. The resolution, as mentioned above, is poor. If it were better the only difference that can be observed is a change in the speckle of the image. The free running beam profile has a clear speckle to it. In the laser with feedback the speckle is blurred and indistinct. This is due to the multi-longitudinal mode structure and occurs with conventional feedback as well. This is the only clear difference between the images.

The return beam is more interesting. In Fig. 5.7 the return from the external cavity is imaged. (The horizontal lines are a product of the processing had have no significance.) The conventional feedback, at a power reflectivity of 4.8%, is shown in Fig. 5.7a. Feedback from the ring PPCM is shown in Fig. 5.7b at a reflectivity of 5.0%. Note that the conventional case suffers from divergence, the intensity is spread out, while the phase-conjugate beam has more of its intensity centered. Keep in mind that the beam quality is about the same for both cases. The conventional case also suffers from self-interference (Fig. 5.7c), shown at a higher reflectivity (26%) to bring out the effect. This never happens with the phase-conjugate light. Figure 5.7d maps the background without reflectivity for comparison.

The buildup of the phase-conjugate return can be quite interesting. In Fig. 5.8 the progression from no feedback to maximum is shown in 2.5 minute increments. Figure 5.8a is just the background without feedback. The illumination of the crystal was started at this point. There is saturation due to back reflections off the optics and the poor resolution available. After 2.5 minutes, the buildup in phase-conjugate feedback is visible (Fig. 5.8b). Additionally, there is a second return beam, which is not phase conjugate. Its existence is analogous to previously observed cones of light emanating from the crystal [55]. These occur due to a relaxation of the phase matching condition given in Eq. 2.15. In that case, when only two of the four wave vectors are specified, the other two beams

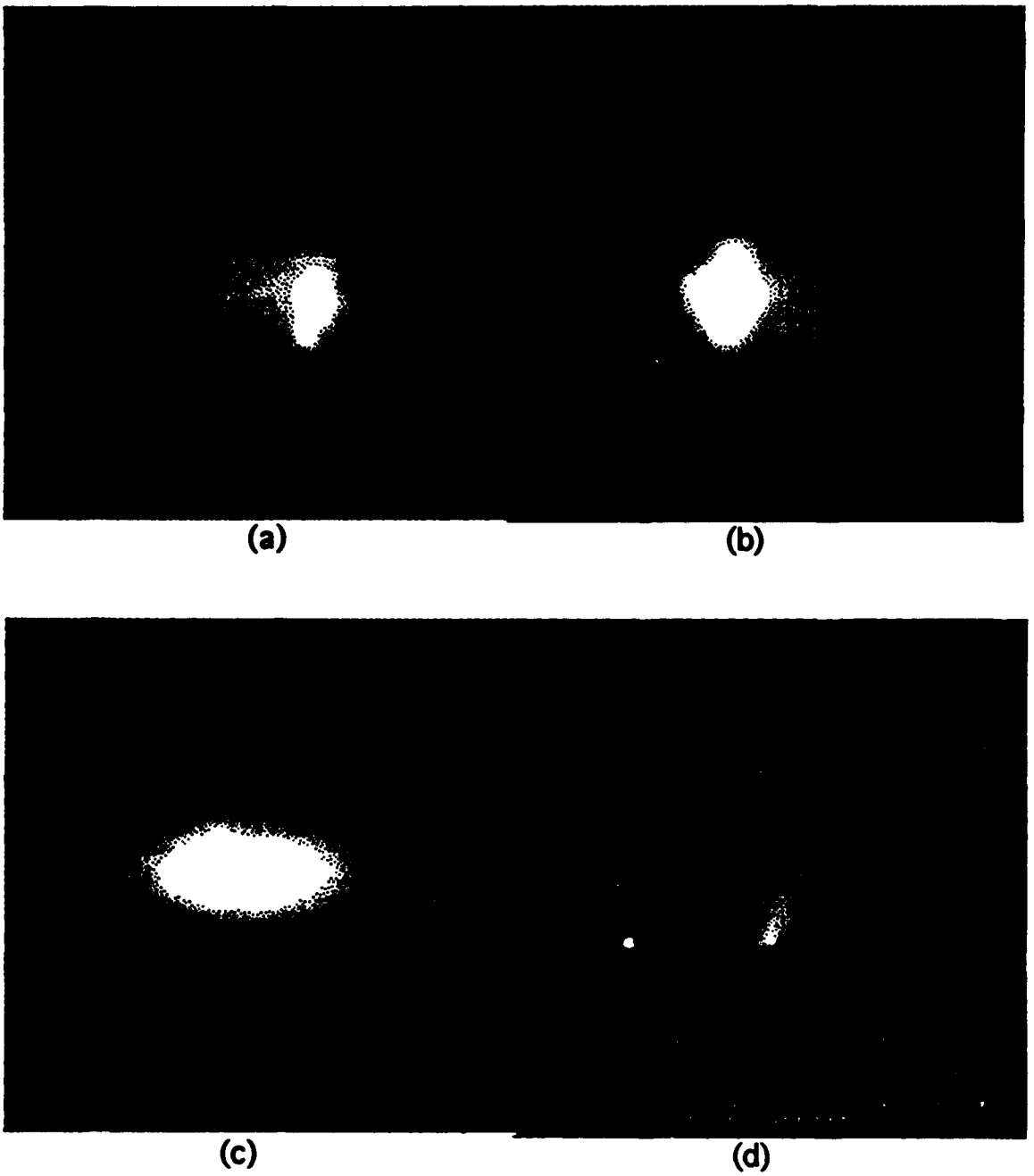

Fig. 5.7. Return beam profiles. (a) Conventional, (b) phase conjugate, (c) conventional showing interference effects, and (d) background.

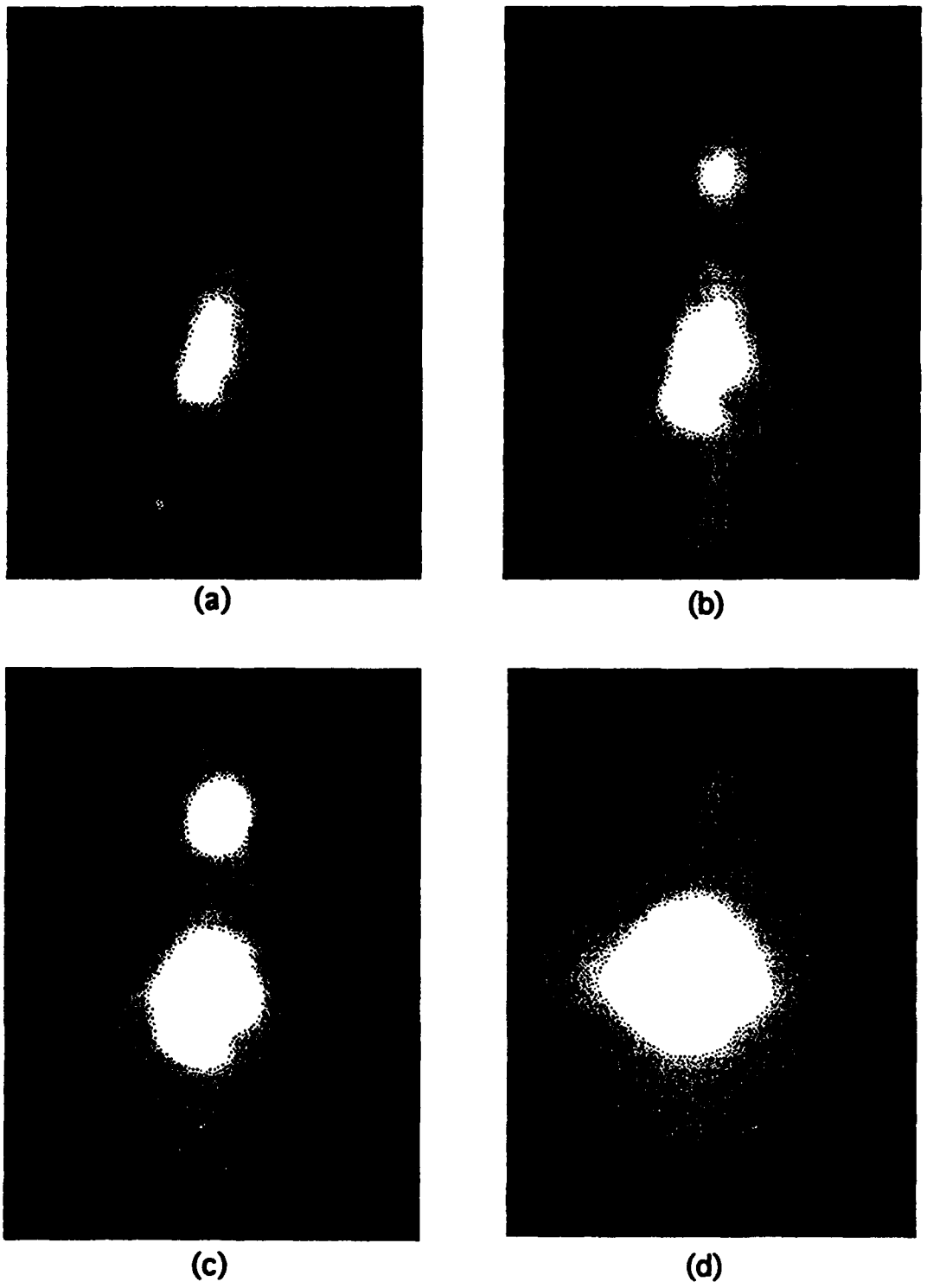

Fig. 5.8. Progress of phase conjugate buildup with off-axis beam. (a) Background, (b) 2.5 minutes, (c) 5 minutes, (d) 7.5 minutes.

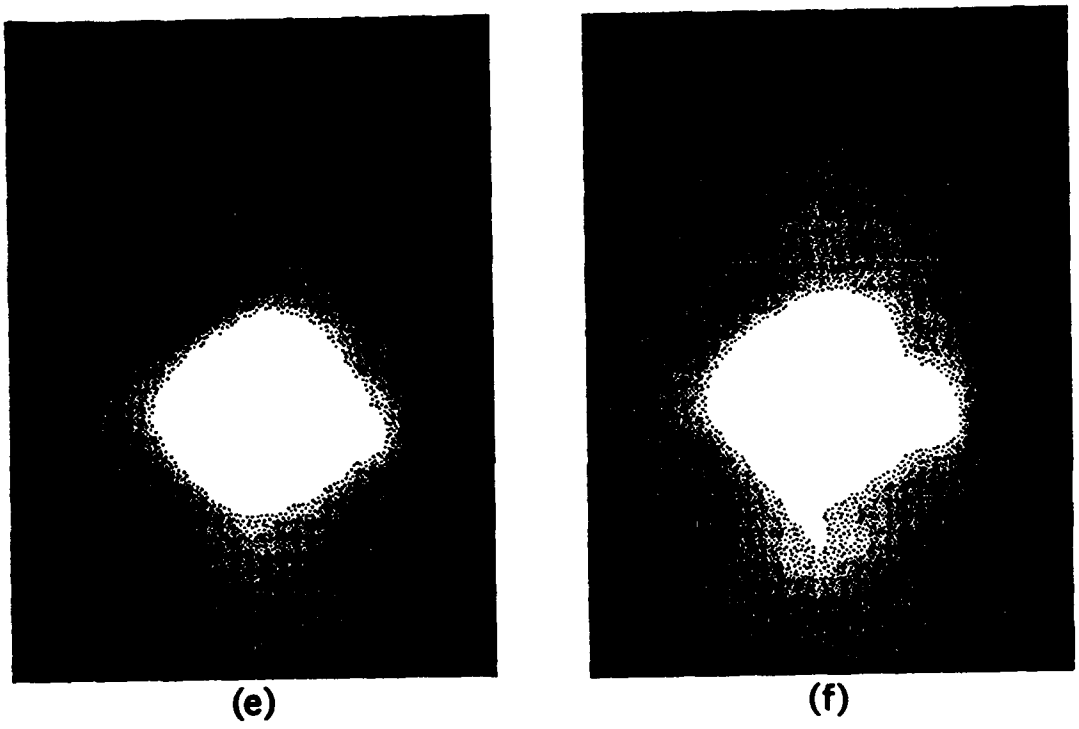

Fig. 5.8. Continued – (e) 10 minutes, and (f) 12.5 minutes.

are free to lase in any direction that preserves phase matching, and they will map out cone of light instead of returning as a single point. That a second beam of light should return instead of a section of a cone has been predicted [102, 103]. In both of those cases the second spot was a steady state phenomena, where the transient data is shown here. In the former reference a ring PPCM was used, but one of the mirrors was intentionally tilted to produce the effect. In the latter case, a different geometry was used, and the parametrs adjusted so that the usual copu;ling would not experience high gain. This dissertation work found the second spot to take appear for coplanar and otherwise optimal alignment.

After 5 minutes (Fig. 5.8c) the second beam has maximized in intensity. The phase-conjugate spot has increased as well. Recall, its buildup time can take many minutes. After 7.5 minutes (Fig. 5.8d) the second beam has almost entirely faded and most of the light is directed back into the phase-conjugate beam. As time progress, Figs. 5.8e and 5.8f the second been is gone. The beam profile starts to grow asymmetrically, indicating a degradation in beam quality.

The above set of images clearly show why the fidelity will lag the reflectivity and then taper off from a maximum (Fig. 5.2). In the early part of the buildup, light is diverted into the second beam (or cone), so that while the reflectivity of the device may be high, only a small portion of the light is directed back on axis. The extraneous light collapses into the phase-conjugate beam as the gratings experience preferential gain and become stronger, as discussed in Chapter 2. That is why the second spot observed is only a transient. Eventually the gratings are strong enough to diffract higher order modes out of the phase-conjugate return and the beam quality begins to degrade.

A second run was conducted for comparison. In that experiment, the beams were realigned in the crystals to create a new set of phase matching conditions. The results are shown in Fig. 5.9, again presented in 2.5 minute increments. In

that case no off axis beam appears. The phase conjugation process starts in Fig. 5.9 with no feedback (only back reflections) and builds up nonuniformly. The exact cause is not known, but it clearly degrades the beam quality. After 5 minutes (Fig. 5.9c) the reflectivity is 3.2%. After 10 minutes (Fig. 5.9e) it had doubled to 6.4%. By the end of the run (Fig. 5.9g) it had increased, at fifteen minutes, to 10.2%.

The second run was presented to show that although the general trends are consistent from run to run, the exact result is highly dependent upon initial conditions. In fact, there was no measurable difference between the crystal orientations in the crystal. Yet the behavior is quite different in each case. The actual coupling process in the crystal is extremely complicated and dependent on many factors.

This last discussion points a significant problem with photorefractives in general, and specifically with regard to laser coupling. The material properties of Barium Titanate have been extensively characterized yet are not well understood. The photorefractive behavior varies greatly from crystal to crystal. Even with the same crystal there can be difficulty in reproducing some results, while other data are easily repeatable. The data presented in this dissertation has been limited to what can be reproduced, except in this last case. Although photorefractives have enormous potential, they will remain in the research lab until better understood.

Summary

In this chapter the beam quality aspects of the unidirectional ring PPCM have been considered experimentally. The time response of the beam quality was shown to lag the reflectivity. The beam quality of the ring PPCM was only slightly better than that of the conventional mirror without an aberration, but it was significantly better than the conventional case when the beam was distorted

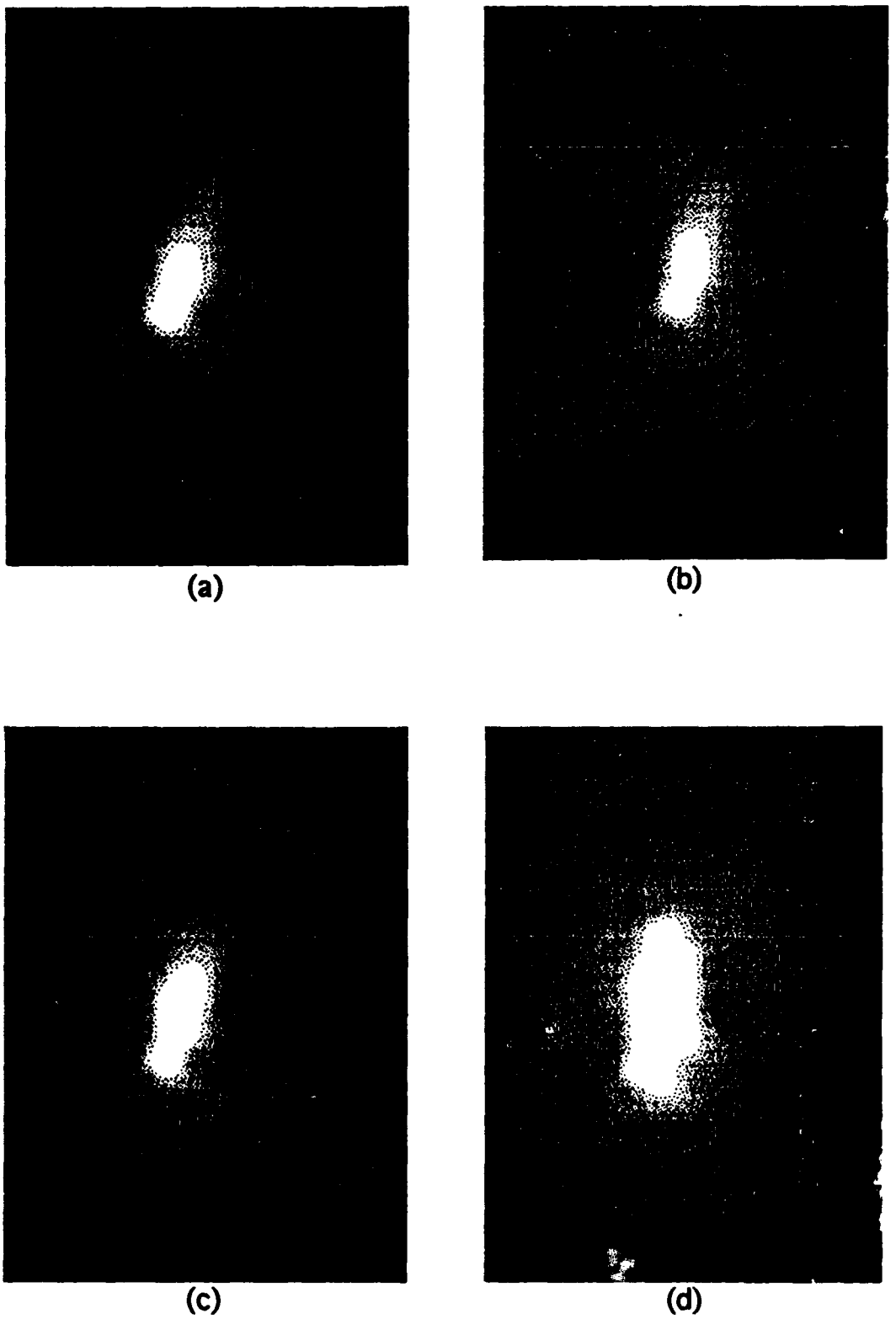

Fig. 5.9. Progression of phase conjugate buildup (a) Background, (b) 2.5 minutes, (c) 5 minutes, (d) 7.5 minutes.

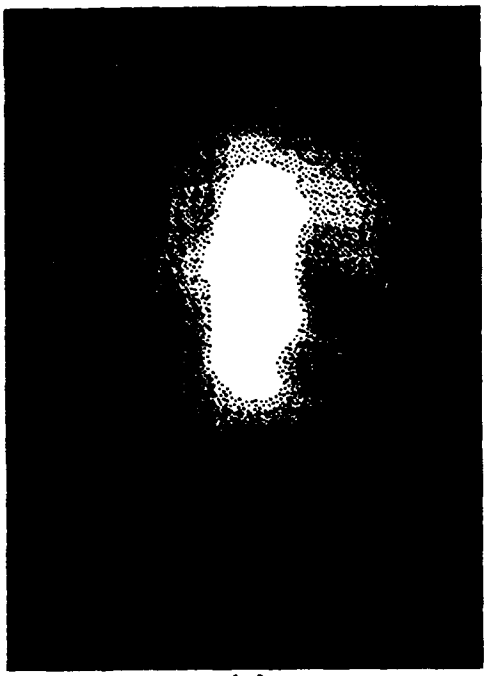

(e)

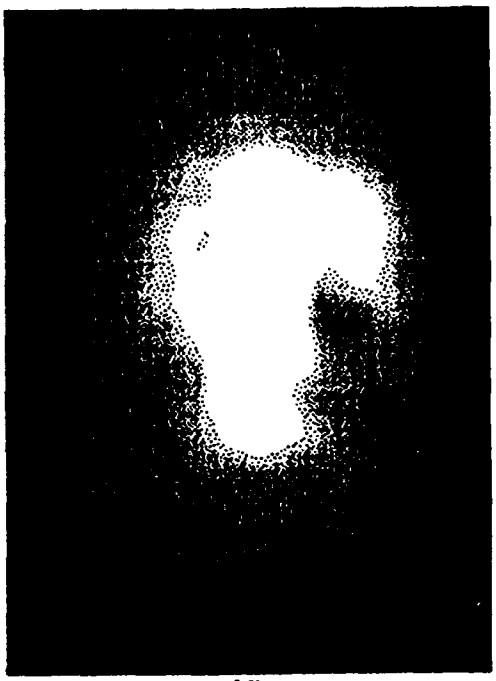

(f)

(g)

Fig. 5.9. Continued – (e) 10 minutes, (f) 12.5 minutes, and (g) 15 minutes.

prior to reflection. This was true only if it had time to write new gratings in the crystal, otherwise it acted as a static hologram, in which case beam quality was comparable to the conventional reflector. The beam profiles of the laser output and return beams were examed. The progression, in time, of the buildup of the phase conjugate feedback was presented. The two runs shown explained the behavior of the time response curve and also demonstrated the problematic nature of photorefractives.

CHAPTER 6

CONCLUSIONS AND FUTURE WORK

The work presented was an attempt to conduct a systematic study of a semiconductor laser with phase-conjugate feedback, that is, a phase-conjugate external cavity semiconductor laser. The motivation was to place in context a body of work that would define the problem, answer basic questions, and point the ways towards meaningful follow up work. It has succeeded, in this respect, to the extent that the unidirectional ring PPCM acted like a phase-conjugate mirror. The possibilities and limitations of the device are more clearly understood, as well as the pitfalls of using a photorefractive PPCM as a phase-conjugator.

Prior to this work, when phase-conjugate feedback into a semiconductor laser was considered, the nonlinear medium has been either another diode laser or Barium Titanate, used in a self-pumped configuration. This is due to the higher powers needed to drive other media. The phase-conjugate aspects have been casually assumed when photorefractive methods have been employed. As shown, a self-pumped device can be considered to be phase conjugating only when the phase matching conditions are met. Otherwise it is only a static hologram. This doesn't devalue the device, rather it allows for greater comprehension of its operation.

The most important result of this was establishing the return phase of the ring PPCM through modeling and experiment, and the likewise modeling of the Ideal PCM. That the return phase is exactly $2n\pi$ may have been intuitive, but prior work was always kept general. This work shows that this needn't be done.

In Chapter 2 the effective reflectivities and the rate equations for the CECL, PCECL, and URECL were derived and compared. The differences in form due to phase shifts between one case and another. Moreover, when the boundary conditions are imposed, the steady state rate equations for the PCECL and the URECL are single valued, in contrast to the CECL.

In Chapter 3 the boundary conditions (that are so significant) were derived and substantiated with experimental evidence. Two methods of obtaining an expression for the effective reflectivity from the data were considered. This in turn allowed for a calculation of the coupling factor f. Linewidth narrowing and broadening for all three cases was discussed and compared. Experimental results were provided for the URECL which were in good agreement with the models developed. The multimode spectra of the CECL and URECL were presented and an empirical explanation of that behavior was shown to be quite plausible.

In Chapter 4 the phenomena of coherence collapse for the URECL was explored. Experimental evidence was presented that clearly demonstrated this effect. External cavity mode suppression at low feedback levels was described. Dynamic rate equations for the three cases were given. The comparison of them neatly illustrated their differences and similarities.

In Chapter 5 beam quality aspects of the URECL were considered. It was shown, as expected, to be better than the CECL. The difference between phase conjugator and static hologram was demonstrated via comparison of the beam cleanup capability of each. The laser output beam profile was seen to be only marginally affected by feedback. The time lag of the fidelity of the ring PPCM, an important device consideration, was measured and discussed. The beam profile of the return beams were compared for conventional and self-pumped phase conjugate were compared. The ring PPCM buildup over time was presented, showing characteristics unique to that device.

Future Work

Any good research will suggest further avenues of investigation. The experiments and modeling done herein have provided a number of possible follow-on efforts.

In the conventional arena two interesting experiments might be performed. The first is to investigate the possibility of using an external reflector as an effective anti-reflection coating. There are many instances were a low facet reflectivity is desirable. However, due to the small surface area of the emitting face of the semiconductor laser, good quality AR coatings have been very difficult (and expensive) to achieve. Using a reflector, conventional or phase conjugate, might be a convenient way to address this problem. The modeling suggests that essentially zero reflectivity can be attained for the proper combination of phase delay and external reflectivity.

Coherence collapse is another fascinating topic. In all previous experiments the phase delay is kept constant. Varying the phase delay rather than the external reflectivity is proposed. As mentioned in Chapter 4 there is some debate on the influence of the product of $\kappa\tau$ on coherence collapse. This experiment would settle that debate once and for all.

Further work on phase-conjugate feedback would be worth the effort; This research has only touched on the possibilities. The first experiment should be to augment the attenuator with an optical isolator. This would provide the opportunity to study the effects of very low feedback into the laser. (Unfortunately for this work, the available instruments were not suited to this technique.) A careful study of the transition to coherence collapse should be carried out, as well as a comparison to conventional low feedback effects such as line narrowing and frequency stability. Further investigation of mode suppression, including both measurements and modeling, would fit in with this study.

Use of a faster medium would permit a thorough investigation into the dynamic effects of phase conjugate feedback. Semiconductor materials are ideal candidates for this, and certainly are the nonlinear materials of the future for diode laser work. This would also allow an investigation of a four-wave mixing geometry which could be compared to the Ideal PCM model in the present work. The validity of neglecting the delay length of the external cavity could then be verified.

There has been some recent work with double external cavities being used for stability and other considerations. Some novel research might include substituting a PCM for one or both of the conventional mirrors. Since the double cavity work is being done to better manage the diode laser instabilities for device applications a PCM would have the added advantage of being self-aligning.

The use of holograms for optical storage has long been pursued. There is potential for an URECL in these situations, especially one that is constrained to be single longitudinal mode. In that case the ring PPCM would only provide reflectivity for the correct frequency. This could be exploited for an optical switch or memory device.

The full dynamic behavior of the external cavity semiconductor laser deserves more attention. The development of a full multimode model would be quite useful and could verify some of the suggestions offered. This treatment would include a complete gaussian transverse profile with multiple transverse modes. It would take into consideration gain competition and mode coupling, as well. The complete mathematical model could then be used to model feedback effects quite accurately. This would require putting a time dependence into the coupling constant κ for photorefractives.

Chaotic effects are quite the rage, these days. It would be worthy investigate the implications of using the multiple round trip equations in the considerations

of chaos. This might shed some insight as to whether chaos is actually affecting the laser, or is just a consequence of the equations.

The original intent of this research was to provide a background for laser diode coupling via nonlinear optics. This work suggests that the use of a faster media might be required for good coupling – this is a natural extension of the work. Coupling via a DPCM, already demonstrated, might be greatly enhanced through the use of optical isolators (to limit the feedback intensities) and an etalon to force single mode coupling between the lasers. Coupling via a true four-wave mixing geometry might be the preferred method, as Dente's work on overcoupling suggests time delay effects have an adverse impact on the coupling quality. These effects could, in theory, be removed with the proper phase-conjugate device.

In summary, the field is rich with potential investigations. Most of the proposed work is possible with only a small expansion of the current experiment, and well worth doing.

BIBLIOGRAPHY

[1] Armstrong, J. A., N. Bloembergen, J. Duciung, and P. S. Pershan, "Interactions between Light Waves in a Nonlinear Dielectric," Phys. Rev. **127**, 1918 (1962).

[2] Kogelnik, H., "Coupled Wave Theory for Thick Hologram Gratings," Bell. Sys. Tech. J. **48**, 2909 (1969).

[3] Glass, A. M., "The Photorefractive Effect," Opt. Eng. **17**, 470 (1978) .

[4] Zeldovich, B. Ya., V. I. Popoichev, V. V. Ragulsky, and F. S. Faizulov, "Connection Between the Wavefronts of the Reflected and Exciting Light in Stimulated Mandel'shta-Brillouin Scattering," JETP Lett. **15**, 109 (1972).

[5] Hellwarth, R., "Generation of Time-Reversed Fronts by Nonlinear Refraction," J. Opt. Soc. Am. **76**, 1 (1977).

[6] Cronin-Golomb, M., B. Fischer, J. O. White, and A. Yariv, "Theory and Applications of Four-Wave Mixing in Photorefractive Media," IEEE J. Quant. Electr. **QE-20**, 12 (1984).

[7] Feinberg, J., "Self-Pumped, Continuous-Wave Phase Conjugator Using Internal Reflection," Opt. Lett. **10**, 486 (1986).

[8] Feinberg, J., "Asymmetric Self-Defocusing of an Optical Beam from the Photorefractive Effect," J. Opt. Soc. Am. **72**, 46 (198[illegible] .

[9] Hall, R. N., G. E. Fenner, J. D. Kingsley, T. J. Soltys, and R. O. Carlson, "Coherent Light Emission from GaAs Junctions," Phys. Rev. Lett. **9**, 366 (1962).

[10] Nathan, M. R., W. P. Dumke, G. Burns, F. H. Dill, Jr., and G. Lasher, "Emission of Radiation from GaAs $p-n$ Junctions," Appl. Phys. Lett. **1**, 62 (1962).

[11] Quist, T. M., R. H. Rediker, R. J. Keyes, W. E. Krag, B. Lax, A. L. McWhorter, and H. J. Zeiger, "Semiconductor Maser of GaAs," Appl. Phys. Lett. **1**, 91 (1962).

[12] Holonyak, N., Jr. and S. F. Bevacqua, "Coherent (Visible) Light Emission from $Ga(As_{1-X}P_X)$ Junctions," Appl. Phys. Lett. **1**, 82 (1962).

[13] Henry, C. H., "Theory of the Linewidth of Semiconductor Lasers," IEEE J. Quant. Electr. **QE-18**, 1982, 259.

[14] Henry, C. H., "Phase Noise in Semiconductor Lasers," J. Light. Tech. **LT-4**, 1986, 298.

[15] Lang, R. and K. Kobayashi, "External Optical Feedback Effects on Semiconductor Laser Properties," IEEE J. Quant. Electr. **QE-16**, 347 (1980).

[16] Goldberg, L., H. F. Taylor, A. Dandridge, J. F. Weller, and R. O. Miles, IEEE J. Quant. Electr. **QE-18**, 555 (1982).

[17] Henry, C. H. and R. F. Kazarinov, "Instability of Semiconductor Lasers Due to Optical Feedback from Distant Reflectors," *IEEE J. Quant. Electr.* **QE-22**, 294 (1986).

[18] Olesen, H., J. H. Osmundsen, and B. Tromberg, "Nonlinear Dynamics and Spectral Behavior for an External Cavity Laser," IEEE J. Quant. Electr. **QE-22**, 762 (1986).

[19] Petermann, K. and N. Schunk, "Laser Diode Characteristics in the Presence of Optical Feedback," SPIE Opt. Fibers. Appl. V. **1085**, 32 (1989).

[20] Bel'dyugin, I. M. and E. M. Zemskov, "Theory of Resonators with Wavefront-Reversing Mirrors," Sov. J. Quantum Electron. **9**, 1198 (1979).

[21] Auyeung, J., D. Fekete, D. M. Pepper, A. Yariv, "A Theoretical and Experimental Investigation of the Modes of Optical Resonators with Phase-Conjugate Mirrors," IEEE J. Quant. Tech., **QE-15**, 1180 (1979).

[22] Lam, J. L. and W. P. Brown, "Optical Resonators with Phase-Conjugate-Mirrors," Opt. Lett. **5**, 61 (1980).

[23] Lind, R. C. and D. G. Steel, "Demonstration of the Longitudinal Modes and Aberration-Correction Properties of a Continuous-Wave Dye Laser with a Phase-Conjugate Mirror," Opt. Lett. **6**, 554 (1981).

[24] Belanger, P. A., "Phase Conjugation and Optical Resonators," Opt. Eng. **21**, 299 (1982).

[25] McFarlane, R. A. and D. G. Steel, "Laser Oscillator Using Resonator with Self-Pumped Phase-Conjugate Mirror," Opt. Lett. **8**, 208 (1983).

[26] Cronin-Golomb, M. and A. Yariv, "Self-Induced Frequency Scanning and Distributed Bragg Reflection in Semiconductor Lasers with Phase-Conjugate Feedback," Opt. Lett. **11**, 455 (1986).

[27] Vahala, K., K. Kyuma, A. Yariv, S-K. Kwong, M. Cronin-Golomb, and K. Y. Lau, "Narrow Linewidth, Single Frequency Semiconductor Laser with a Phase Conjugate External Cavity Mirror," Appl. Phys. Lett. **49**, 1563 (1986).

[28] Weiss, S., M. Segev, and B. Fischer, "Line Narrowing and Self Frequency Scanning of Laser Diode Arrays Coupled to a Photorefractive Oscillator," IEEE J. Quant. Electr. **24**, 706 (1988).

[29] Segev, M. and B. Fischer, "Laser Diode Arrays with Apertured Phase Conjugate Feedback," IEEE J. Quant. Electr. **26**, 1318 (1990).

[30] Segev, M., Y. Ophir, B. Fischer, and G. Eisenstein, "Mode Locking and Frequency Tuning of a Laser Diode Array in an Extended Cavity with a Photorefractive Phase Conjugate Mirror," Appl. Phys. Lett. **57**, 2523 (1990).

[31] Champagne, Y., N. McCarthy, and R. Tremblay, "Optical Phase-Conjugate Feedback Effects on Gain-Guided Diode Laser Characteristics," IEEE J. Quant. Electr. **25**, 595 (1989).

[32] Nietzke, R., P. Fenz, W. Elsasser, and E. O. Gobel, "Cascade Four-Wave Mixing in Semiconductor Lasers," Appl. Phys. Lett. **51**, 1298 (1987).

[33] McMicheal, I. and M. Khoshnevisan. P. Yeh, "Phase Conjugation in Semiconductor Lasers," SPIE **739**, 7 (1987).

[34] Patterson, F. G. and J. C. Brock, "Correction of Optical Path Differences using Phase Conjugation in Single-Mode Diode Lasers," Opt. Lett. **16**, 1322 (1991).

[37] Adler, R., "A Study of Locking Phenomena in Oscillators," Proc. IRE **34**, 351 (1946).

[38] Tang, C. L. and H. Statz, "Phase-Locking of Laser Oscillators by Injected Signal," J. Appl. Phys. **38**, 323 (1967).

[39] Spencer, M. B. and W. E. Lamb, Jr., "Laser with a Transmitting Window," Phys. Rev. A **5**, 884 (1972).

[40] Spencer, M. B. and W. E. Lamb, Jr., "Theory of Two Coupled Lasers," Phys. Rev. A **5** 893 (1972).

[41] Lang, R., "Injection Locking Properties of a Semiconductor Laser," IEEE J. Quant. Electr. **QE-16**, 976 (1982).

[42] Marcuse, D., "Coupled Mode Theory of Optical Resonant Cavities," IEEE J. Quant. Electr. **QE-21**, 1819 (1985).

[43] Fader, W. J., "Theory of Two Coupled Lasers," IEEE J. Quant. Electr. **QE-21**, 1838 (1985).

[44] Tsacoyeanes, J. G., "Phase Locking and Stability Properties for Two Coupled Semiconductor Lasers," J. Appl. Phys. **64**, 32 (1988).

[45] Dente, G. C., C. E. Moeller, and P. S. Durkin, "Coupled Oscillators at a Distance: Applications to Coupled Semiconductor Lasers," IEEE J. Quant. Electr. **26**, 1014 (1990).

[46] Feinberg, J. and G. D. Bacher, "Phase-Locking Lasers with Phase Conjugation," Appl. Phys. Lett. **48**, 570 (1986).

[47] Rockwell, D. A. and C. R. Giuliano, "Coherent Coupling of Laser Gain Media Using Phase Conjugation," Opt. Lett. **11**, 147 (1986).

[48] White, J. O., G. C. Valley, and R. A. McFarlane, "Coherent Coupling of Pulsed Dye Oscillators Using Nonlinear Phase Conjugation," Appl. Phys. Lett. **50**, 890 (1987).

[49] Kramer, M. A., S. Sifuentes, and C. M. Clayton, "Phase Locking of Ring Dye Lasers Using Incoherent Beam Coupling," Appl. Opt. **27**, 1371 (1988).

[50] Moeller, C. E., P. S. Durkin, and G. C. Dente, "Mapping the Injection-Lock Band of Semiconductor Lasers," IEEE J. Quant. Electr. **25**, 1603 (1989).

[51] Cronin-Golomb, M. and A. Yariv, I. Ury, "Coherent Coupling of Diode Lasers by Phase Conjugation," Appl. Phys. Lett. **48**, 1240 (1986).

[52] Sternklar, S., S. Weiss, M. Segev, and B. Fischer, "Beam Coupling and Locking of Lasers Using Photorefractive Four-Wave Mixing," Opt. Lett. **11**, 528 (1986).

[53] Stephens, R. R., R. C. Lind, and C. R. Giuliano, "Phase Conjugate Master Oscillator-Power Amplifier Using $BaTiO_3$ and AlGaAs Semiconductor Diode Lasers," Appl. Phys. Lett. **50**, 647 (1987).

[54] Segev, M., S. Weiss, and B. Fischer, "Coupling of Diode Laser Arrays with Photorefractive Passive Phase Conjugate Mirrors," Appl. Phys. Lett. **50**, 1397 (1987).

[55] Statman, D. and B. Liby, "Two-Beam Cross Coupling from Mutually Incoherent Lasers," J. Opt. Soc. Am. B **6**, 1884 (1989).

[56] Cronin-Golomb, M., K. Y. Lau, and A. Yariv, "Infrared Photorefractive Passive Phase Conjugation with BaTiO3: Demonstrations with GaAlAs and 1.09-μm Ar^+ Lasers," Appl. Phys. Lett. **47**, 567 (1984).

[57] Weiss, S., S. Sternklar, and B. Fischer, "Double Phase-Conjugate Mirror: Analysis, Demonstration, and Applications," Opt. Lett. **12**, 114 (1987).

[58] Ewbank, M. D., "Mechanism for Photorefractive Phase Conjugation Using Incoherent Beams," Opt. Lett. **13**, 47 (1988).

[59] Wu, C., J. G. McInerney, and B. W. Liby, to be published.

[60] Gauthier, D. J., P. Narum, and R. W. Boyd, "Observation of Deterministic Chaos in a Phase-Conjugate Mirror," Phys. Rev. Lett. **58**, 1640 (1987).

[61] Shaw, K., Private communication.

[62] Park, J. D., "Nonlinear Dynamics of External Cavity Semiconductor Lasers," Ph.D. Dissertation, Department of Electrical and Computer Engineering, University of New Mexico (1989).

[63] Agrawal, G. P. and J. T. Klaus, "Effect of Phase-Conjugate Feedback on Semiconductor Laser Dynamics," Opt. Lett. **16**, 1325 (1991).

[64] Boyd, R. W., Habashy, T. M., A. A. Jacobs, L. Mandel, M. Nieo-Vesperinas, W. R. Tompkin, and E. Wolf, "Nature of the Interference Pattern Produced on Reflection at a Phase-Conjugate Mirror," Opt. Lett, **12**, 42 (1987).

[65] Wolf, E., L. Mandel, R. W. Boyd, T. M.Habshy, and M. Nieto-Vesperinas, "Interference Pattern Produced on Reflection at a Phase-Conjugate Mirror. I: Theory," J. Opt. Soc. Am. B **4**, 1260 (1987).

[66] A. A. Jacobs, W. R. Tompkin, R. W. Boyd, and E. Wolf, "Interference Pattern Produced on Reflection at a Phase-Conjugate Mirror. II: Experiment," J. Opt. Soc. Am. B **4**, 1266 (1987).

[67] Yeh, P., "Theory of Unidirectional Photorefractive Ring Oscillators," J. Opt. Soc. Am. B **2**, 1924 (1985).

[68] MacDonald, K. R. and J. Feinberg, "Theory of a Self-Pumped Phase Conjugator with Two Coupled Interaction Regions," J. Opt. Soc. Am. **73**, 548 (1983).

[69] Feinberg, J., "Interferometer with a Self-Pumped Phase-Conjugating Mirror," Opt. Lett. **8**, 569 (1983).

[70] *Long Wavelength Semiconductor Lasers*, G. P. Agrawal and N. K. Dutta, Van Nostram Reinhold Co. Inc. (1986).

[71] McInerney, J. G., and G. C. Dente, Private communications.

[72] Chung, K. H., J. G. McInerney, M. Osinski, "Measurement of the Semiconductor Laser Linewidth Enhancement Factor," SPIE Proc. **1043**, 175 (1989).

[73] Lee, S. S., L. Figueroa, R. Ramaswamy, "Variations of Linewidth Enhancement Factor and Linewidth as a Function of Laser Geometry in (AlGa)As Lasers," IEEE J. Quant. Electr. **25**, 862 (1989).

[74] Dente G. C., P. S. Durkin, K. A. Wilson, and C. E. Moeller, "Chaos In[sic] the Coherence Collapse of Semiconductor Lasers," IEEE J. Quant. Electr. **24**, 2441 (1988).

[75] Mork, J., *Nonlinear Dynamics and Stochastic Behaviour of Semiconductor Lasers with Optical Feedback*," Ph. D. Dissertation, Laboratory of Applied Mathematics, Technical University of Denmark (1988).

[76] Hitachi Optoelectronics Devices Data Book (1988).

[77] Several months after my experiments were completed the FSR was measured by another researcher and found to be 2100GHz. Evidently the continual alignment and adjusting moved the position of the mirrors over time. I believe that the 4000GHz number was fairly constant during the course of my experiments and the data taken from them was good. At any rate, I largely employed this device just to check for single mode operation, so extreme accuracy was not required.

[78] Sanders Associates, Nashua, NH.

[79] *Physics of Semiconductor Laser Devices*, G. H. B. Thompson, John Wiley & Sons (1980).

[80] Seo, D. S., "Multimode Feedback Effects in External Cavity Semiconductor Lasers: Quasistatic Analysis," Ph.D. Dissertation, Department of Electrical and Computer Engineering, University of New Mexico (1989).

[81] Agrawal, "Line Narrowing in a Single-Mode Injection Laser Due to External Optical Feedback," G. P., IEEE J. Quant. Electr. **QE-20**, 468 (1984).

[82] Kazarinov, R. F. and C. H. Henry, "The Relation of Line Narrowing and Chirp Reduction Resulting from the Coupling of a Semiconductor Laser to a Passive Resonator," IEEE J. Quant. Electr. **QE-23**, 1401 (1987).

[83] Saito, S. and Y. Yamamoto, "Direct Observation of Lorentzian Lineshape of Semiconductor Laser and Linewidth Reduction with External Grating Feedback," Electrn. Lett. **17**, 325 (1981).

[84] Nilsson, O., S. Saito, and Y. Yamamoto, "Oscillation Frequency, Linewidth Reduction and Frequency Modulation Characteristics for a Diode Laser with External Grating Feedback," Electrn. Lett. **17**, 589 (1981).

[85] Kikuchi, K. and T. Okoshi, "Simple Formula Giving Spectrum-narrowing Ratio of Semiconductor-laser Output Obtained by Optical Feedback," Electrn. Lett. **18**, 10 (1982).

[86] Ohtsu, M., I. Koshiishi, and Y. Teramachi, "A Semiconductor as a Stable Phase Conjugate Mirror for Linewidth Reduction of Another Semiconductor Laser," Jap. J. Appl. Phys. **29**, 2060 (1990).

[87] Dahmani, B., L. Hollberg, and R. Drullinger, "Frequency Stabilization of Semiconductors Lasers by Resonant Optical Feedback," Opt. Lett. **12**, 876 (1987).

[88] Lenstra, D., B. H. Verbeek, and A. J. den Boef, "Coherence Collapse in Single-Mode Semiconductor Lasers Due to Optical Feedback," IEEE J. Quant. Electr. **QE-21**, 674 (1985).

[89] Temkin, H., N. A. Olsson, J. H. Abeles, R. A. Logan, and M. B. Panish, "Reflection Noise in Index-Guided InGaAsP Lasers," IEEE J. Quant. Electr. **QE-22**, 286 (1986).

[90] Helms, J., and K. Petermann, "A Simple Analytic Expression for the Stable Operation Range of Laser Diodes with Optical Feedback," IEEE J. Quant. Electr. **26**, 833 (1990).

[91] Schunk, N. and K. Petermann, "Stability Analysis for Laser Diodes with Short External Cavities," IEEE Phot. Lett. **1**, 49 (1989).

[92] Helms, J. and K. Petermann, "Microwave Modulation Charactersitics of Semiconductor Lasers with Optical Feedback," Electron. Lett. **25**, 1369 (1989).

[93] Mork, J., B. Tromberg, and P. L. Christiansen, "Bistability and Low-frequency Fluctuations in Semiconductor Lasers with Optical Feedback: A Theoretical Analysis," IEEE J. Quant. Electr. **24**, 123 (1988).

[94] Bloom, D. M. and G. C. Bjorkland, "Conjugate Wave-Front Generation and Image Reconstruction by Four-Wave Mixing," Appl. Phys. Lett. **31**, 592 (1977).

[95] Suni, P. and J. Falk, "Measurements of Stimulated Brillouin Scattering Phase-Conjugate Fidelity," Opt. Lett. **12**, 838 (1987).

[96] Cronin-Golomb, M., B. Fischer, J. O. White, and A. Yariv, "Passive (Self-Pumped) Phase Conjugate Mirror: Theoretical and Experimental Investigation," Appl. Phys. Lett. **41**, 689 (1982).

[97] Chiou, A. E. T. and P. Yeh, "Beam Cleanup Using Photorefractive Two-Wave Mixing," Opt. Lett. **10**, 621 (1985).

[98] Cronin-Golomb, M. A. M. Biernacki, C. Lin, H. Kong, "Photorefractive Time Differentiation of Coherent Optical Images," Opt. Lett. **12**, 1029 (1987).

[99] Levenson, M. D., K. M. Jonhson, V. C. Hanchett, K. Chiang, "Projection Photolithography by Wave-Front Reversal," J. Opt. Soc. Am. **71**, 737 (1981).

[100] Brody, P. S. and C. G. Garvin, "Processing Microscope Using Phase-Conjugate Illumination Generated by Self-Pumping in Barium Titanate," Ferroelectrics **107**, 1255 (1990).

[101] Beckwith, P. H. and W. R. Christian, "Two-Wave Mixing and Phase Conjugation at 830nm in $BaTiO_3$," Opt. Lett. **14**, 642 (1989).

[102] Mazur, A. and S. Odoulov, "Ring Photorefractive Oscillator with Linear Cavity Distortions," IEEE J. Quant. Electr. **26**, 963 (1990).

[103] He, Q. B., P. Yeh, C. Gu, R. R. Neurgaonkar, "Multigrating Competition Effects in Photorefractive Mutually Pumped Phase Conjugation," J. Opt. Soc. Am. **B9**, 114 (1992).